


**Quarterly Research Performance Progress Report**

Federal Agency and Organization Element to Which Report is Submitted	U.S. Department of Energy Office of Fossil Energy
FOA Name	Advanced Technology Solutions for Unconventional Oil & Gas Development
FOA Number	DE-FOA-0001722
Nature of the Report	Research Performance Progress Report (RPPR)
Award Number	DE-FE0031606
Award Type	Cooperative Agreement
Name, Title, Email Address, and Phone Number for the Prime Recipient	<p><b>Technical Contact (Principal Investigator):</b> Abhijit Dandekar, Professor, <a href="mailto:adandekar@alaska.edu">adandekar@alaska.edu</a> 907-474-6427</p> <p><b>Business Contact:</b> Rosemary Madnick Executive Director UAF Office of Grants and Contracts Administration <a href="mailto:rmadnick@alaska.edu">rmadnick@alaska.edu</a>, 907-474-6446</p>
Name of Submitting Official, Title, Email Address, and Phone Number	Same as PI
Prime Recipient Name and Address	University of Alaska Fairbanks Grants and Contracts Administration PO Box 757880, Fairbanks AK 99775
Prime Recipient Type	Not for profit organization
Project Title	<b><u>FIRST EVER FIELD PILOT ON ALASKA'S NORTH SLOPE TO VALIDATE THE USE OF POLYMER FLOODS FOR HEAVY OIL EOR a.k.a ALASKA NORTH SLOPE FIELD LABORATORY (ANSFL)</u></b>

Principal Investigator(s)	<b>PI:</b> Abhijit Dandekar, <i>University of Alaska Fairbanks</i> <b>Co-PIs:</b> Yin Zhang, <i>University of Alaska Fairbanks</i> John Barnes and Samson Ning, Hilcorp Alaska LLC Randy Seright, <i>New Mexico Institute of Mining &amp; Technology</i> Baojun Bai, <i>Missouri University of Science and Technology</i> Dongmei Wang, <i>University of North Dakota</i>
Prime Recipient's DUNS number	615245164
Date of the Report	March 30, 2020
Period Covered by the Report	December 1, 2019-February 29, 2020
Reporting Frequency	Quarterly
Signature of Principal Investigator:	 Abhijit Dandekar

**TABLE OF CONTENTS**

1. ACCOMPLISHMENTS	8
a. Project Goals	8
b. Accomplishments	8
c. Opportunities for Training and Professional Development	67
d. Dissemination of Results to Communities of Interest	67
e. Plan for Next Quarter	67
2. PRODUCTS	71
3. PARTICIPANTS & OTHER COLLABORATING ORGANIZATIONS	71
4. IMPACT	71
5. CHANGES/PROBLEMS	71
6. SPECIAL REPORTING REQUIREMENTS	71
7. BUDGETARY INFORMATION	71
8. PROJECT OUTCOMES	72
9. REFERENCES	73

**LIST OF FIGURES**

Figure 2.1: Effect of reservoir heterogeneity on field assessment of polymer retention.	10
Figure 2.2: Attempted matches of Pack-5 polymer breakout using simulation.	12
Figure 3.1: The sand-filled channeled core model	14
Figure 3.2: Swelling of the microgel	15
Figure 3.3: The experimental procedure	16
Figure 3.4: Before gel treatment (sand size=10-20 mesh)	17
Figure 3.5: Before gel treatment (sand size=20-30 mesh)	18
Figure 3.6: Before gel treatment (sand size=30-60 mesh)	18
Figure 3.7: Gel placement (sand size=30-60 mesh)	19
Figure 3.8: Gel placement (sand size=20-30 mesh)	19
Figure 3.9: Gel placement (sand size=10-20 mesh)	20
Figure 3.10: Injection pressure during gel treatment	20
Figure 3.11: Oil recovery performance after gel treatment	21
Figure 3.12: Transport mechanisms of PPG in porous media	22
Figure 4.1: Oil viscosity calculations by EOS using different hydrocarbon composition lumping numbers	26
Figure 4.2a: Improved oil viscosity calculations	26
Figure 4.2b: Improved gas viscosity calculations	27
Figure 4.3: K-value (gas phase) calculations	27
Figure 4.4: Fluid density calculations	28
Figure 4.5: Oil rate history match for Well J-27	29
Figure 4.6: Oil rate history match for Well J-28	29
Figure 4.7: Areas corresponding to the different relative permeability curves	30
Figure 4.8: Modified relative permeability curves	31
Figure 4.9: Water-cut history match using the multiple relative permeability curves	32
Figure 4.10: The relationships of (a) oil recovery factor and (b) polymer utilization with polymer injection	

time	34
Figure 4.11: The relationships of (a) oil recovery factor and (b) polymer utilization with polymer concentration	36
Figure 4.12: The relationships of polymer utilizations at different polymer injection concentrations with time for Cases 1, 2 and 3 respectively, and shown in that order	38
Figure 4.13: The relationships of (a) oil recovery factor and (b) polymer utilization with polymer retention	39
Figure 4.14: The relationships of polymer utilizations at different polymer retention with time for Cases 1, 2 and 3 respectively, and showed in that order.	41
Figure 5.1: Polymer concentration and viscosity vs. time.	43
Figure 5.2: J-23A injection rate and pressure.	44
Figure 5.3: J-24A injection rate and pressure.	45
Figure 5.4: Hall plot for J-23A and J-24A.	45
Figure 5.5: Voidage replacement ratio	46
Figure 5.6: J-27 production performance.	47
Figure 5.7: J-28 production performance.	48
Figure 5.8: Predicted total oil rate under waterflood and polymer flood processes.	49
Figure 5.9: Tracer concentration in produced water.	50
Figure 6.1: The effect of salinity on oil-water separation	52
Figure 6.2: The demulsification performance of NaCl for emulsion at 75% WC	53
Figure 6.3: The demulsification performance of KCl for emulsion at 75% WC	54
Figure 6.4: The demulsification performance of KCl for emulsion with 800 ppm polymer at 75% WC	55
Figure 6.5: The effect of polymer on the demulsification performance of KCl	55
Figure 6.6: The effect of KCl on the formation of the intermediate layer	
Figure 6.7: The demulsification performance of E12+E18 for emulsion with 800 ppm polymer at 75% WC	56
Figure 6.8: The performance of KCl combined with demulsifier for emulsion with 800 ppm polymer at 75% WC	57
Figure 6.9: Schematic of Dynamic Scale Loop (DSL)	59
Figure 6.10: Deposit rate comparison at different temperatures and polymer concentrations	60
Figure 6.11: Tubes (original and after 5 runs) in both 400ppm and 160ppm test conditions compared with tubes from the 1 <sup>st</sup> attempt	61
Figure 6.12: Cloud point test solutions after 12 hours at 160°F	61
Figure 6.13: Cloud point test solutions after 12 hours at 190°F	62
Figure 6.14: Cloud point test solutions after 12 hours at 220°F	62
Figure 6.15: Cloud point test solutions after 4 hours at 240°F	62
Figure 6.16: Cloud point test solutions after 10 hours at 240°F	63
Figure 6.17: Cloud point test solutions after 4 hours at 250°F	63
Figure 6.18: Cloud point test solutions after 12 hours at 250°F.	64
Figure 6.19: DSL test result at 165F at 60mL/min with 0ppm polymer	65
Figure 6.20: DSL test result at 350F at 60mL/min with 0ppm polymer	65
Figure 6.21: DSL test result at 165F at 2mL/min with 0ppm polymer	66

Figure 6.22: DSL test result at 350F at 2mL/min with 0ppm polymer 67

**LIST OF TABLES**

Table 3.1: The key parameters of the models	14
Table 3.2: Oil recovery performance before gel treatment	17
Table 3.3: Different mechanisms behind transport of PPG in fractures and porous media	22
Table 3.4: Current empirical and theoretical models for preformed gel transport in open fractures	23
Table 3.5: Capability of current available models and simulator	23
Table 4.1: Comparison of different polymer injection time	33
Table 4.2: Comparison of different polymer injection concentrations	35
Table 4.3: Comparison of different polymer retention	38
Table 6.1: Compositions of synthetic brine	51
Table 6.2: Experimental approach for cloud point testing	58
Table 6.3: Experimental plan for Dynamic Scale Loop (DSL)	58
Table A: Summary of milestone status.	67
Table B: Budgetary information for Budget Period 2, Q3.	72

**NOMENCLATURE**

ANS	Alaska North Slope
BS&W	Basic Sediment and Water
bpd	Barrel Per Day
BHP	Bottomhole Pressure
BP	Budget Period
BS	Backscattering
CMG	Computer Modeling Group
cp or cP	Centipoise
DMP	Data Management Plan
DSL	Dynamic Scale Loop
EB	Emulsion Breaker
EOR	Enhanced Oil Recovery
EOS	Equations of State
FPV	Fracture Pore Volume
FR	Filter Ratio
Fr	Resistance Factor
Frr	Residual Resistance Factor
f <sub>w</sub>	Fractional Flow of Water
G'	Elastic Modulus
G''	Viscous Modulus
HPAM	Hydrolyzed Polyacrylamide
HM	History Matching
HSPF	High Salinity Polymerflood
HSWF	High Salinity Waterflood
IAPV	Inaccessible Pore Volume

*University of Alaska Fairbanks*

ICD	Inflow Control Device
IMEX	Implicit Pressure Explicit Saturation Simulator
I PROF	Injection Profile Log
KI	Potassium Iodide
k or K	Permeability (generally absolute)
K <sub>ro</sub>	Relative Permeability to Oil
K <sub>rw</sub>	Relative Permeability to Water
LSWF	Low Salinity Waterflood
LSPF	Low salinity Polymerflood
md or mD	MilliDarcy
mg	Milligram
nm	Nanometer
N <sub>o</sub>	Corey Exponent for Oil
N <sub>w</sub>	Corey Exponent for Water
OIW	Oil in Water
OOIP	Original Oil in Place
PF	Polymerflood
PFO	Pressure Falloff
PMP	Project Management Plan
PPB	Parts Per Billion
PPG	Preformed Particle Gel
PPM	Parts Per Million
PRV	Pressure Release Valve
PSU	Polymer Skid Unit
PV	Pore Volume
QC	Quality Control
RF	Recovery Factor
RPM	Rotation Per Minute
SC	Standard Conditions
SCTR	Abbreviation of Sector as used in CMG
SEM	Scanning Electron Microscopy
S <sub>or</sub>	Residual Oil Saturation
S <sub>orw</sub>	Residual Oil Saturation due to Water
S <sub>orp</sub>	Residual Oil Saturation due to Polymer
SPE	Society of Petroleum Engineers
STB	Stock Tank Barrel
STOOIP	Stock Tank Original Oil in Place
S <sub>wc</sub> or S <sub>wi</sub>	Connate/Irreducible Water Saturation
T <sub>o</sub>	Oil Content in the Water Sample
TPV	Total Pore Volume
μ	Viscosity
μg	Microgram
ULSPF	Ultra Low Salinity Polymerflood
URTeC	Unconventional Resources Technology

*University of Alaska Fairbanks*

USBM	United State Bureau of Mines
UV	Ultraviolet
VE	Viscoelasticity
VRR	Voidage Replacement Ratio
VRV	Vacuum Release Valve
WC	Water Cut
WF	Waterflood
WOR	Water Oil Ratio
XRD	X-ray Diffraction
XRF	X-ray Fluorescence

## **1. ACCOMPLISHMENTS**

### **a. Project Goals**

The overall objective of this project is to perform a research field experiment to validate the use of polymer floods for heavy oil Enhanced Oil Recovery (EOR) on the Alaska North Slope (ANS).

The main scientific/technical objectives of the proposed project are:

1. Determine the synergy effect of the integrated EOR technology of polymer, low salinity water, horizontal wells, and conformance treatments (e.g., gels), and its potential to economically enhance heavy oil recovery.
2. Assess polymer injectivity into the Schrader Bluff formations for various polymers at various concentrations.
3. Assess and improve injection conformance along horizontal wellbore and reservoir sweep between horizontal injectors and producers.
4. Evaluate the water salinity effect on the performance of polymer flooding and gel treatments.
5. Optimize pump schedule of low-salinity water and polymer.
6. Establish timing of polymer breakthrough in Schrader Bluff N-sands.
7. Screen an optimized method to control the conformance of polymer flooding at the various stages of the polymer flooding project.
8. Estimate polymer retention from field data and compare with laboratory and simulation results.
9. Assess incremental oil recovery vs. polymer injected.
10. Assess effect of polymer production on surface facilities and remediation methods.

The technical tasks proposed in these studies focus on the following: (1) optimization of injected polymer viscosity/concentration and quantification of polymer retention via laboratory scale experiments; (2) optimization of injection water salinity and identification of contingencies for premature polymer breakthrough via laboratory scale experiments and numerical analyses; (3) reservoir simulation studies for optimization of polymer injection strategy; (4) design and implementation of a field pilot test at Milne Point on the ANS; (5) identification of effective ways to treat produced water that contains polymer (including polymer fouling of heater tubes), and finally (6) the feasibility of commercial application of the piloted method in ANS heavy oil reservoirs. The project milestones, and current milestone status are shown toward the end in **Table A**.

### **b. Accomplishments**

The primary focus of the research program, since the start of the polymer injection in August 2018, has been monitoring the performance of the pilot in the injection wells J-23A and J-24A, and production wells J-27 and J-28 respectively. In order to complement the field pilot, focus of other supporting tasks has been advancing reservoir simulation, tackling flow assurance challenges and laboratory corefloods. The accomplishments to date are summarized in the following bullet points:



*University of Alaska Fairbanks*

- Publications resulting from the project continues to be a success. In the reporting quarter three completed papers were successfully submitted to 2020 SPE-IOR, and one to the 2020 SPE WRM. Complete citations were in the previous quarterly report. All three SPE-IOR conference papers were submitted for consideration to the SPE refereed journals. The review for the paper on emulsions has been received and the editorial committee ranked the paper among the “top 20%” of papers reviewed. We are currently preparing the rebuttal. The joint paper by NMT and UND has been accepted for refereed publication in the SPE Journal. Finally, an abstract also has been submitted (details under products) to the 2020 SPE ATCE conference to be held in Denver. The outcome of this is currently awaited.
- Plungers of pumps have been replaced and the filter ratio test for polymer QC has been automated. As such the pilot operations seamlessly continued in this reporting quarter.
- No polymer production or breakthrough has been observed more than 18 months after start of polymer injection, which has been monitored with both the clay flocculation and water composition analyses. Although clay flocculation test shows positive results, water composition analysis still could not detect presence of polymer.
- The project team continues to be cautiously optimistic from the standpoint of incremental oil, which is estimated to be ~600 bopd (over waterflood) from polymer injection.

Since the official project start date of June 1, 2018, the entire project team has continued the practice of working meetings every other Friday for three hours to discuss the various tasks and the project as a whole. A summary of these bi-weekly meetings is provided to the project manager. Additionally, separate meetings, as needed, between the sub-groups also take place. In the bi-weekly meeting of February 28 the team extensively discussed the possibility of lowering the polymer concentration from the current 1700 ppm down to 1400 ppm to lower the viscosity to ~30 cP and potentially improve the injectivity. If this is implemented the results will be reported in the next quarterly report.

The following summarizes the team’s progress to date in relation to the various tasks and sub-tasks outlined in the Project Management Plan (PMP):

- Task 1.0 - Project Management and Planning

Revised PMP and DMP are on file with DOE, which were submitted on April 30<sup>th</sup> 2019.

- Task 2.0 - Laboratory Experiments for Optimization of Injected Polymer Viscosity/Concentration and Quantification of Polymer Retention

Reported in this quarter was a collaborative effort from New Mexico Tech (Task 2) and the University of North Dakota (Task 4).

***Effect of Heterogeneity on Field Determination of Retention.*** Reservoir heterogeneity can affect field-based measurements of polymer retention. Consider the case where a fracture allows direct channeling between an injector and producer. Polymer retention in this fracture will probably be low or zero, so that

part of the flow stream may have no separation between the tracer and polymer fronts. In contrast, the part of the flow stream that passes through the porous rock should have a detectable difference between the tracer and polymer transit times.

For illustration, assume that the fracture/high-permeability channel accounts for 10% of the pattern pore volume, while homogeneous matrix accounts for the remaining 90%. Also assume that 50% of the flow that arrives at the production well travels through the fracture, while the other 50% travels through the matrix. Assume that polymer retention in the fracture is zero, but is  $110 \mu\text{g/g}$  in the porous rock. Given a polymer concentration of 1750 ppm and matrix porosity of 0.25, this retention value means that the polymer bank in the matrix will travel 50% slower than the tracer bank. (See Eq. 1 of Manichand and Seright, 2014, to perform this calculation.)

For this scenario, **Figure 2.1** plots the expected concentrations of polymer and tracer in the produced water. Because retention is zero in the fracture, tracer and polymer breakthrough together after about 0.2 PV of polymer injection. If the field observations were stopped here, polymer retention would appear to be zero. If the concentrations were continued to be monitored up to 3 PV (of continuous polymer/tracer injection), another bank of tracer would appear to breakthrough about 1.8 PV and a second bank of polymer would break through about 2.6 PV. If the field data were then used to calculate polymer retention, a value of  $55 \mu\text{g/g}$  would result—if the correct assumptions about reservoir heterogeneity were not made. Thus, field-based observations could result in a wide range of polymer retention calculations, depending on when the tracer and polymer concentrations were measured and the assumptions made about reservoir heterogeneity.

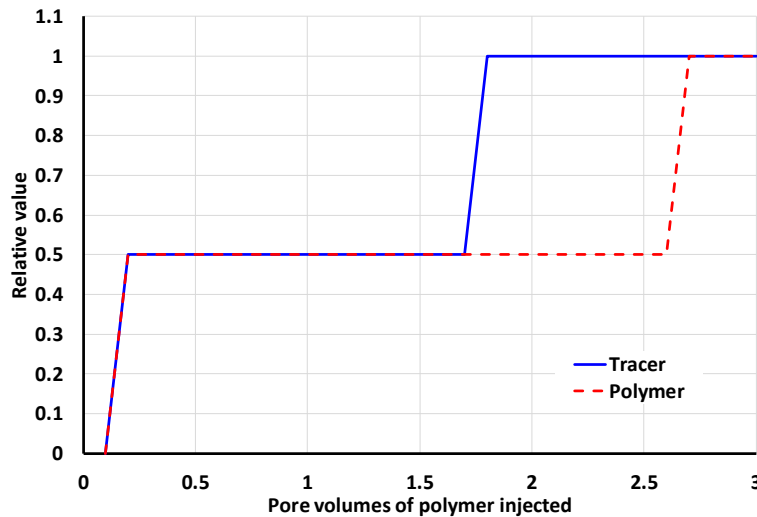


**Figure 2.1: Effect of reservoir heterogeneity on field assessment of polymer retention.**

**Examination of Models of Polymer Retention.** Simulators have options when treating polymer retention. Models often recognize that polymer adsorption is irreversible—i.e., once the polymer adsorbs onto the rock, it will not desorb under practical conditions. This discussion will not consider “hydrodynamic retention”, which can be reversible. Hydrodynamic retention is typically only of interest at velocities seen near a well (Chauveteau and Lecourtier 1988, Zhang and Seright 2015).

The simplest model assumes that polymer retention is independent of concentration. In this case, once polymer enters a given grid block, no polymer will flow to the next grid block until the entire adsorption capacity of that first grid block has been satisfied.

A second, very common model of polymer (and other chemical) adsorption is the Langmuir isotherm:

$$R_{pret} = R_{pretmax} K_a C / (1 + K_a C) \quad (2.1)$$

where  $R_{pretmax}$  is the maximum allowable adsorption and  $K_a$  is a constant. This model predicts that some free (un-adsorbed polymer) will always exist once polymer enters a given grid block (until brine is injected after polymer). As a consequence, some polymer will always be available to flow to the next grid block. If ten grid blocks separate an injection well from a production well, the simulator may predict some low concentration of polymer at the production well after the tenth time step. This effect is an artifact, but it could be misinterpreted as supporting false positives associated with the clay flocculation test (for detection of produced polymer in a field application) that will be discussed in the next section.

A third model of polymer retention was introduced by Zhang and Seright (2014). They noted that polymer adsorption was constant at low concentrations (e.g., <100 ppm), increased with increased polymer concentration at intermediate values (e.g., 100-1000 ppm), and was relatively constant at high concentrations (e.g., >1000 ppm). (A mechanistic explanation of this behavior can be found in their paper.) Some existing simulators can accommodate this behavior by allowing tabular input of polymer retention as a function of concentration.

As part of this work, CMG STARS and IMEX simulators were routinely used to model behavior in laboratory corefloods and in the field application. Details of this work will be presented in a future paper. Here, we briefly discuss some issues concerning use of the simulators to match our laboratory data.

Both STARS and IMEX could be made to approximate the observed laboratory retention data, although STARS consistently yielded greater dispersion of the polymer fronts. A false molecular mass must be used in the STARS modules because the actual polymer molecular weight (e.g., 18 million g/mol) will calculate extremely small polymer mole fractions (on the order of  $10^{-9}$  or  $10^{-10}$ ), and then lead to numerical convergence difficulties. Even though the false polymer molecular weight reduces numerical convergence difficulties, differences in simulation results between using IMEX and STARS still exist. These differences may be acceptable for some analyses.

**Figure 2.2** plots results from several attempts using IMEX to match the polymer breakout observed during our Pack-5 experiment. This experiment was performed in a 548-mD NB#1 sand pack, with  $k_w=50$  mD at  $S_{or}$ . The solid circles in **Figure 2.2** show the experimental results, based on nitrogen analysis of the effluent. The simulations were one-dimensional and had 61 grid blocks in the direction of flow. Other parameters in the simulation matched conditions of the experiment. The red curve shows the projected polymer breakout with a single retention input value in the model—specifically that retention is 240  $\mu\text{g/g}$  if polymer concentration is 1750 ppm. This model assumes that polymer retention is zero at zero concentration, and that polymer retention increased linearly between zero and 1750 ppm. The red curve is fairly symmetrical and has the proper shape observed in some experiments—but not this one.

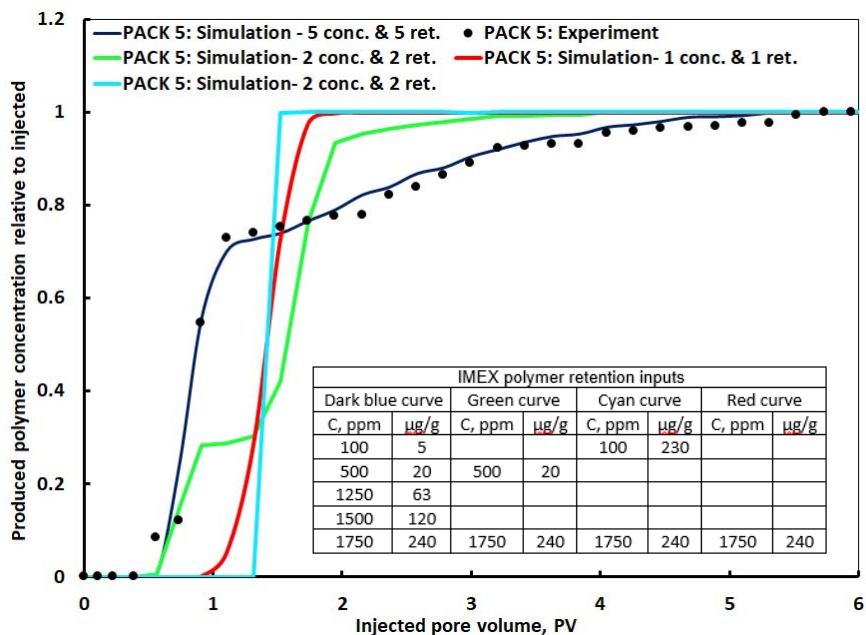


**Figure 2.2: Attempted matches of Pack-5 polymer breakout using simulation.**

The cyan curve shows a projection with two retention inputs—specifically that retention is 230  $\mu\text{g/g}$  at 100 ppm and 240  $\mu\text{g/g}$  at 1750 ppm. Again, the simulator assumes that polymer retention is zero at zero concentration, and retention values are interpolated at intermediate concentrations. This case is close to an assumption that retention is independent of concentration. The cyan curve is similar to the red curve, but is sharper (less dispersion).

The green curve also shows a projection with two retention inputs—specifically that retention is 20  $\mu\text{g/g}$  at 500 ppm and 240  $\mu\text{g/g}$  at 1750 ppm. The green curve shows rapid breakthrough of low-concentration polymer (~30% of injected value), followed by delayed breakthrough of higher concentrations.

The dark blue curve uses five retention inputs, as listed in the table within **Figure 2.2**. Depending on concentration, retention values range from 5  $\mu\text{g/g}$  to 240  $\mu\text{g/g}$ . This set of inputs provides the closest match to the experimental data (the black circles).

All four of the simulations shown in **Figure 2.2** are associated with 240  $\mu\text{g/g}$  polymer retention. However, they will all predict different efficiencies of oil displacement. Cases associated with the cyan and red curves predict a substantial delay (roughly double the time and polymer requirement) for an oil response as the case for zero retention. In contrast, the dark blue curve (and the experimental data points) predicts timing and an oil response equivalent to injecting a polymer bank with zero retention, but with only 70% of the injected polymer concentration (i.e., a much faster response than from the blue and red curves, but with higher water cuts). The green curve predicts something intermediate. Thus, the form assumed for the retention input into a simulator can have an important impact on the timing and magnitude of the oil response from a polymer flood.

**Activity is ongoing.**

- Task 3.0 - Laboratory Experiments for Optimization of Injection Water Salinity and Identification of Contingencies in Premature Polymer Breakthrough in the Field

During this quarter, experiments were carried out to investigate the impact of heterogeneities on polymer flooding performance and the effectiveness of gel treatment. Our previous experiments with Milne Point Liviano NB core plug, Liviano NB sandpack, silica sand, and Berea sandstone cores have all demonstrated that polymer with low salinity could improve the oil recovery efficiency even after extensive water flooding. A satisfactory overall oil recovery performance could be achieved after polymer flooding. It should be noted that the results were observed from homogeneous core/sandpack models. But the field condition may not be as optimistic as in the lab. Heterogeneities (e.g. super-k channels, fractures) may be present in the reservoir. To what extent does the heterogeneity influence the water breakthrough, water cut, and oil recovery performance? Is polymer still effective and sufficient to overcome the impact of heterogeneity and achieve a satisfactory oil recovery performance? Whether a conformance treatment can improve the situation or not?

Three experiments were conducted in this quarter. The cores used were 2-inch Berea cores with a permeability of about 500 md. The key parameters of the model are shown in **Table 3.1**. As shown in **Figure 3.1**, the cores were cut into two halves. A 0.3-cm fracture was created between the two half parts. The fracture was filled with NB sand with a specific range of mesh size. The detailed preparation procedure of the sand-filled channel model has been presented in last quarter report. For the three models, sand with different sizes (10-20 mesh, 20-30 mesh, and 30-60 mesh) was used to fill the fracture and make the channel with different permeabilities. The channel would have a higher permeability when filled with larger sand, and therefore, the permeability contrast between the channel and matrix became larger and the heterogeneity of the model became more enhanced. Following the same procedure, another model would be prepared using 60-80 mesh sand. The results of a previous experiment using a homogeneous core was included for comparison purpose. The main objectives of these experiments include:

- 1) To evaluate the impact of the presence of heterogeneity on the injection pressure, water breakthrough, water cut response, and oil recovery performance;
- 2) To test whether polymer flood is still effective and sufficient to overcome the impact of heterogeneity, control the water cut, and achieve a satisfactory oil recovery performance;
- 3) To test whether a conformance treatment (microgel injection) can improve the situation and evaluate how much improvement can be achieved after the treatment; and
- 4) To assess the damage caused by the treatment and figure out solutions to recover/minimize the damage.

In this report, we will present the major observations made from the three experiments. Another two experiments are planned to be carried out following this quarter. The results will be presented in next report.

**Table 3.1: The key parameters of the models**

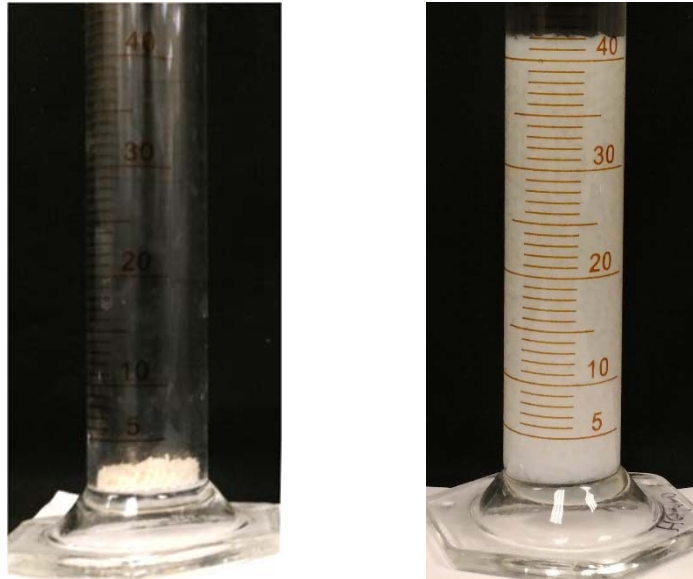
Exp. #	L×d, cm	Channel thickness, cm	Channel width, cm	Sand size, mesh	Heterogeneity
Homogenous model	30×3.8	/	/	/	Low ↓ ↓ High
Channeled #3	14.5×5	0.3	4.1	30-60	
Channeled #2	14.5×5	0.3	4.1	20-30	
Channeled #1	14.5×5	0.3	4.1	10-20	



**Figure 3.1: The sand-filled channeled core model**

Microgel was used as the conformance treatment agent. The microgel used was a kind of preformed

particle gel with the swelling ratio around 40. **Figure 3.2** shows the microgel before and after swelling in Milne Pt injection brine. The dry microgel had a size of 170-230 mesh. The gel was carried with Milne Pt injection brine with a microgel concentration of 1 wt%.



(a) Dry microgel particles      (b) Swelling microgel in brine

**Figure 3.2: Swelling of the microgel**

The procedure of the experiments is shown in **Figure 3.3**. After establishing initial water saturation condition, waterflooding and polymer flooding were performed before a microgel treatment was implemented.

The initial waterflooding was run until the water cut increased to ~80%, as comparable to the pilot situation. Polymer flooding was then performed until no oil produced and the injection pressure became stable. Microgel dispersion was injected until the gel was observed at the outlet (if possible). After the gel treatment, post polymer flooding and waterflooding were followed sequentially. The residual resistance factor established by the microgel treatment was evaluated.

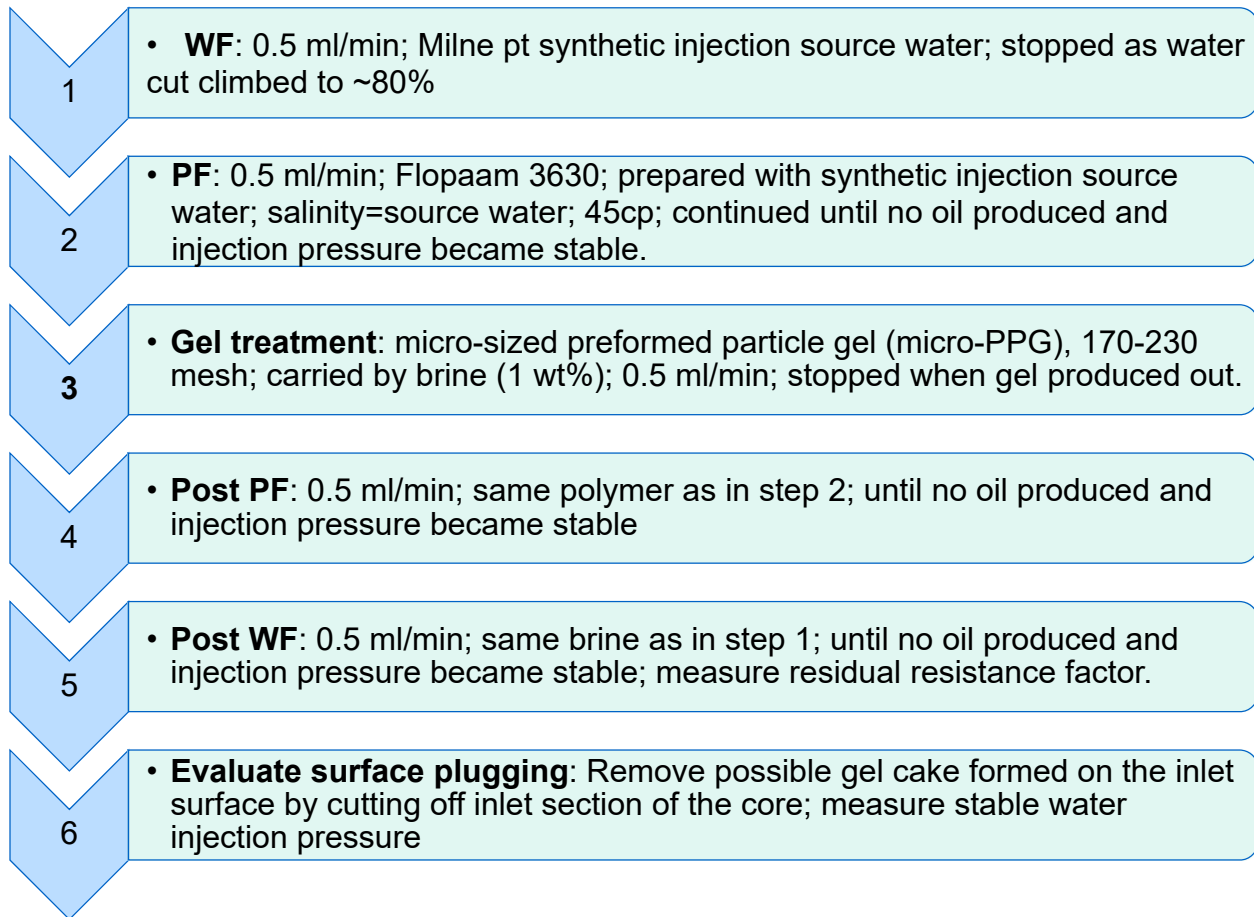


**Figure 3.3: The experimental procedure**

**Oil Recovery Performance before Gel Treatment.** The oil recovery performance before gel treatment is shown in **Table 3.2** and **Figure 3.4-3.6**. As the size of the filled sand increases, the severity of the heterogeneity becomes greater. The water broke through to the outlet (producer) earlier. The oil recovery factor of waterflood at the water cut of about 80% decreased. In the following polymer flooding process, the pressure buildup was smaller as the heterogeneity became more severe. The polymer flooding remarkably improved the oil recovery (22.7-32.2% OOIP). However, as the water breakthrough occurred earlier, the water cut increased more quickly and the low-water-cut production period was much shorter, and it would enter a high-water-cut production stage at very early time. After switching to polymer flooding, though the water cut was declined, it would increase back up to a high level. The water increased back more quickly as the heterogeneity was more enhanced. The seemingly encouraging incremental oil by polymer was mostly obtained in the long period of high-water-cut production process with continuous polymer injection. The overall oil recovery (58.4%, 48.9% and 34.7%) after waterflooding and extensive polymer flooding was much lower than that of the homogeneous model. The results indicate the impact of heterogeneity is significant and polymer alone is not sufficient to control the water cut and achieve a satisfactory oil recovery performance.



**Table 3.2: Oil recovery performance before gel treatment**

Sand size	Heterogeneity	K, D (channel)	Water breakthrough	Pp/Pw	WF, % fw=80%	PF, %	WF+PF
Homogenous	Low ↓ ↓ High	0.86	0.24PV	14.4	49.0	22.7	72.9
30-60		11	0.11PV	6.7	19.0	32.2	58.4
20-30		26.5	0.10PV	3.4	16.7	32.0	48.9
10-20		60	0.09PV	3.0	10.8	22.7	34.7

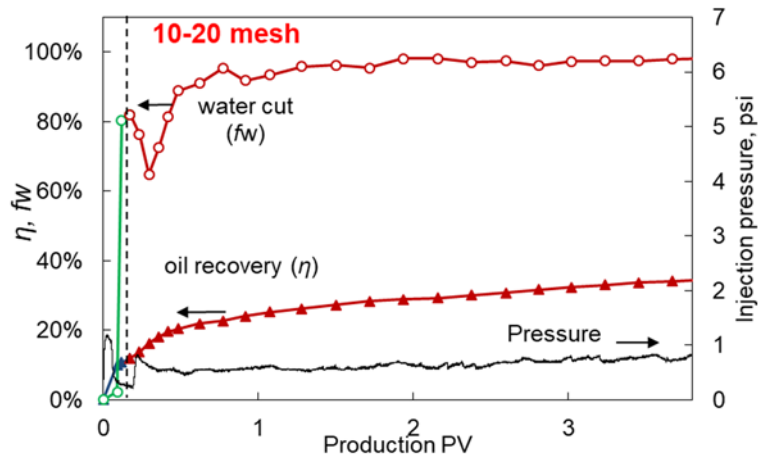


**Figure 3.4: Before gel treatment (sand size=10-20 mesh)**

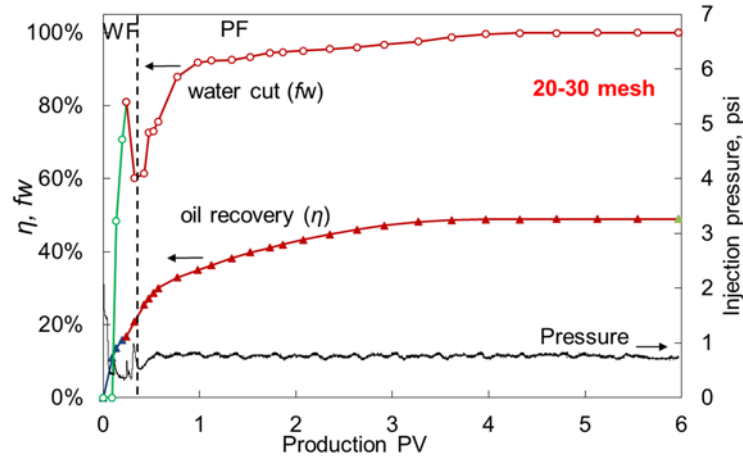


Figure 3.5: Before gel treatment (sand size=20-30 mesh)

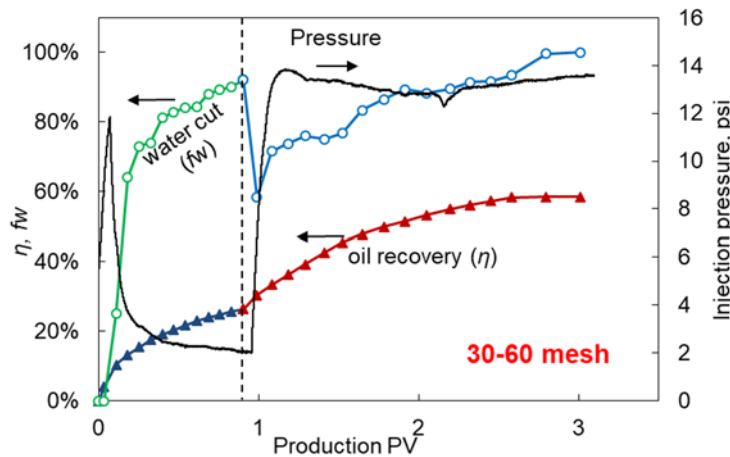
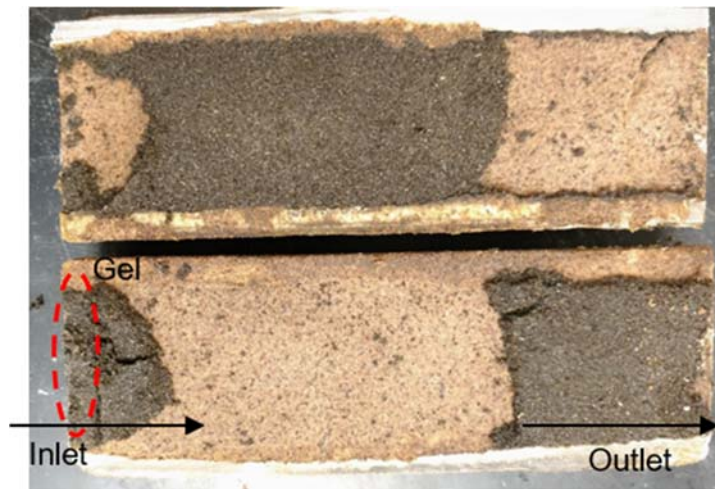


Figure 3.6: Before gel treatment (sand size=30-60 mesh)

**Gel Treatment.** The gel placement in the channel is shown in **Figures 3.7-3.9**. In the case with 30-60 mesh sand, about 4 fracture pore volumes (FPV) of gel dispersion was injected. No gel was produced out. Examination of the gel placement indicated that the gel only penetrated a small section at the inlet of the channel, as shown in **Figure 3.7**. The injection pressure is shown in **Figure 3.10(a)**. Gel was produced out in the other two experiments, and gel occupied the entire channel space, as shown in **Figures 3.8** and **3.9**. The gel came out earlier in the case with 10-20 mesh sand, at 7.4 FPVs of injection. For the case with 20-30 mesh sand, the gel came out at 9.7 FPVs. The injection pressure first showed a steady increase at the early stage and then showed fluctuation in a wide range. At the very beginning, the gel dispersion entered the super-k channel. As the retention of the particle microgel was very high, the pressure gradient would build up very quickly. It became harder for the following gel to go into the channel. Meanwhile,

due to the established pressure gradient, leak-off would occur at the matrix surface. In this process, the water of the gel dispersion was forced into the matrix while the microgel was left at the surface. As more gel accumulated at the surface, a gel cake would be formed. The gel cake prevented further leak-off of the gel dispersion into the matrix. The injection pressure in this stage showed a steady increase, as illustrated in **Figure 3.10**.

In the channel, the microgel particles would accumulate at the pore-throat structures. As the injection pressure increased, the gel would deform or break into smaller pieces and then passed through the pore-throat structures (Bai et al., 2004). The injection pressure would sharply drop down as the gel clusters broke out downstream. The gel again accumulated at the downstream pore-throat structures. Consequently, the injection pressure was built up, the newly-formed gel clusters were broken out, and the pressure was sharply released. With the repeat of accumulation and breakout of the microgel particles, a gel bank was gradually formed and grew in the channel from the inlet towards the outlet. Note that the injection pressure required for the breakout to occur was increased as the gel bank became larger, as shown in **Figure 3.10**. The front of the gel bank advanced towards the outlet, and gel particles would be produced out as the front arrived at the outlet, because the accumulation/breakdown of the gel particles occurs near the outlet.



**Figure 3.7: Gel placement (sand size=30-60 mesh)**

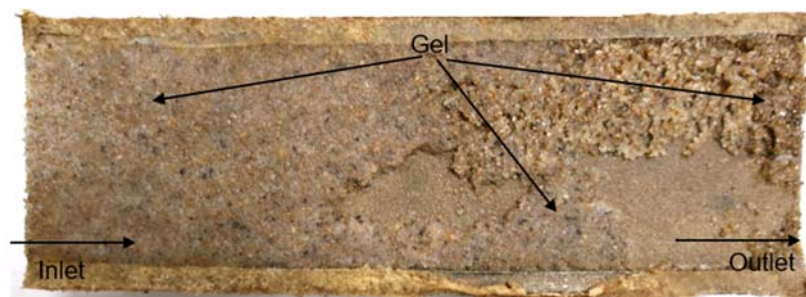


**Figure 3.8: Gel placement (sand size=20-30 mesh)**

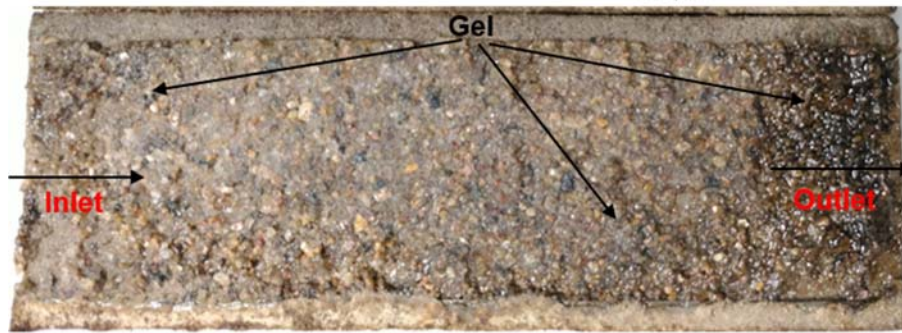
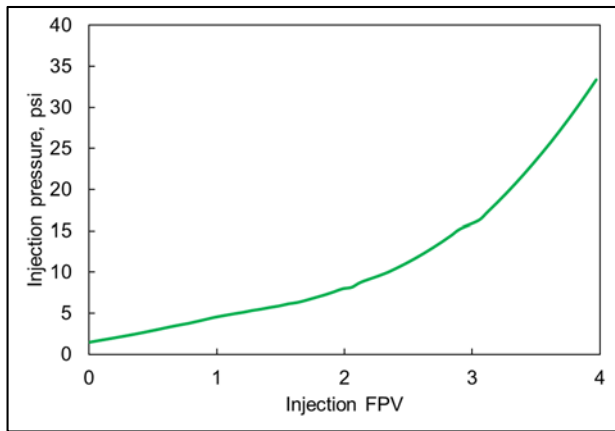
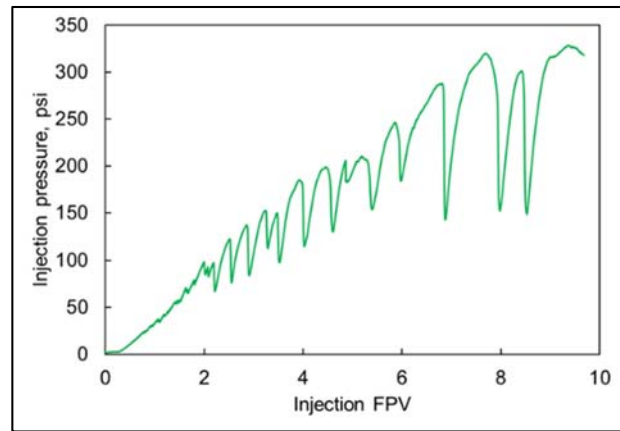


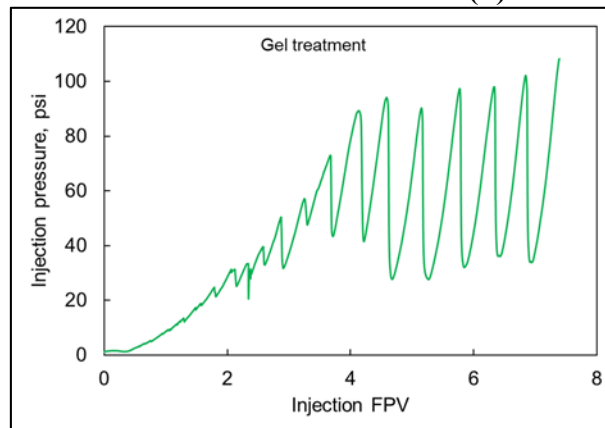
Figure 3.9: Gel placement (sand size=10-20 mesh)



(a) sand size=30-60 mesh



(b) sand size=20-30 mesh



(c) sand size=10-20 mesh

Figure 3.10: Injection pressure during gel treatment

**The Performance after Gel Treatment.** The oil recovery performance after gel treatment is shown in Figure 3.11. For the case of 30-60 mesh sand model, the overall improvement was quite limited, only

2.7% OOIP. The injected gel volume was insufficient and no gel was produced out. The gel was not successfully injected into the channel and a gel pack was not formed. Also, the permeability of the channel was not as high as in the other two models, thus it is harder for the gel to enter the channel. More likely, the gel accumulated and formed a gel cake at the surface, as observed in the experiment. Nevertheless, the final oil recovery efficiency was not poor (61.08%) compared with the other two cases. This is because the heterogeneity of the model was not as severe as the other two cases and a much higher oil recovery had achieved before the gel treatment. The improvement after gel treatment was 18.0% and 21.4% for the 20-30 and 10-20 mesh model, respectively. The improvement was noticeably greater when the model was more heterogeneous. For the case with the most serious heterogeneity problem, the water cut was effectively reduced as low as 63% from 100%, and the oil recovery efficiency was increased from 34.7% to 56.1%.

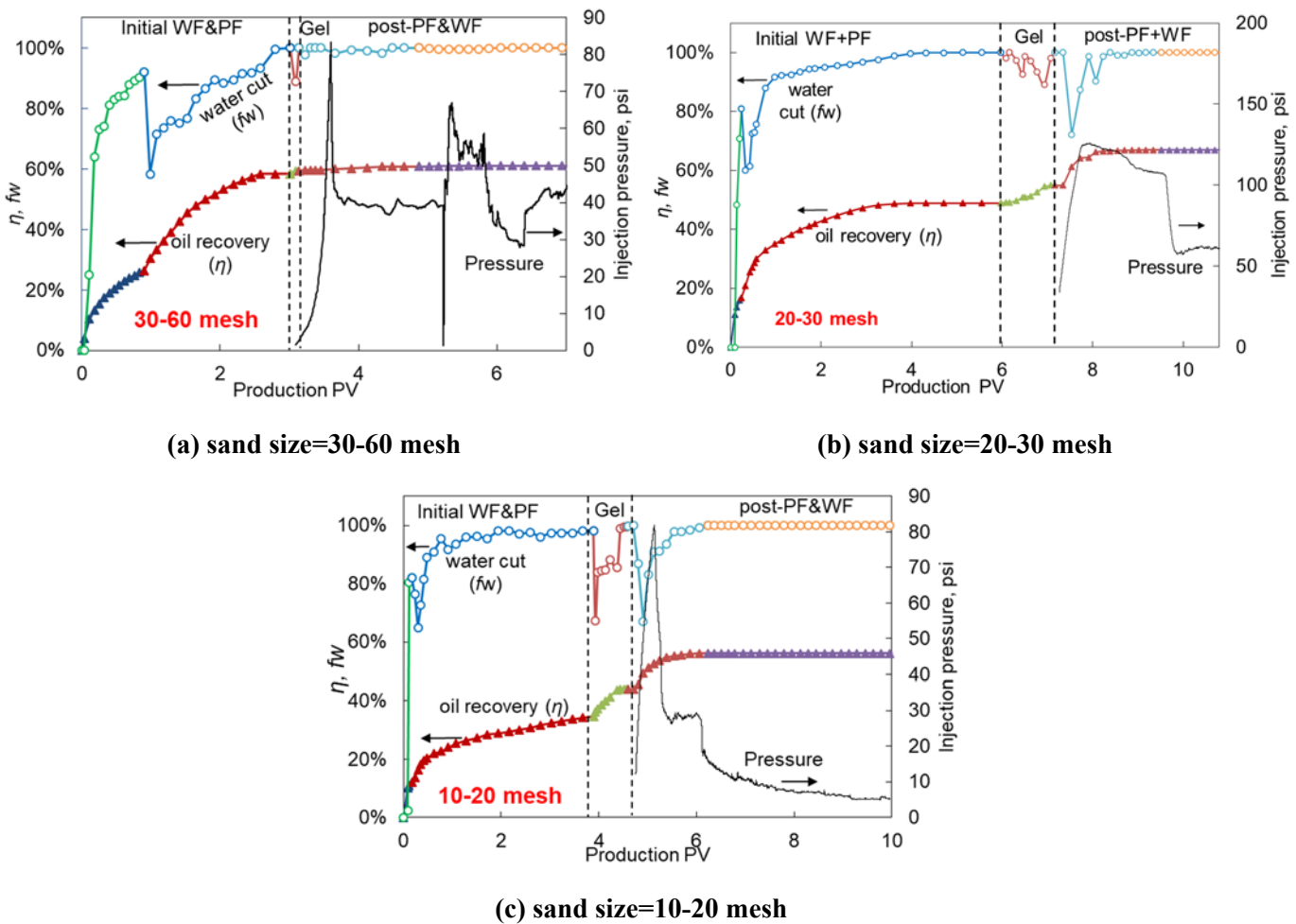


Figure 3.11: Oil recovery performance after gel treatment

**Challenges for Simulation of Microgel**

The objective of the simulation work is to link particle gel experimental results to the field applications. First of all, we need to understand particle gel transport mechanisms and use CMG simulators to establish a conceptual model and mimic the processes with eligible simplifications.

PPG performs different transport mechanisms in porous media and fracture, as shown in **Table 3.3**.

**Table 3.3: Different mechanisms behind transport of PPG in fractures and porous media**

Open Fracture	Porous Media
PPG propagation	PPG pass through large size pores
Gel packing	Deformation
Fluid leak-off	Totally plug at small size pores

In porous media, microscopically, Bai et al., (2007) depicts the propagation of particle gel through the pore throat and states that particles either pass, exhibit deformation or totally plug pore throats, as shown in **Figure 3.12**.

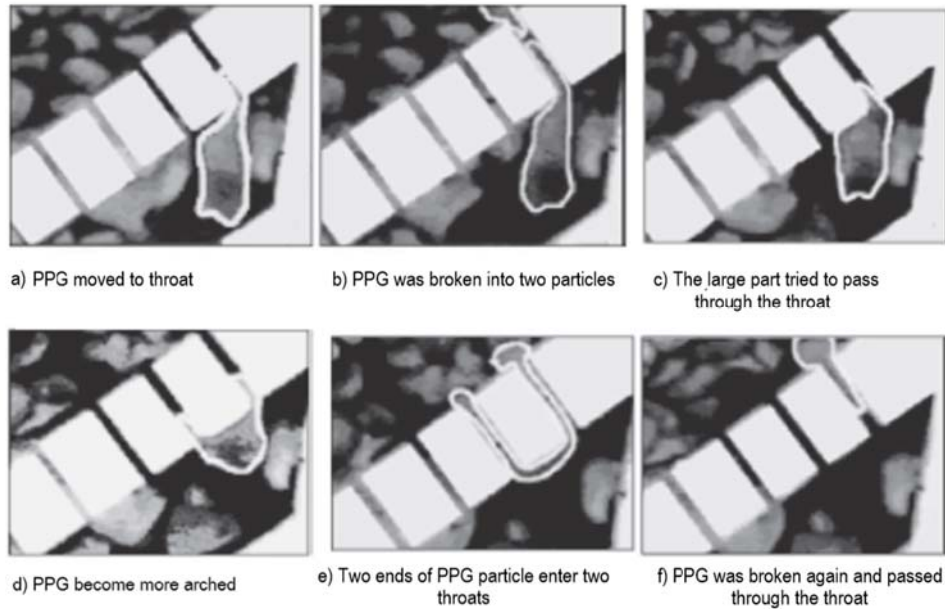


**Figure 3.12: Transport mechanisms of PPG in porous media**

Macroscopically, Bai, (2004) concluded conditions for passing PPG through pore throat: for weak PPG particles, if PPG diameter is less than 5.7 X pore throat diameter, and; for strong PPG particles, if PPG diameter is less than 1.3 X pore throat diameter. Whether PPG can pass through the pore throat depends on concentration, velocity,  $D_g/D_p$ , and gel strength.

In open fractures, PPG transport mechanisms in fracture are similar to bulk gel. Researchers, shown in **Table 3.4**, discussed several available models.

**Table 3.4: Current empirical and theoretical models for preformed gel transport in open fractures**

Mechanism	Model Description	Key Functions	Reference
<b>Gel Filtration</b>	Evenly Leakoff Model	$u_l = 0.05t^{-0.55}$	Howard, G.C, 1970
	Unevenly Leakoff Model	$u_l = \frac{u_m}{1 + \frac{\int u_l dt}{w_f}}$	Seright, 2003
	Compression Model	$C_g = 1 - C_w = 1 - \phi_g$ $K_g = \frac{(1 - C_g)^3}{2\tau C_g^2 S_0^2}$ $\Delta p = \frac{1}{\sigma_g} \ln\left(\frac{1 - C_g}{1 - C_{g,0}}\right)$	Andersen & Stavland 2018
<b>Gel Propagation</b>	Propagation Bingham Model	$q = \frac{h_f w_f^3 \Delta p}{12\mu_0 L} \left(1 - \frac{3y_0}{w_f} + \frac{4y_0^3}{w_f^3}\right)$	Seright, 1998
	Propagation Buckley Model	$q = 2h_f A \left(\frac{w_f}{2} - y_0\right) - 2h_f \frac{A}{\frac{\Delta p}{\mu_0 L} \left(1 + \frac{1}{n}\right) \left(2 + \frac{1}{n}\right)} + 2h_f y_0 A, A = \frac{\left(\frac{-\Delta p w_f - \tau_0}{\mu_0 L} \frac{2}{\mu_0}\right)^{1+\frac{1}{n}}}{\frac{-\Delta p}{\mu_0 L} \left(\frac{1}{n} + 1\right)}$	Ouyang, L., 2013
	Propagation Empirical Bulk Gel Model	$\frac{\Delta p}{\Delta l} = \begin{cases} 156 \left(\frac{q}{h_f}\right)^{0.26} \frac{1}{w_f^{1.52}}, 1X \text{ GEL: } 0.5\%, 0.0417\% \\ 760 \left(\frac{q}{h_f}\right)^{0.21} \frac{1}{w_f^{1.42}}, 2X \text{ GEL} \\ 1796 \left(\frac{q}{h_f}\right)^{0.19} \frac{1}{w_f^{1.38}}, 3X \text{ GEL} \end{cases}$	Wang, Y., 2006
	Propagation Empirical PPG Model	$F_r = 3831.3(3e^{-17} G'^{5.6391})^{0.2709} \gamma^{-0.6001} (3e^{-17} G'^{5.6391})^{-0.01}$	Imqam, A., 2014

In our simulation, with simulator’s limitation, we cannot implement any of the empirical or theoretical model directly. The capability of simulator is shown in **Table 3.5**.

**Table 3.5: Capability of current available models and simulator**  
(Y: Available. N: Not available)

Critical Mechanisms	Theoretical Model	Empirical Model	Simplification	CMG Capability
Extrusion	Y	Y	Y	Y
Fluid Leakoff	Y	Y	Y	N

Pass	N	N	Y	Partially Y
Deform	Y	N	Y	Partially Y
Plug	N	Y	N	N

Alternatively, we have to simplify some models from lab experiments and mathematical derivation so that the mechanism can be simulated correctly. We will further study this in future work.

**Summary and Future work.**

The experiments carried out during this quarter demonstrate that the injection pressure, water breakthrough behavior, water cut response and oil recovery performance could be significantly impacted when a heterogeneity is present in the porous media. The overall oil recovery efficiency was much lower in the model with serious heterogeneity problem. Without additional conformance treatment, though the polymer could reduce the water cut, it increased back very quickly to high level. The seemingly remarkable improvement by the polymer flooding was obtained over long period of high-water-cut production process with continuous polymer injection. Significant water cut reduction and oil recovery improvement were observed after gel treatment. In the near future, two more experiments (60-80 mesh sand model and open fracture model) will be carried out. The residual resistance factor in both the channel/fracture and matrix will be evaluated. Effective solutions will be investigated to remove the filter cake formed at the matrix surface. Also, the relative permeability is an important parameter for simulation. We will summarize this parameter from the NB sandpack coreflooding experiments we had performed (endpoint  $K_{rw}$ ). To obtain a more reliable endpoint  $K_{rw}$ , experiments will be carried out using NB core plugs to test the endpoint relative permeability of high salinity water and low salinity water. The experiment is expected to verify whether LSW can lower the endpoint  $K_{rw}$  in the NB sand and provide support for reservoir simulation work. No mechanisms of PPG transport can be directly simulated. Some mechanisms can be mimicked with appropriate simplification, however, the other mechanisms need more research studies.

**Activity is ongoing.**

- Task 4.0 - Reservoir Simulation Studies for Coreflooding Experiments and Optimization of Field Pilot Test Injection Strategy

Activities and progress during December 2019, through February 2020, completed by UND include:

- Completed and submitted manuscript of the paper SPE-200428-MS along with NMT, “Laboratory Evaluation of Polymer Retention in A Heavy Oil Sand for A Polymer Flooding Application on Alaska’s North Slope” to *SPE* Journal, which will be presented in the SPE IOR Conference in August, 2020. The paper has been modified based on peer reviewer suggestions and accepted for publication.
- Continued to investigate the polymer propagation function using the CMG/GEM model, working especially on the WINPROP function to generate EOS models for GEM hydrocarbon geochemistry input.



- Continued to match the newer production index using field-scale models through multiple relative permeability curves, focusing especially on the low water-cut of the producers within the last period of 2019.

#### 4.1 Examining Core Flooding Behavior on Polymer Retention

The key points here were presented in the aforementioned paper and referred to Task 2.0.

#### 4.2 Field-Scale Models for Production History Match

As mentioned in previous reports, in order to increase confidence in numerical simulations for polymer flooding, all three modules of CMG (including STARS, IMEX, and GEM with polymer functions) were examined for production history matching and forecasting. Also, using multiple components of hydrocarbon geochemistry in the GEM Module, the Equation of State (EOS) model was specifically investigated through the CMG module, WINPROP.

Technically, WINPROP/EOS can be used to predict phase behavior and characterize reservoir fluids, especially the heavy fraction of the petroleum fluids during simulation. Since we are simulating a heavy oil reservoir, oil viscosity is a key matching factor when using EOS modeling. Prior to simulation using the GEM field-scale model, EOS components for heavy oil in the target reservoir were incorporated in oil viscosity matching, along with the other composition matches on K-value, oil phase density, gas phase density, and gas viscosity from more than 30 hydrocarbon components. Those hydrocarbon compositions were then combined into the GEM model as ‘Heavy’ and ‘CH<sub>4</sub>’. After several attempts at EOS calculations, the production history match on oil rates compared favorably to other modules (IMEX, for example).

During the EOS calculations, we made two observations:

(1) **Figure 4.1** describes oil viscosity modeling when calculated by two lumped hydrocarbon compositions (left) and by ten hydrocarbon compositions including N<sub>2</sub> to H<sub>2</sub>S, CH<sub>4</sub>, and other compositions (right) through EOS. The blue dots were the data obtained through laboratory results (provided by Hilcorp) and the orange dots were the results of EOS calculations. Based on these illustrations, the EOS results for oil viscosity that lumped 10 hydrocarbon compositions provided similar results compared to lumping 2 hydrocarbon compositions (**Figure 4.1**, left), but with slight differences from the experimental data (**Figure 4.1**, right).

(2) When only focused on the oil viscosity calculation by EOS, the production history match was not very good, regardless of the number of component lumping. However, when the other parameter matching results were incorporated into the component lumping (‘Heavy’ and ‘CH<sub>4</sub>’) after the EOS calculation (K-value, oil density, gas viscosity, gas density, for instance, **Figures 4.2 to 4.4**), the production history matches on oil rates were good (**Figures 4.5 and 4.6**).

In the following discussions, two components utilized in the EOS calculation will be examined in **Figures 4.2 to 4.6**.

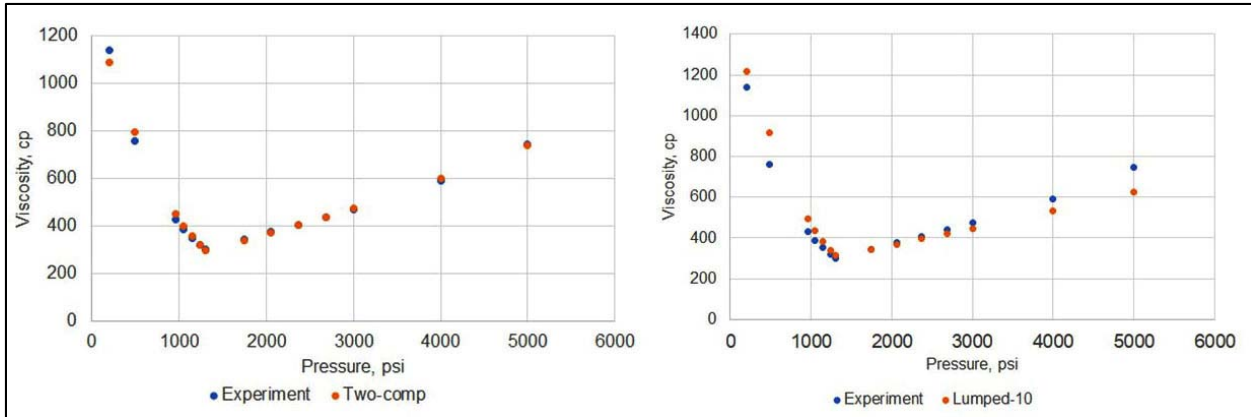


**Figure 4.1: Oil viscosity calculations by EOS using different hydrocarbon composition lumping numbers**

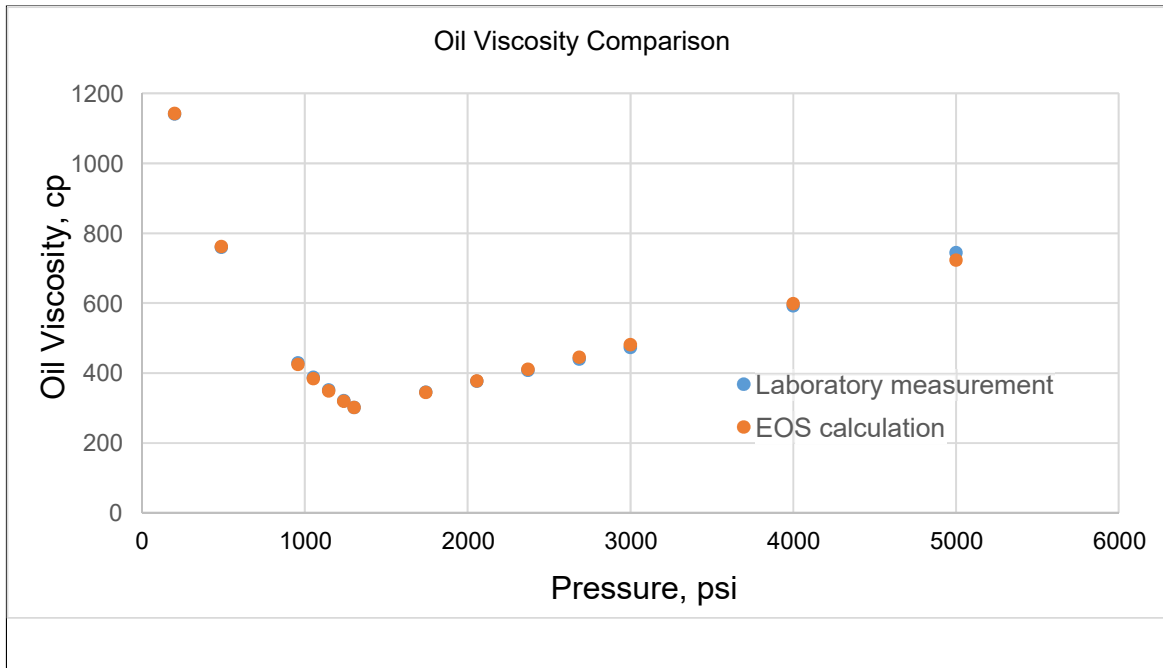


**Figure 4.2a: Improved oil viscosity calculations**

Figures 4.2a and 4.2b present the oil and gas viscosities calculation using EOS, and Figure 4.3 provides the EOS flash calculation results of K-Value matching with two components of ‘Heavy’ and ‘CH<sub>4</sub>’ based on input from the STARS model (i.e., based on the laboratory measurements). Note that the first component flash calculation was ignored when the K-value flash was calculated (data in even rows in the column “after regression”) because the K-value was focused on the gas phase. The K-value of CH<sub>4</sub> was calculated as a function of pressure and temperature, based on the PVT table input. Figure 4.4 presents the calculation results by the EOS model for oil and gas densities as functions of pressure.

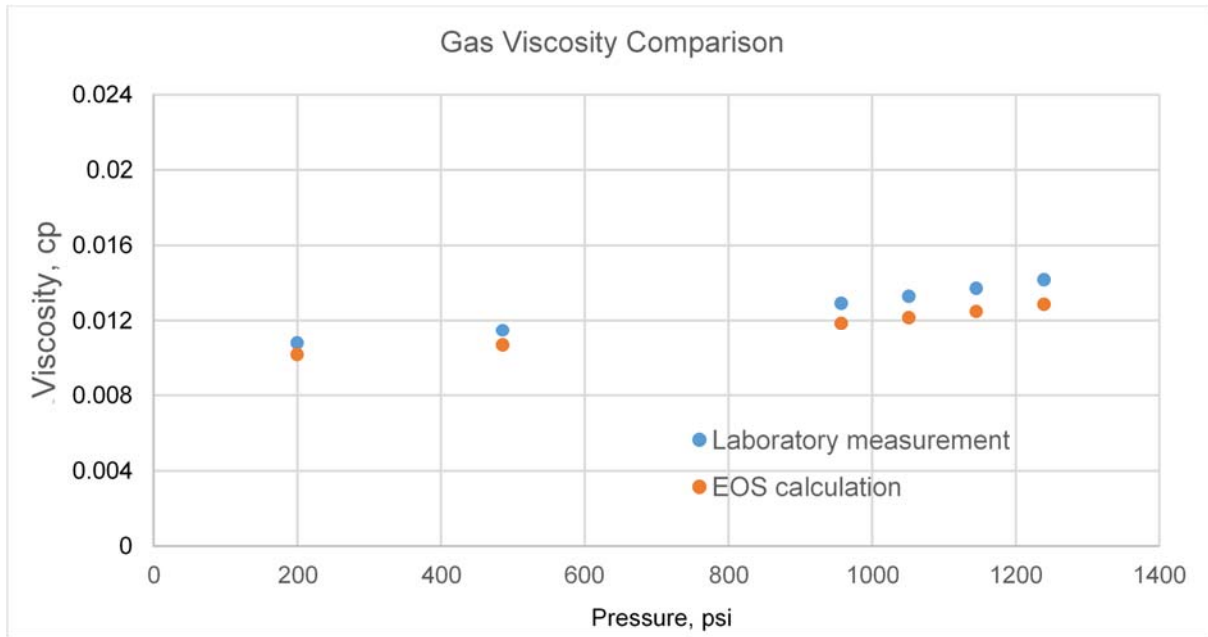


Figure 4.2b: Improved gas viscosity calculations

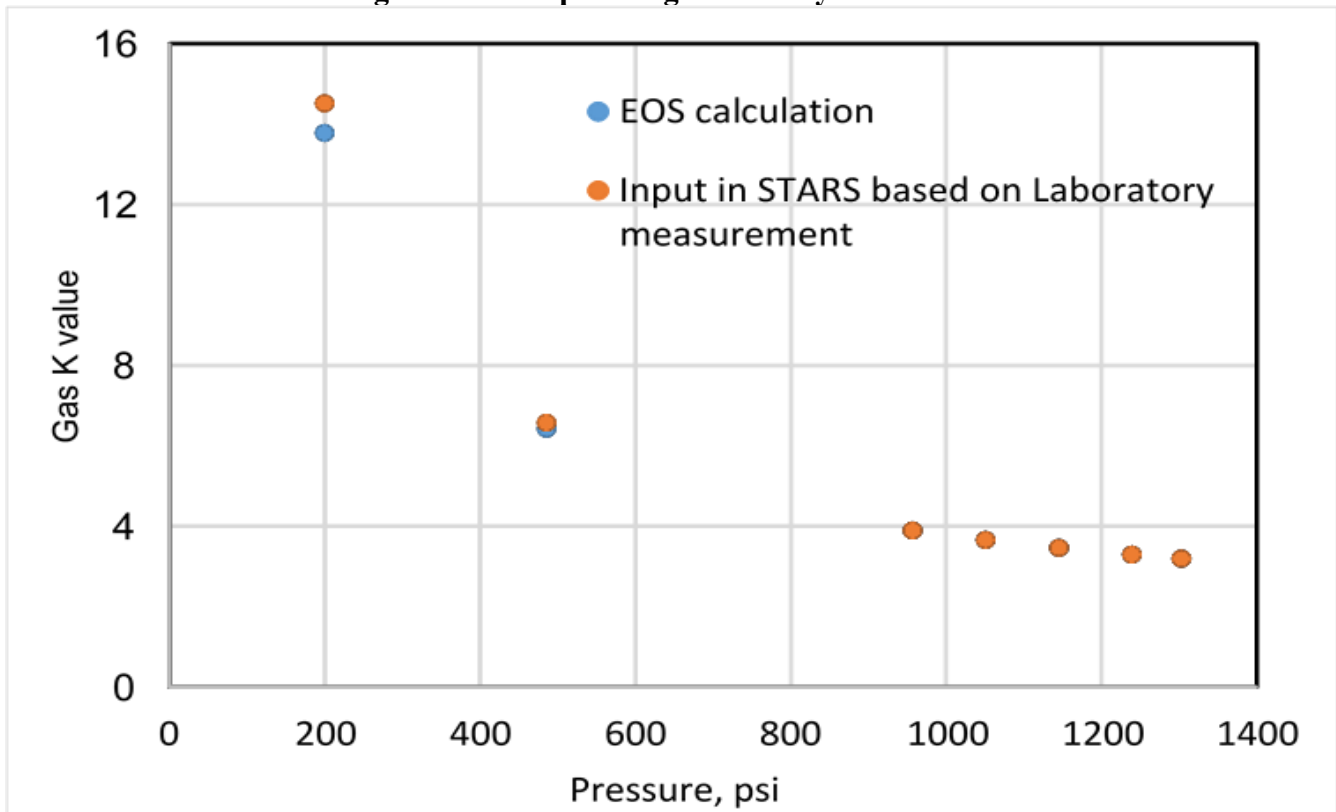
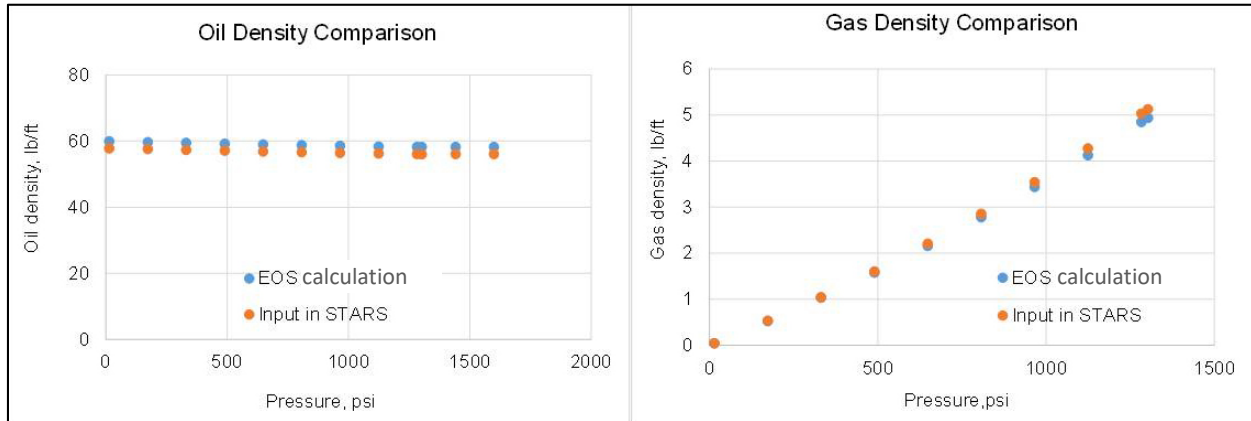


Figure 4.3: K-value (gas phase) calculations



**Figure 4.4: Fluid density calculations**

**Figures 4.5 and 4.6** present the history match using the GEM and IMEX modules for oil rates of the two production wells. In these two figures, actual production data are depicted by the green circles, and the dashed lines in orange and blue colors represent the simulation results using two hydrocarbon components in GEM (orange) and IMEX (blue), respectively. Note that in **Figures 4.5 and 4.6**, the purple lines are where the orange and blue lines overlapped. Because the PVT parameter inputs used in GEM after EOS flash modeling were similar to the parameters used IMEX, similar history match results were observed compared to the real production data on oil rates. In other words, the use of EOS flash calculations was a feasible approach for reaching a satisfactory numerical simulation result in GEM. However, for water-cut, the history matching was a challenge for the most recent production period due to exceptional water-cut decreases experienced by the two producers in the studied oil field. Therefore, in the following section, the water-cut history match in IMEX will be discussed.

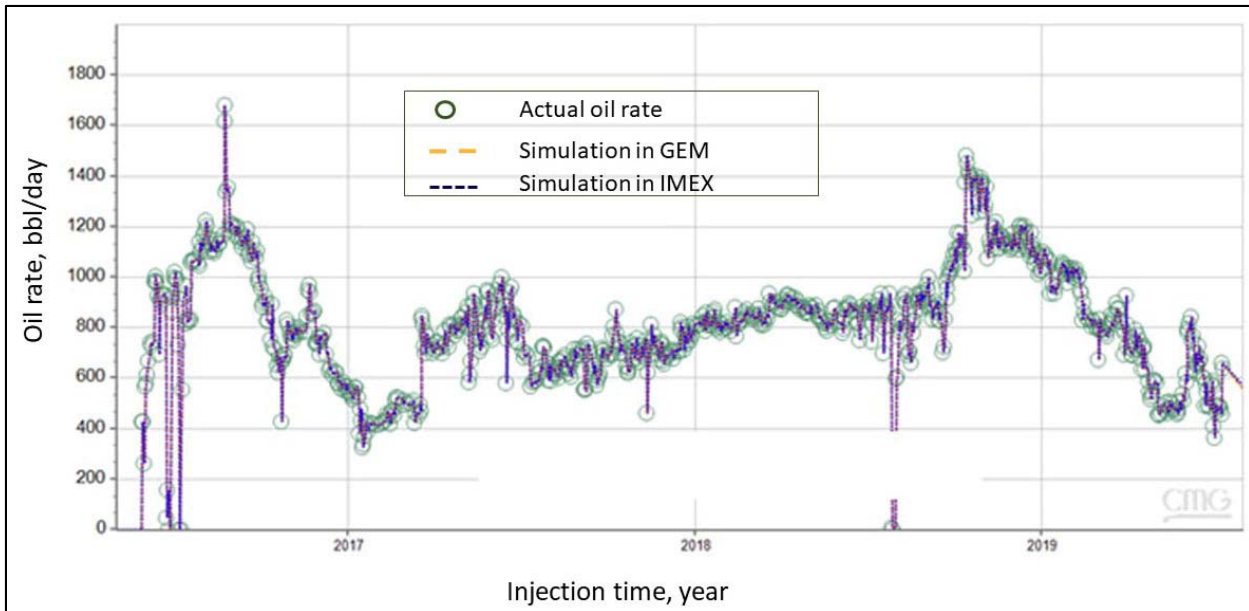


Figure 4.5: Oil rate history match for Well J-27

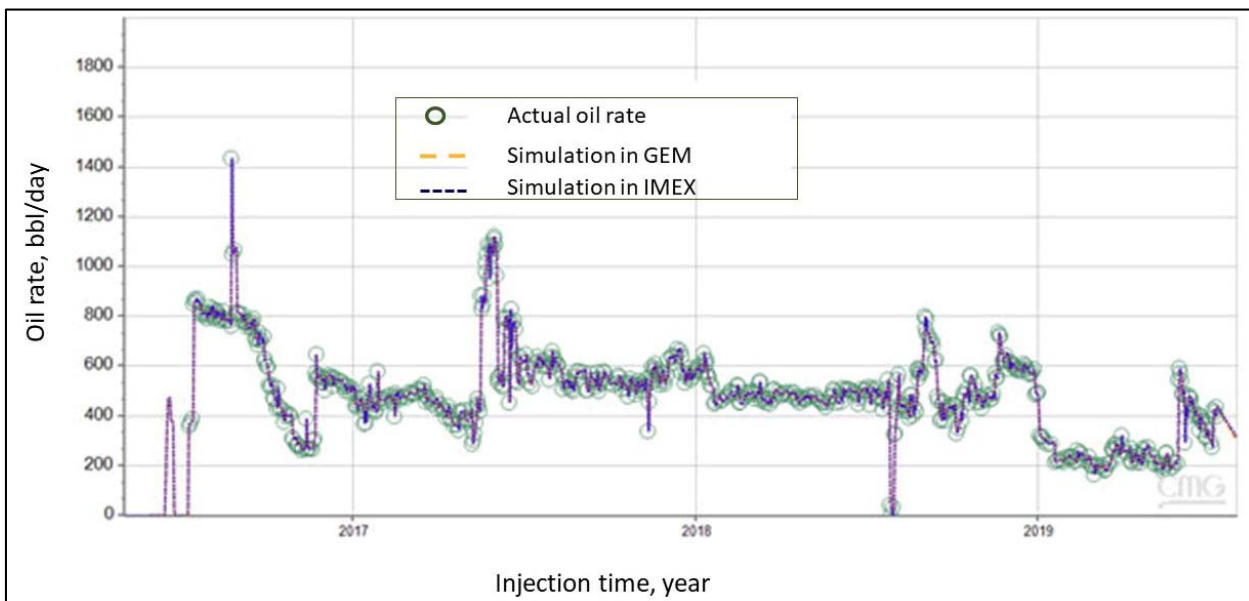


Figure 4.6: Oil rate history match for Well J-28

### 4.3 Multiple Relative Permeability Curves used in Water-Cut History Matching

Water-cut production history matched well for the entire water injection period and earlier portion of the polymer injection. However, due to the exceptional water-cut reduction experienced by the two producers (70% to 15%) since then, water-cut history match has been challenging using the original relative permeability curves and fluid transmissibility adjustment dynamically. In order to obtain a reasonable

history match, three more approaches were attempted for water-cut history match, including: (CASE-1) modifying the original relative water permeability curve for the entire region of the reservoir and decreasing the end point of  $K_{rw}$ ; (CASE-2) to add an additional relative permeability curve to the area containing Wells J28 and J23, and the area containing Well J24. The original relative permeability curve was still applied to the area containing Well J27 as **Figure 4.7** (left) illustrates; and (CASE-3) two additional relative permeability curves corresponding to the near wellbores of J24-J23-J28 and J27, while retaining the rest area of the gridblocks of the simulation model using the original permeability curve, as illustrated in **Figure 4.7** (right). The lowest relative water permeability at the end point was reduced to a value of 0.04, more than 75% lower than the original end point of 0.18. With these multiple curves (**Figure 4.8**) present in the model, the water-cut history match in the latter part of 2019 exhibited fair agreement for Well J28, and a big improvement for the Well J-27 (**Figure 4.9**). Further studies will be continued for improved water-cut history match.

In **Figure 4.9**, the blue circles represent the actual product data, and the dark blue dashed lines represent the water-cut history using the original relative permeability curves, as indicated on the two curves with the same colors in **Figure 4.8**. The green dashed lines in **Figure 4.9** indicates the first modification for CASE-1, corresponding to the revised green line in **Figure 4.8**. The pink line in **Figure 4.9** corresponds to the area of CASE-2 (left of **Figure 4.7**), and the red lines (**Figure 4.9**) were a modification of CASE-3, which corresponds to the right—hand image of **Figure 4.7**.

There is not enough evidence that high molecular weight polymer solutions (18 million Daltons, for instance) could mobilize the trapped residual oil with a low injection rate (1 ft/day, for instance). We believe that with low water permeability endpoint for the relative permeability curve could be reasonable for a heavy oil reservoir (Seright, et al., 2019). Further laboratory investigation may be needed on this point.

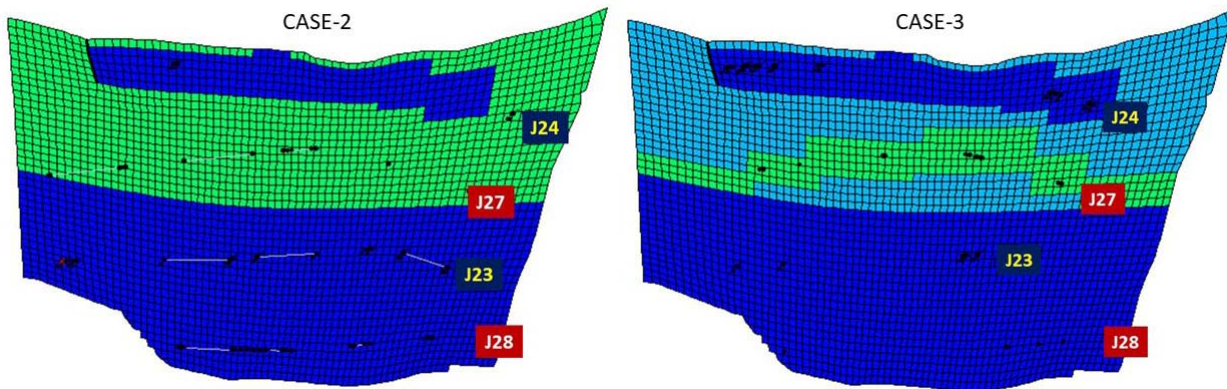


**Figure 4.7: Areas corresponding to the different relative permeability curves**

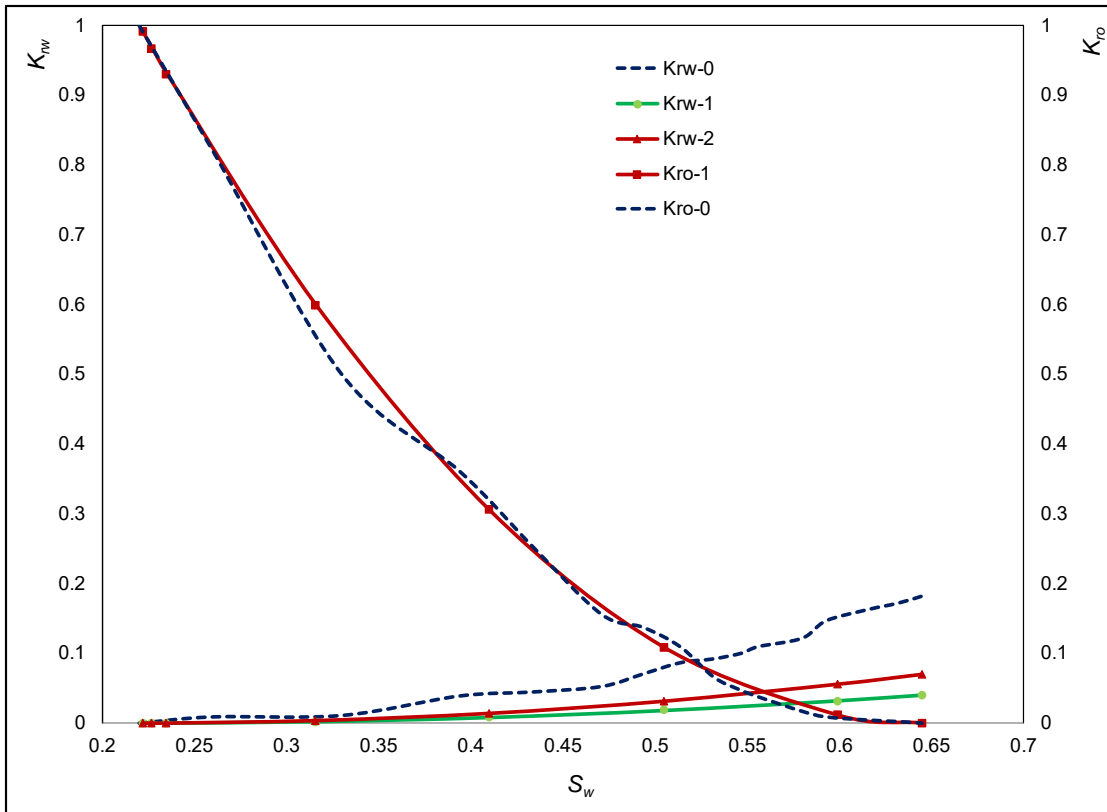
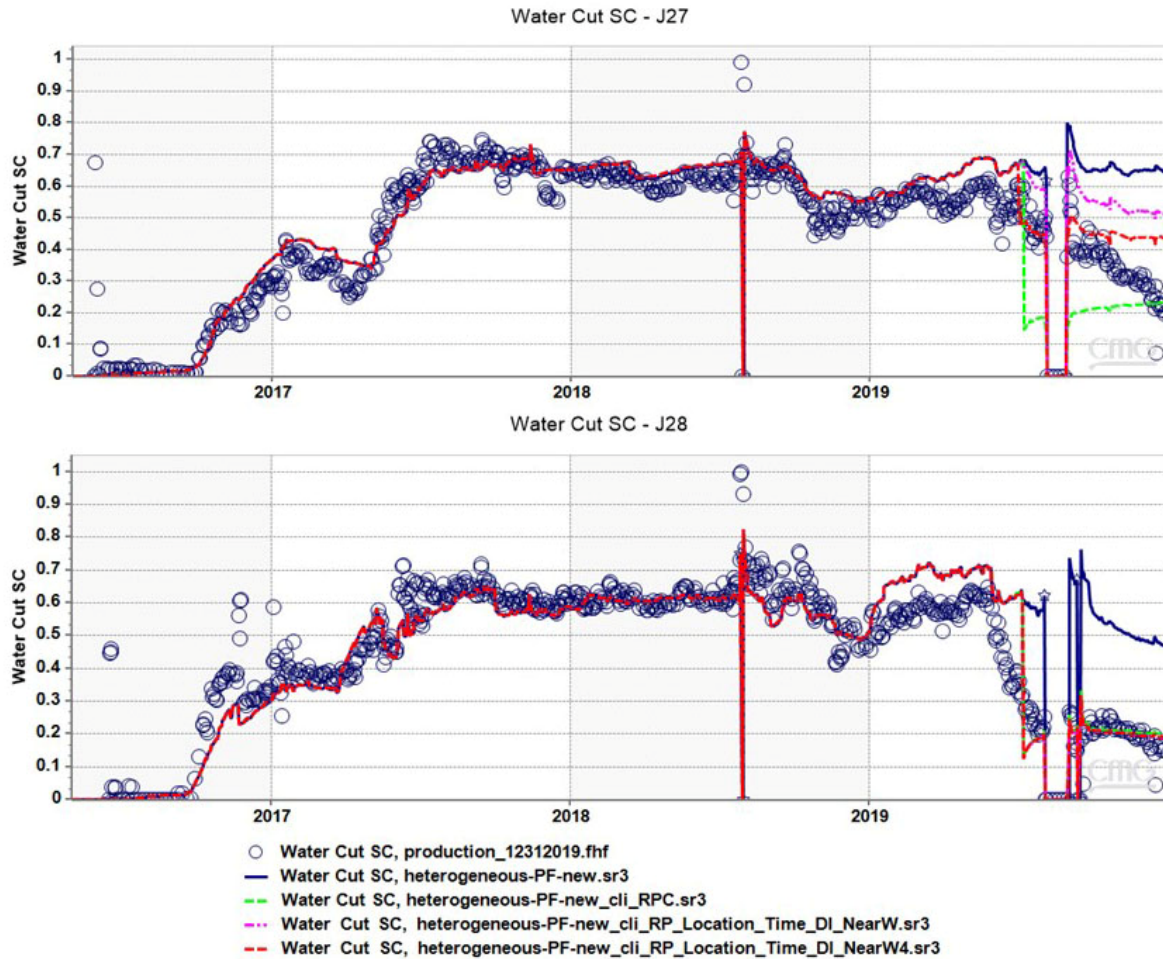


Figure 4.8: Modified relative permeability curves



**Figure 4.9: Water-cut history match using the multiple relative permeability curves**

In this quarter, UAF’s work focused on investigating the influence of polymer injection time, polymer concentration and retention on the oil recovery factor and polymer utilization, which is reported below.

**Sensitivity analysis**

The history matching results of water cut and tracer mass rate for two production wells have been improved by manually tuning the transmissibility multipliers and widths of the high permeable channels. Then the updated reservoir simulation model has been employed to investigate the influence of polymer injection time, polymer concentration and retention on the oil recovery factor and polymer utilization. The polymer utilization is described as

$$\text{Polymer utilization} = \frac{\text{Cumulative polymer injection}}{\text{Cumulative oil production}} \tag{4.1}$$

In the reservoir simulations, the updated reservoir model is used to forecast the production performance



of the polymer flooding for 30 years from July 6, 2019. During the prediction period, the water injection rates for injection wells J23A and J24A are fixed at 1400 bbl/day and 600 bbl/day, respectively, and the liquid production rates for production wells J27 and J28 are fixed at 1400 bbl/day and 600 bbl/day, respectively. The maximum bottom-hole pressure for injection wells is set to 2500 psi, while the minimum bottom-hole pressure for production wells is set to 500 psi.

**Polymer injection time.** The following six case studies have been designed and conducted to investigate the effect of polymer injection time on the oil recovery factor and polymer utilization. In each case, the polymer injection concentration is 1800 ppm, and the polymer retention is 153 µg/g.

- Case #1: inject polymer for 5 years followed by 25 years of waterflooding
- Case #2: inject polymer for 10 years followed by 20 years of waterflooding
- Case #3: inject polymer for 15 years followed by 15 years of waterflooding
- Case #4: inject polymer for 20 years followed by 10 years of waterflooding
- Case #5: inject polymer for 25 years followed by 5 years of waterflooding
- Case #6: inject polymer for 30 years

The oil recovery factors and polymer utilizations of the six cases are listed in **Table 4.1**. The relationships of oil recovery factor and polymer utilization with polymer injection time in 2049 are shown in **Figure 4.10**. As can be seen, the oil recovery factor increases with the increase of polymer injection time, though the increased rate of oil recovery is generally reduced. The polymer utilization increases linearly with the polymer injection time.

**Table 4.1: Comparison of different polymer injection time**

	Case #1	Case #2	Case #3	Case #4	Case #5	Case #6
Polymer injection time (yrs)	5	10	15	20	25	30
Oil recovery factor (%)	26.1	29.8	32.5	34.6	36.3	37.4
Polymer utilization (lb/bbl)	0.79	1.31	1.74	2.14	2.51	2.89

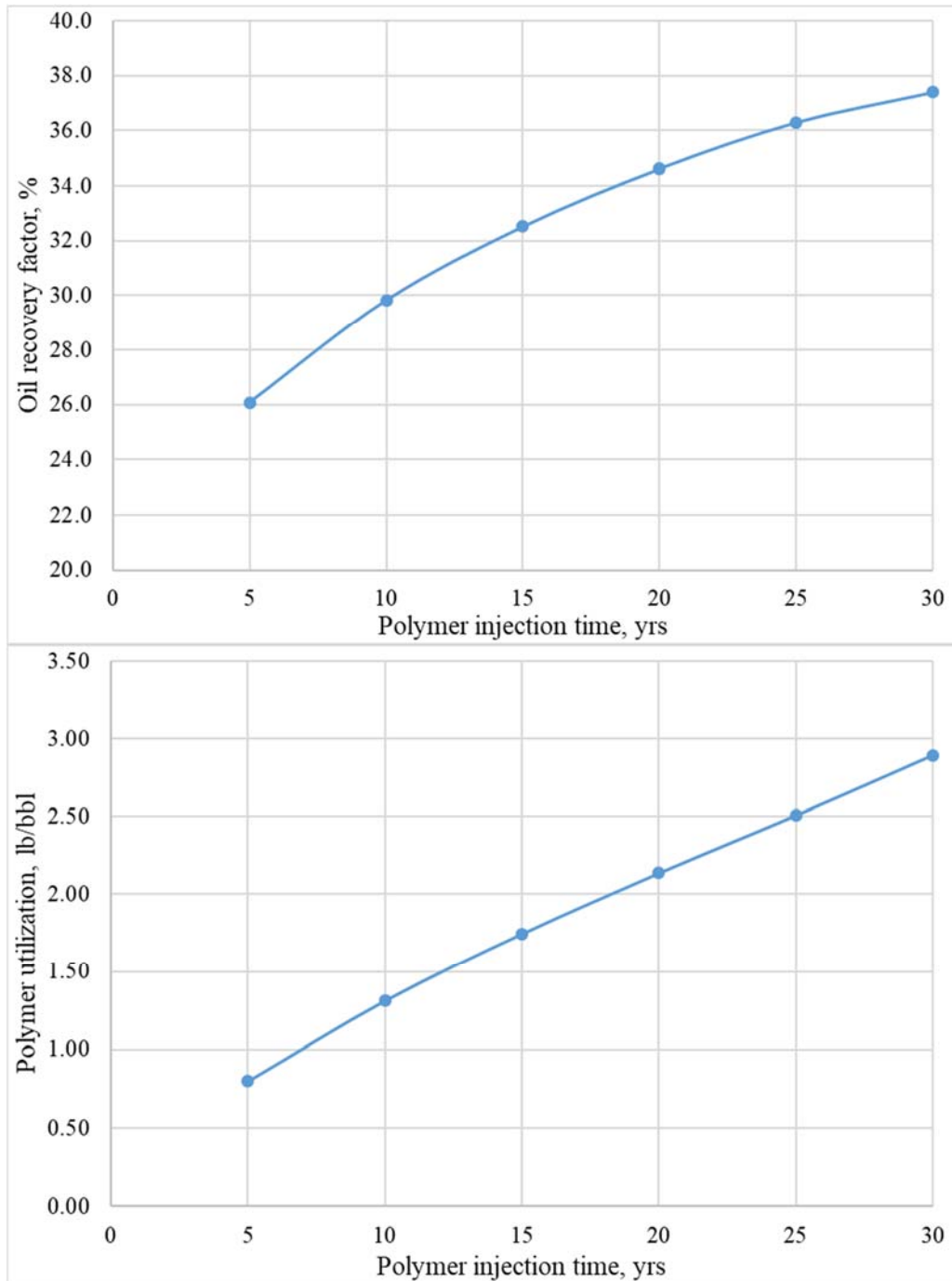


**Figure 4.10: The relationships of (a) oil recovery factor and (b) polymer utilization with polymer injection time**

**Polymer concentration.** The following three case studies have been designed to investigate the effect of polymer concentration on the oil recovery factor and polymer utilization. In each case, reservoir

simulations with the polymer injection concentrations ranging from 1000 ppm to 1800 ppm at intervals of 200 ppm have been conducted, and the polymer retention is 153  $\mu\text{g/g}$  in all the simulations.

Case #1: inject polymer for 10 years followed by 20 years of waterflooding

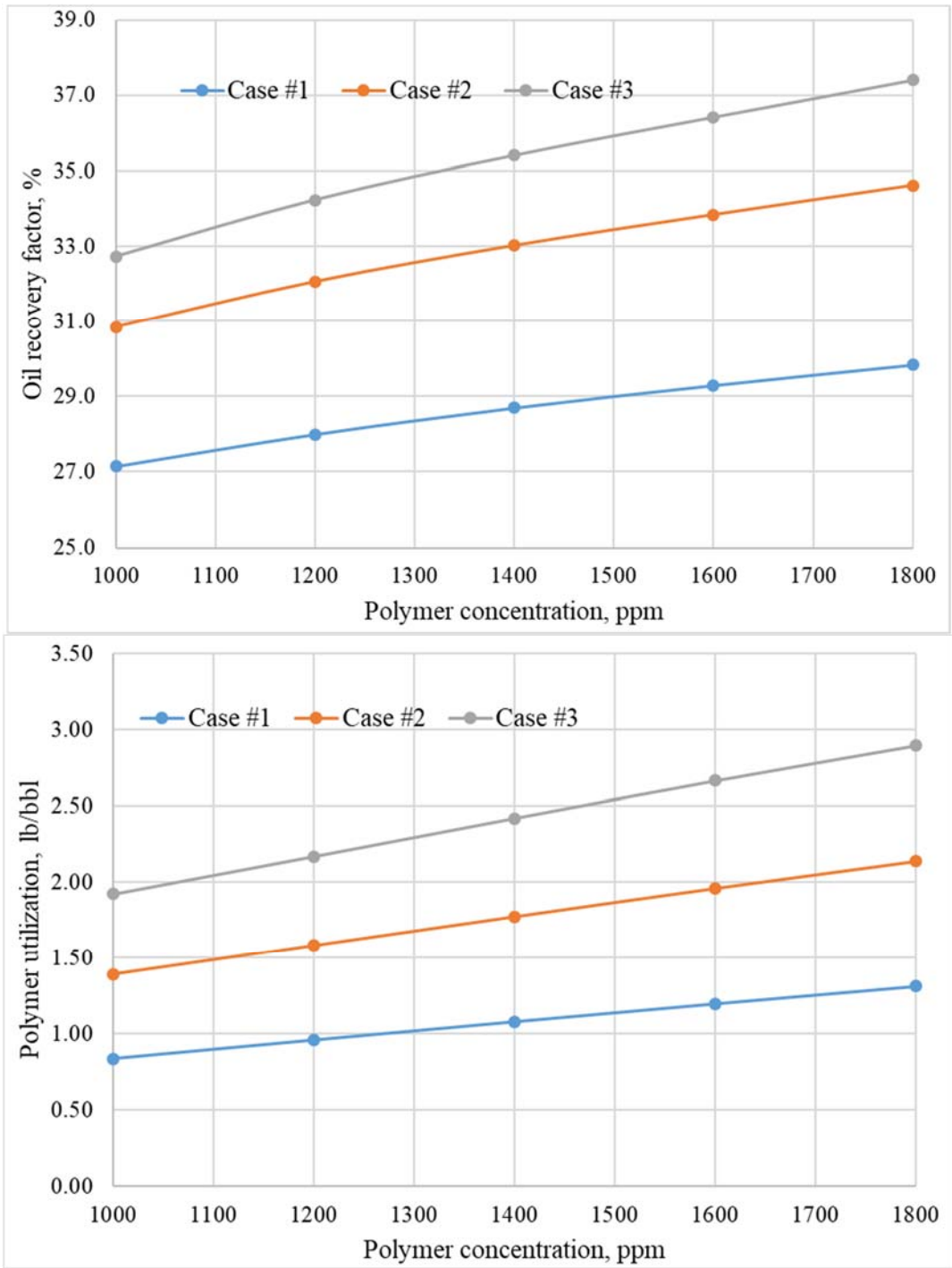
Case #2: inject polymer for 20 years followed by 10 years of waterflooding

Case #3: inject polymer for 30 years

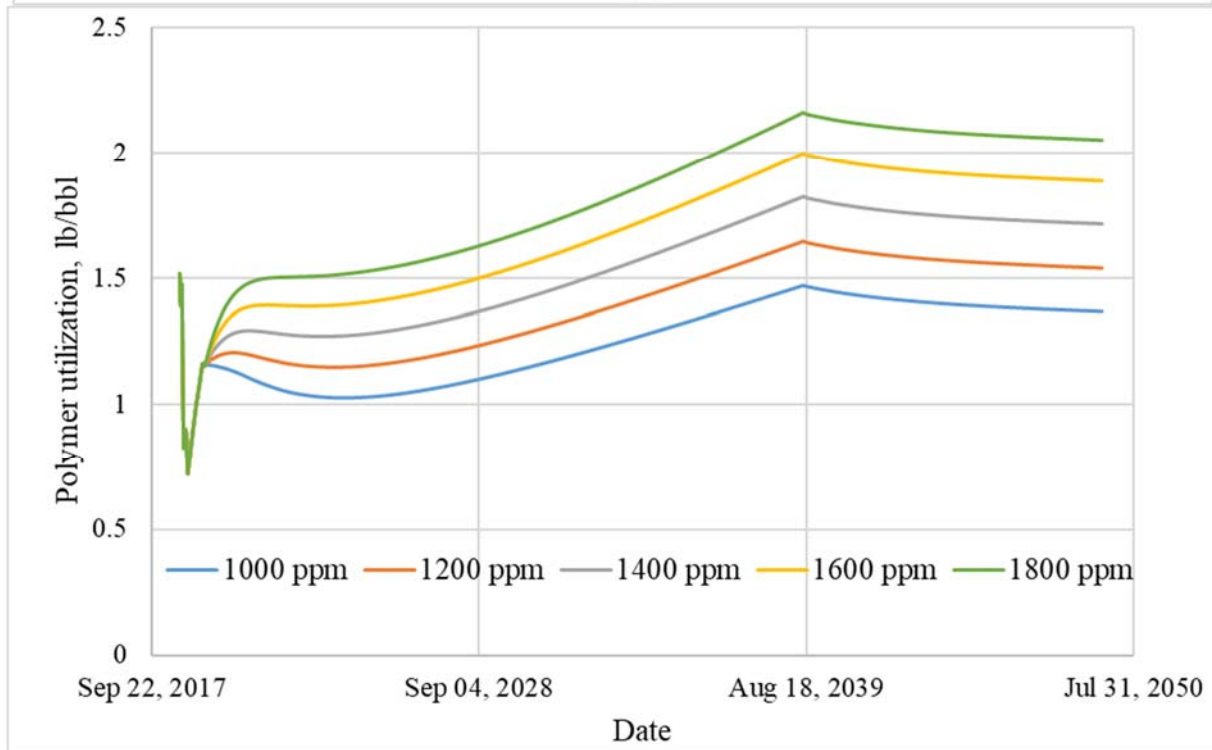
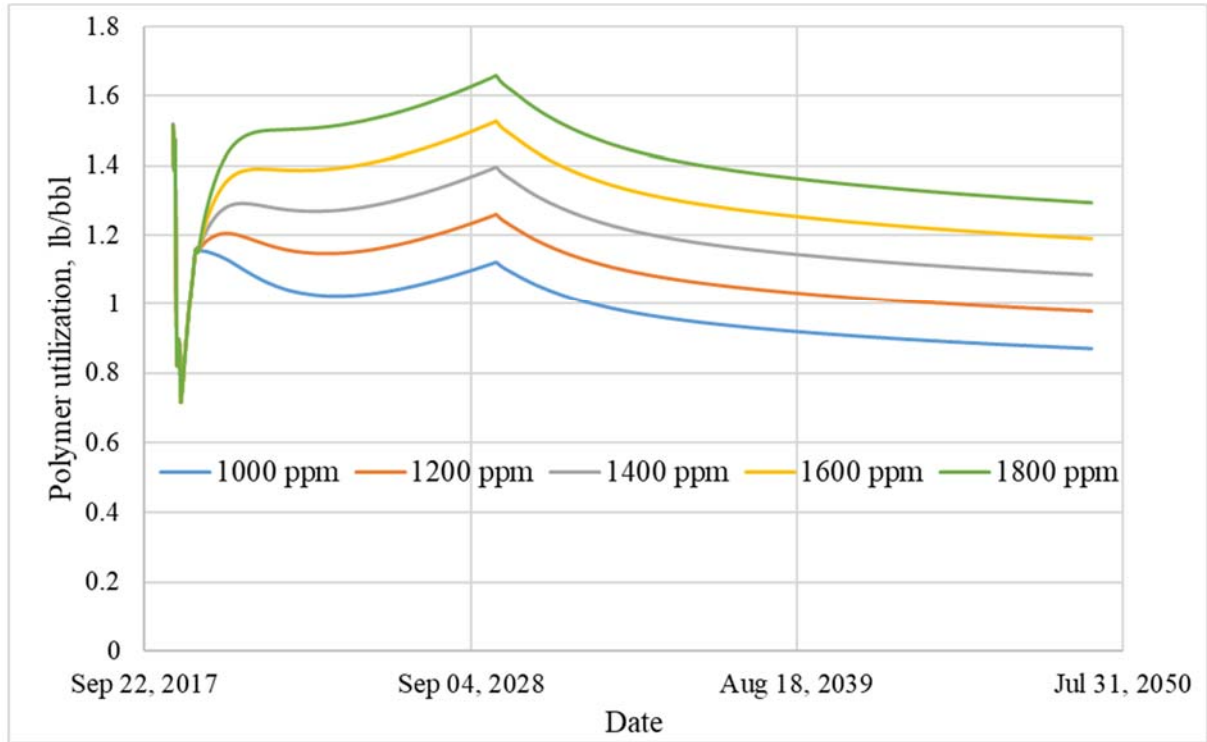
The oil recovery factors and polymer utilizations of the three cases with different polymer injection concentrations are listed in **Table 4.2**. The relationships of oil recovery factor and polymer utilization with polymer concentration in 2049 are shown in **Figure 4.11**. As can be seen, for each case study, the oil recovery factor increases with the increase of polymer concentration, and the polymer utilization increases linearly with the increase of polymer concentration. The relationships of polymer utilizations at different polymer concentrations with time are illustrated in **Figure 4.12**. It can be found that, during the prediction period, the higher the polymer concentration, the greater the polymer utilization. And the polymer utilization decreases gradually after stopping injection of polymer.

**Table 4.2: Comparison of different polymer injection concentrations**

Polymer concentration (ppm)		1000	1200	1400	1600	1800
Case #1	Oil recovery factor (%)	27.2	28.0	28.7	29.3	29.8
	Polymer utilization (lb/bbl)	0.83	0.96	1.08	1.20	1.31
Case #2	Oil recovery factor (%)	30.8	32.1	33.0	33.8	34.6
	Polymer utilization (lb/bbl)	1.39	1.58	1.77	1.96	2.14
Case #3	Oil recovery factor (%)	32.7	34.2	35.4	36.4	37.4
	Polymer utilization (lb/bbl)	1.92	2.17	2.42	2.66	2.89



**Figure 4.11: The relationships of (a) oil recovery factor and (b) polymer utilization with polymer concentration**



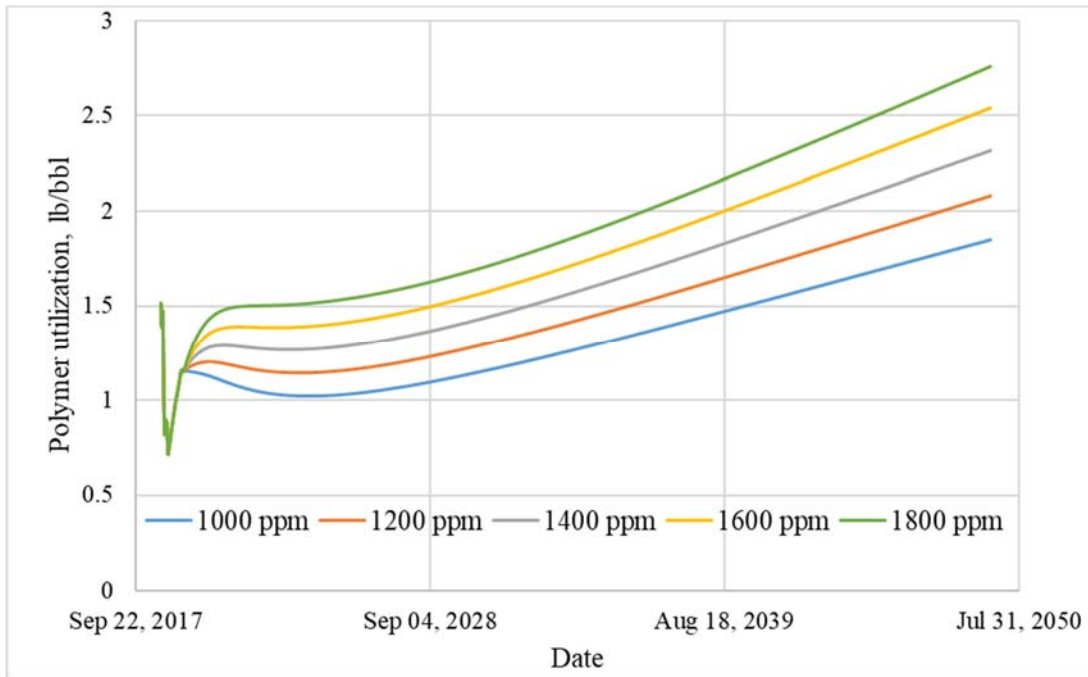


**Figure 4.12: The relationships of polymer utilizations at different polymer injection concentrations with time for Cases 1, 2 and 3 respectively, and shown in that order.**

**Polymer retention.** The following three case studies have been designed to investigate the effect of polymer retention on the oil recovery factor and polymer utilization. In each case, reservoir simulations with polymer retention ranging from 50  $\mu\text{g/g}$  to 300  $\mu\text{g/g}$  at intervals of 50  $\mu\text{g/g}$  have been conducted, and the polymer injection concentration is 1800 ppm in all the simulations.

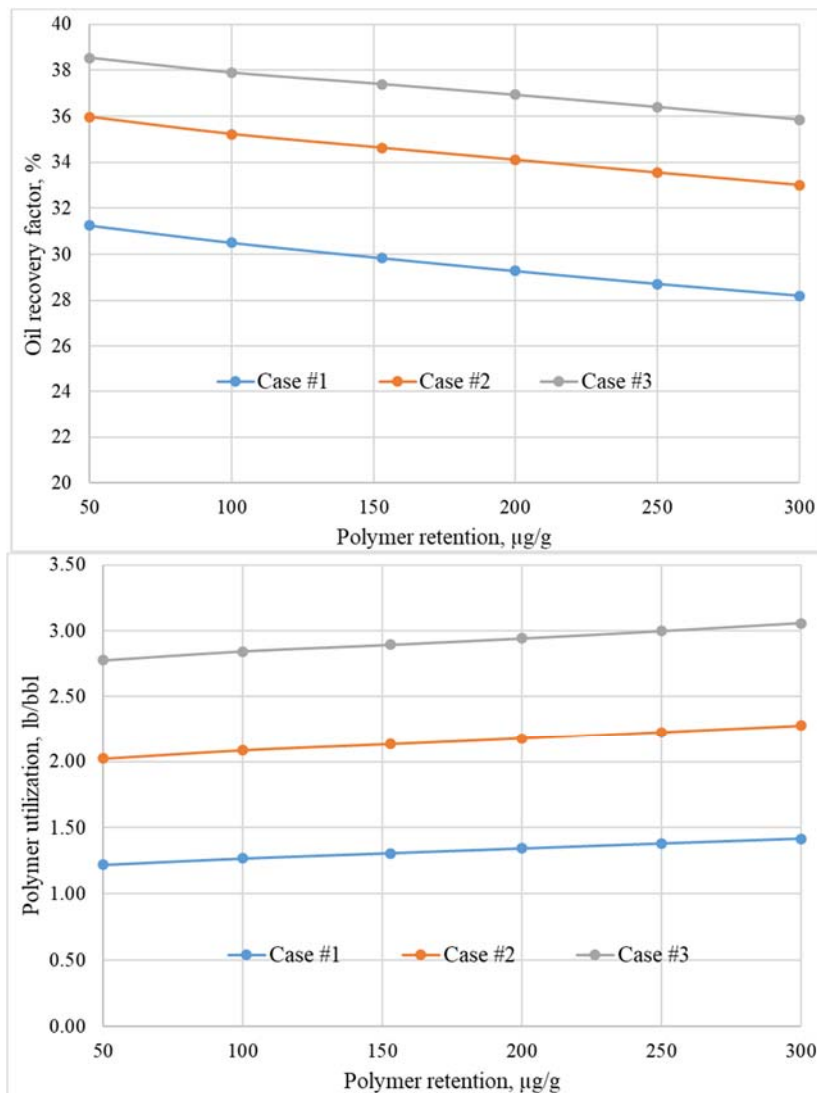
- Case #1: inject polymer for 10 years followed by 20 years of waterflooding
- Case #2: inject polymer for 20 years followed by 10 years of waterflooding
- Case #3: inject polymer for 30 years

The oil recovery factors and polymer utilizations of the three cases with different polymer retention are listed in **Table 4.3**. The relationships of oil recovery factor and polymer utilization with polymer retention in 2049 are shown in **Figure 4.13**. As can be seen, for each case study, the oil recovery factor decreases linearly with the increase of polymer retention, and the polymer utilization increases linearly with the increase of polymer retention. The relationships of polymer utilizations at different polymer retention with time are illustrated in **Figure 4.14**. It can be seen that during the prediction period, the higher the polymer retention, the larger the polymer utilization. The difference between polymer utilizations at various retention values is obvious at the early stage of prediction, but the difference diminishes steadily with time.

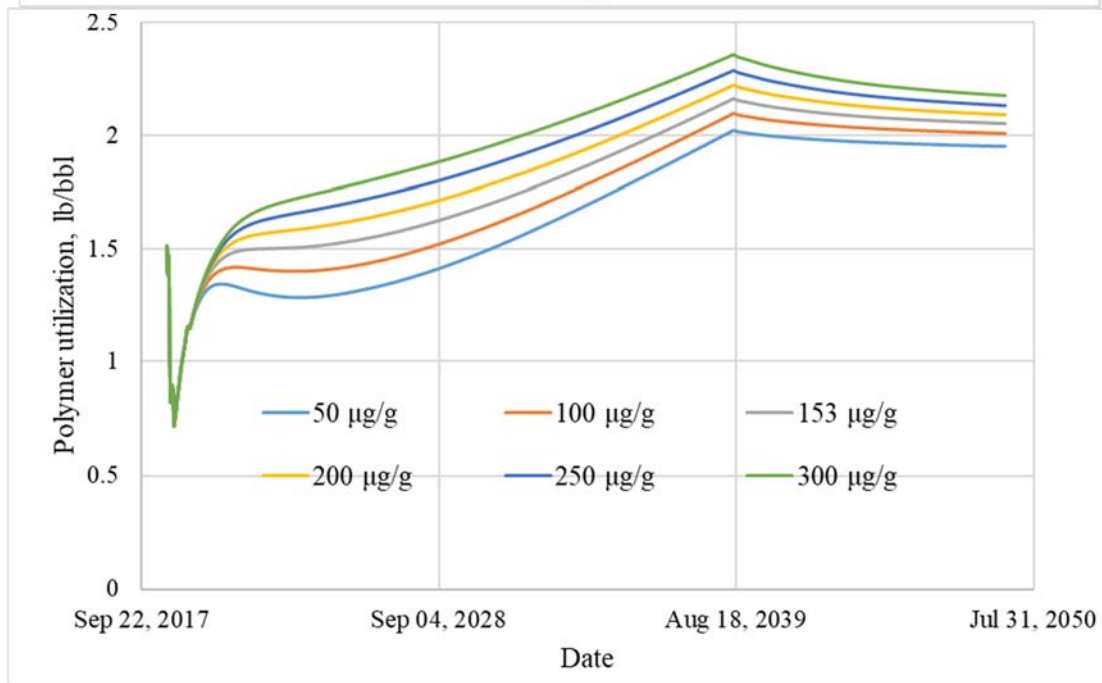
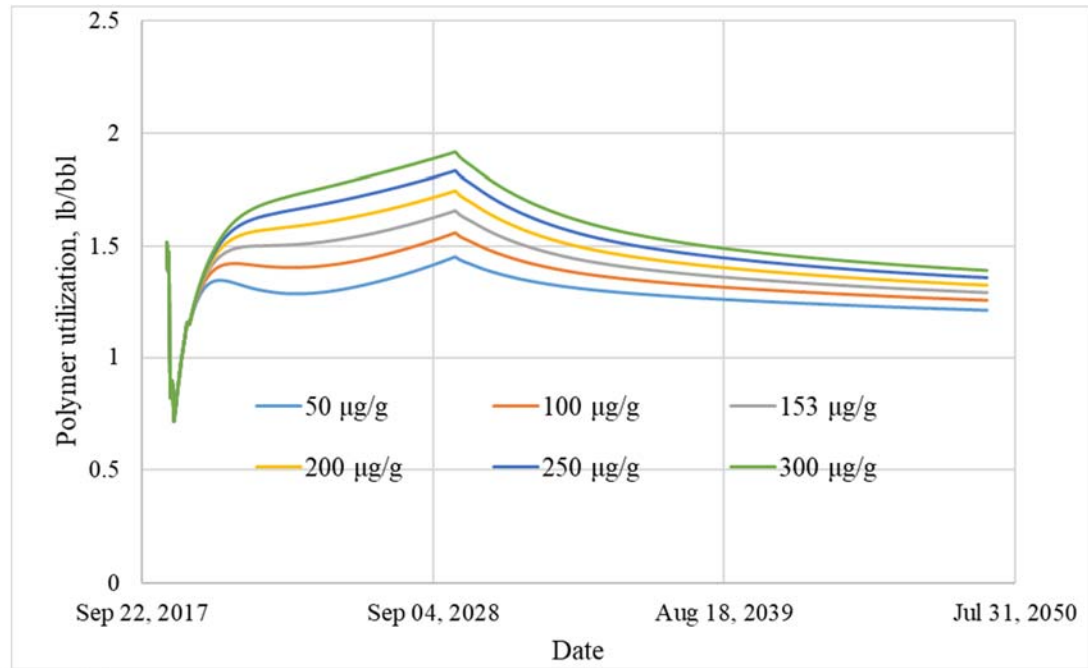
**Table 4.3: Comparison of different polymer retention**

Polymer retention ( $\mu\text{g/g}$ )	50	100	153	200	250	300
---------------------------------------	----	-----	-----	-----	-----	-----

Case #1	Oil recovery factor (%)	31.3	30.5	29.8	29.3	28.7	28.2
	Polymer utilization (lb/bbl)	1.22	1.27	1.31	1.35	1.38	1.42
Case #2	Oil recovery factor (%)	36.0	35.2	34.6	34.1	33.5	33.0
	Polymer utilization (lb/bbl)	2.02	2.09	2.14	2.18	2.23	2.28
Case #3	Oil recovery factor (%)	38.5	37.9	37.4	36.9	36.4	35.9
	Polymer utilization (lb/bbl)	2.78	2.84	2.89	2.94	3.00	3.06



**Figure 4.13: The relationships of (a) oil recovery factor and (b) polymer utilization with polymer retention**





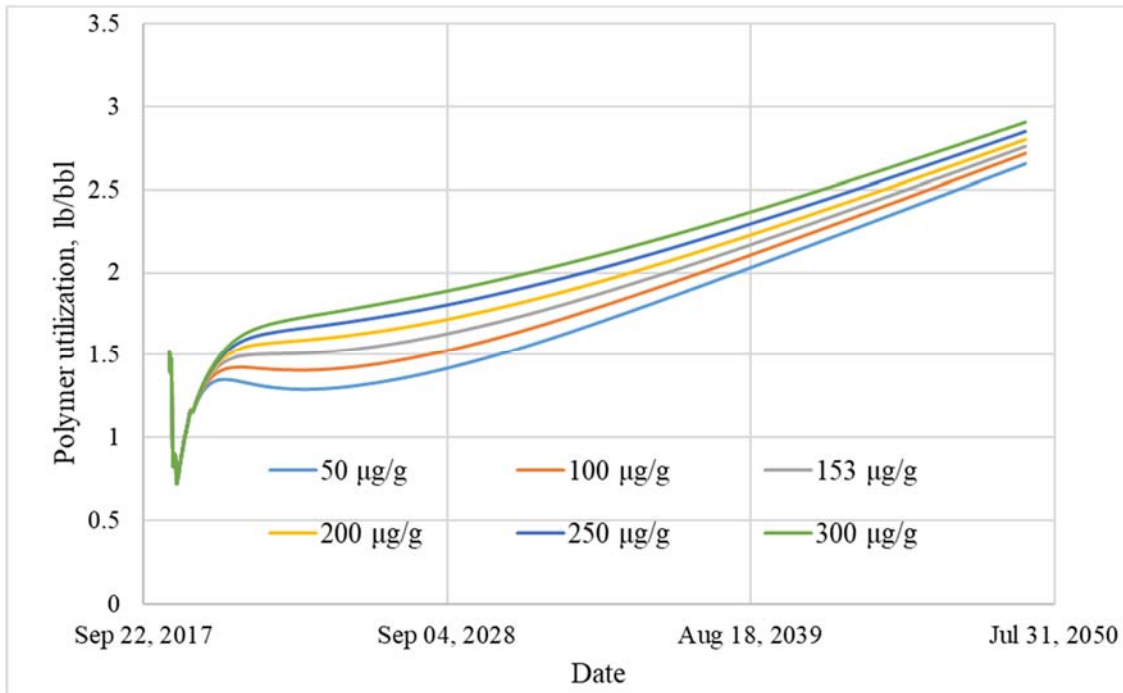


**Figure 4.14: The relationships of polymer utilizations at different polymer retention with time for Cases 1, 2 and 3 respectively, and showed in that order.**

UAF’s future work will focus on history matching the water cut of polymer flooding using the extended production data. The relative permeability will be tuned to improve the history matching results of polymer flooding.

**Both UND and UAF activities are ongoing.**

- Task 5.0 - Implementation of Polymer Flood Field Pilot in Milne Point

Polymer injection into the two horizontal injectors (J-23A and J-24A) started on August 28<sup>th</sup>, 2018. There were two shutdowns in 2018 due to necessary equipment modifications and repairs, one in September and another in November. Then from mid-June through late-August 2019, polymer injection was interrupted due to polymer hydration issues. After 2 months of hard work by the Milne Point team assisted by SNF staff, the polymer hydration problem has been resolved and normal polymer injection has resumed since August 29<sup>th</sup>, 2019. Ultimately as a team we have learned a lot about polymer, polymer facilities and onsite QC required.

Detailed pilot activities are summarized below:

**Polymer Injection Status Timeline**

- 8/23/2018 polymer skid (PSU) online with water
- 8/28 polymer injection starts

*University of Alaska Fairbanks*

- 9/25 PSU shutdown
  - More HC gas found in SW
  - Need to modify and reclassify PSU to Class I Div II
- 10/15 Resume polymer injection
  - Ran downhole gauge
  - Performed post polymer step rate test
- 11/9 J-23A shut in for PFO while waiting for pump repair
- 11/16 J-24A shut in for PFO while repairing augur
- 12/3 Resume polymer injection
- 1/17/19 Attempted Injection Profile Log (IPROF) for J-23A, but tool covered by black goo
- 3/28/19 Pumped 8 kg Tracer T-801 into J-24A
- 3/29/19 Pumped 8 kg Tracer T-803 into J-23A
- 3/29/19 Coil tubing clean out J-23A, repeat IPROF.
  - Tool did not go all the way down, got partial results
  - ICD#1=5.6%, ICD#2=27.8%, ICD#3=40.7%
  - 74% polymer injecting into first segment (heel-2766')
- 6/7/19-6/14/19 J-28 false polymer positive by flocculation test
- 6/19/19 shut down PSU due to polymer hydration issues
- 6/22/19 PSU back online, J-23A rate decreased by 400 bpd, J-24A by 200 bpd
- 7/6/19 J-23A PFO test, no damage identified
- 7/8/19 Treat injectors with hot KCL water to remove damage – not effective
- 7/15/19 J-23A and J-24A step rate test
- 7/18-8/28/19 straight water or low concentration polymer while diagnosing
- 8/29/19 polymer hydration problems resolved, resume polymer injection
- 9/2/19 J-23A and J-24A step rate test
- 12/2/19 shut down PSU to repair augur and replace plungers
- 12/6/19 back on line with new plungers
- 1/9/20 install automated filter ratio test

### **Polymer Injection Performance**

Polymer injection progressed smoothly in this quarter. The only shutdown happened December 2-6, to repair the PSU augur and install pump plungers with higher pressure ratings. As of end of February 2020, total cumulative polymer injected was 604,000 lbs into the two injectors and the total amount of polymer solution injected was 1.22 million barrels which was approximately 7.6% of the total pore volume in the 2 flood patterns. During the reporting period, injected polymer concentration was between 1700 and 1740 ppm to achieve a target viscosity of 40 cP as shown in **Figure 5.1**.

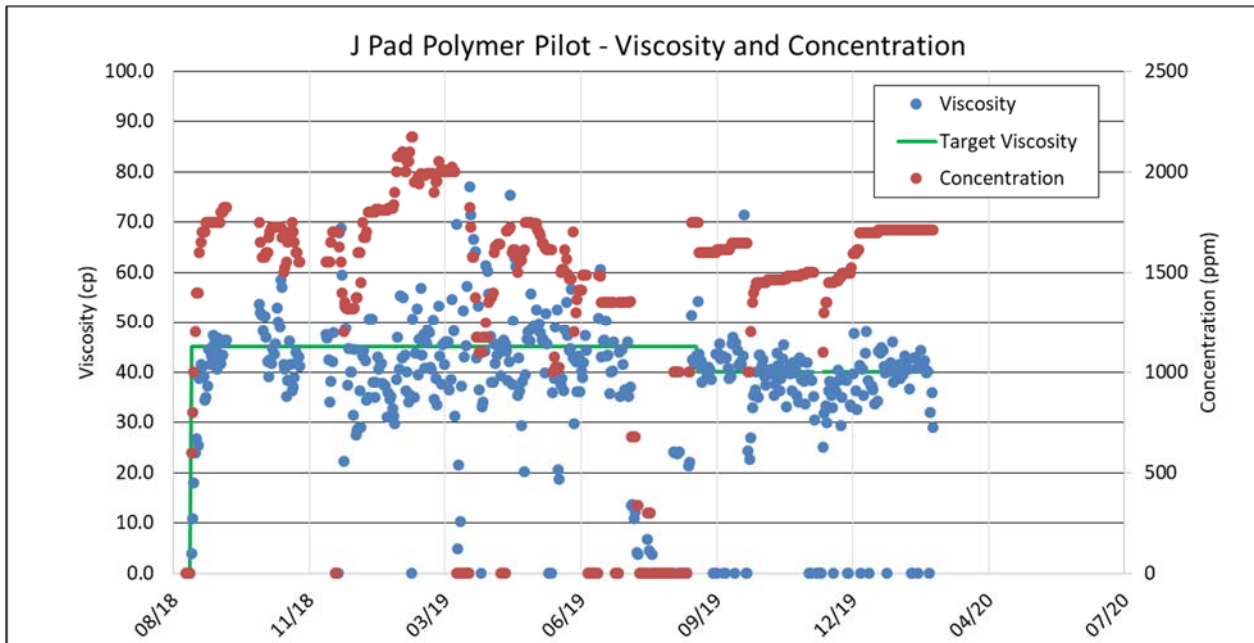


**Figure 5.1: Polymer concentration and viscosity vs. time.**

Polymer solution filter ratio is defined as the ratio of the time needed to filtrate from 180 cc to 200 cc to the time needed to filtrate from 60 cc to 80 cc using a specified filtration device. If this ratio is less than 1.2, the polymer solution is considered good enough to flow through the reservoir rocks without blocking. Therefore, filter ratio is monitored daily for polymer solution quality control. Previously, the operators had to measure and record this parameter manually every day which was time consuming and prone to human errors. To improve this process, filter ratio test has been automated at the project site by installing an electronic scale connected to a computer with automatic data acquisition and processing. This has eliminated human errors during the test and significantly reduced man hours needed for the daily filter ratio tests.

**Figure 5.2** presents daily injection rate and pressure for J-23A. The injection rate stabilized at 1350 barrels per day (bpd) while the wellhead pressure stabilized around 1000 psi for the reporting period. To date 417,000 pounds of polymer have been injected into J-23A and the cumulative volume of polymer

solution injected is 840,000 barrels representing 8.4% of the total pore volume of the flood pattern.

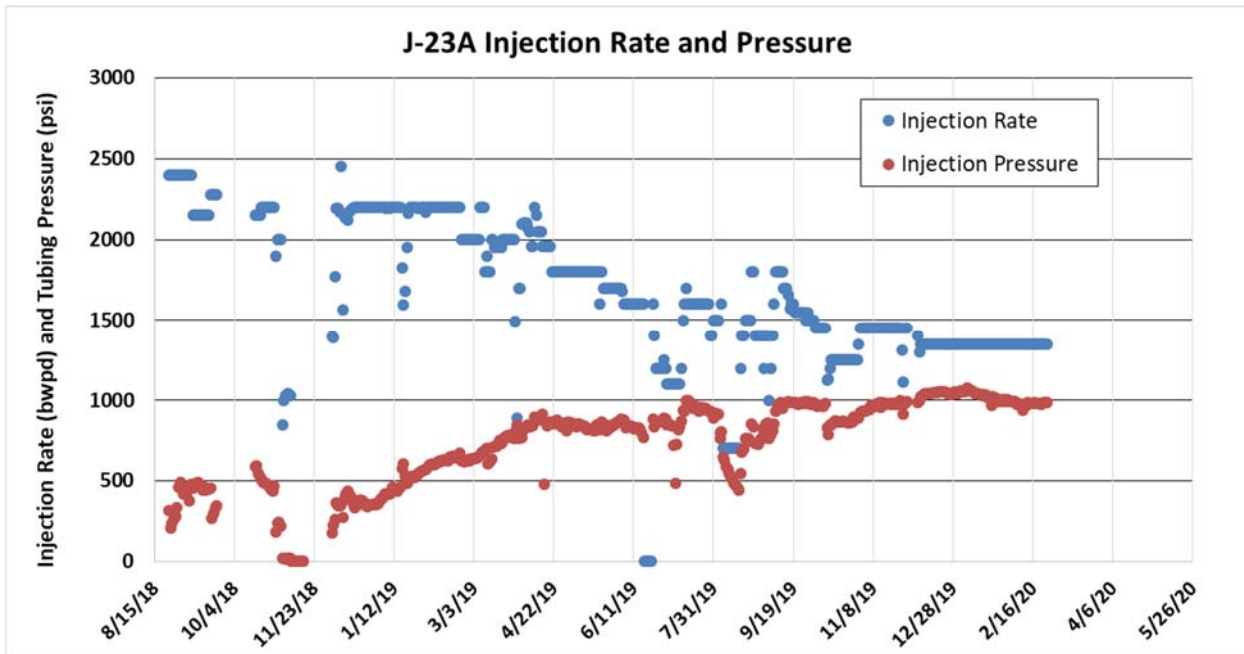


Figure 5.2: J-23A injection rate and pressure.

Figure 5.3 presents daily injection rate and pressure for J-24A. The injection rate stabilized at 700 bpd at a wellhead pressure of approximately 1000 psi, although higher injection rate was achieved at higher pressure for a short period of time prior to stabilization. To date 187,000 pounds of polymer have been injected into J-24A and the cumulative volume of polymer solution injected is 384,000 barrels representing 6% of the total pore volume of the flood pattern.

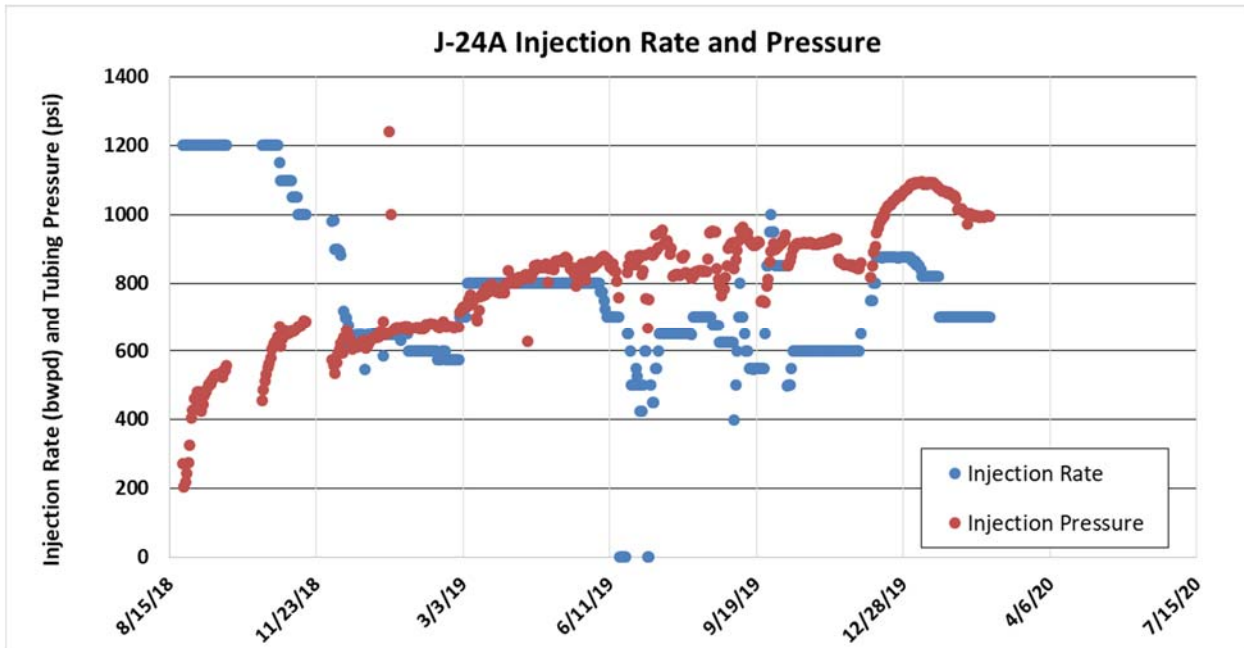


Figure 5.3: J-24A injection rate and pressure.

Figure 5.4 is a Hall Plot for both J-23A and J-24A, which plots the integration of the differential pressure between the injector and the reservoir versus cumulative water injection. The data would form a straight line if the injectivity stays constant over time, curve up if the injectivity decreases and vice versa. After a decrease in the injectivity earlier, current Hall plot diagnostic indicates that the injectivity of both J-23A and J-24A have stabilized.

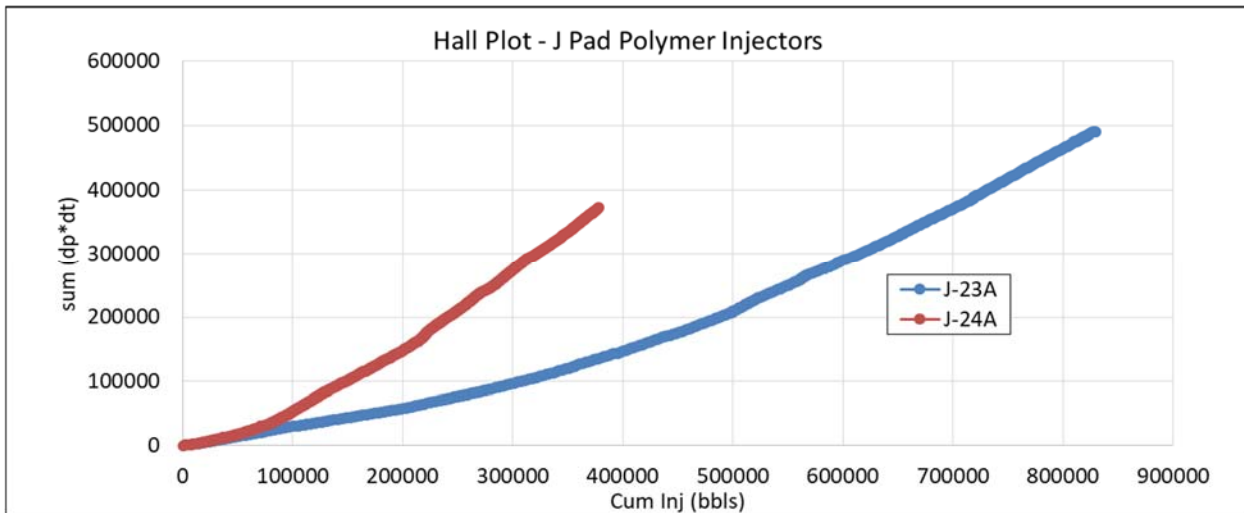


Figure 5.4: Hall plot for J-23A and J-24A.

### Voidage Replacement Ratio

Figure 5.5 presents the instantaneous (blue circles) and cumulative (red line) voidage replacement ratios (VRR) of the project patterns. VRR is defined as the ratio of the injection volume to production volume at reservoir conditions. During the first 4 months of polymer injection from August to December 2018, instantaneous  $VRR < 1$  meaning that the polymer injection volume was less than the production voidage. However, since January 2019, instantaneous  $VRR > 1$  meaning that the polymer injection volume was greater than the production voidage due to the decline in total liquid (oil + water) production rate.

Cumulative VRR of the project pattern was 0.85 at the beginning of polymer injection and currently at ~ 0.88 meaning that we have injected more polymer solution than the production voidage during the last 18 months. Note that this is the delta VRR of 0.03, which is relative over WF prior to polymer startup. In order to increase oil production rate, the current plan is to continue to over inject to catch up with the voidage replacement to elevate the reservoir pressure to its initial value.

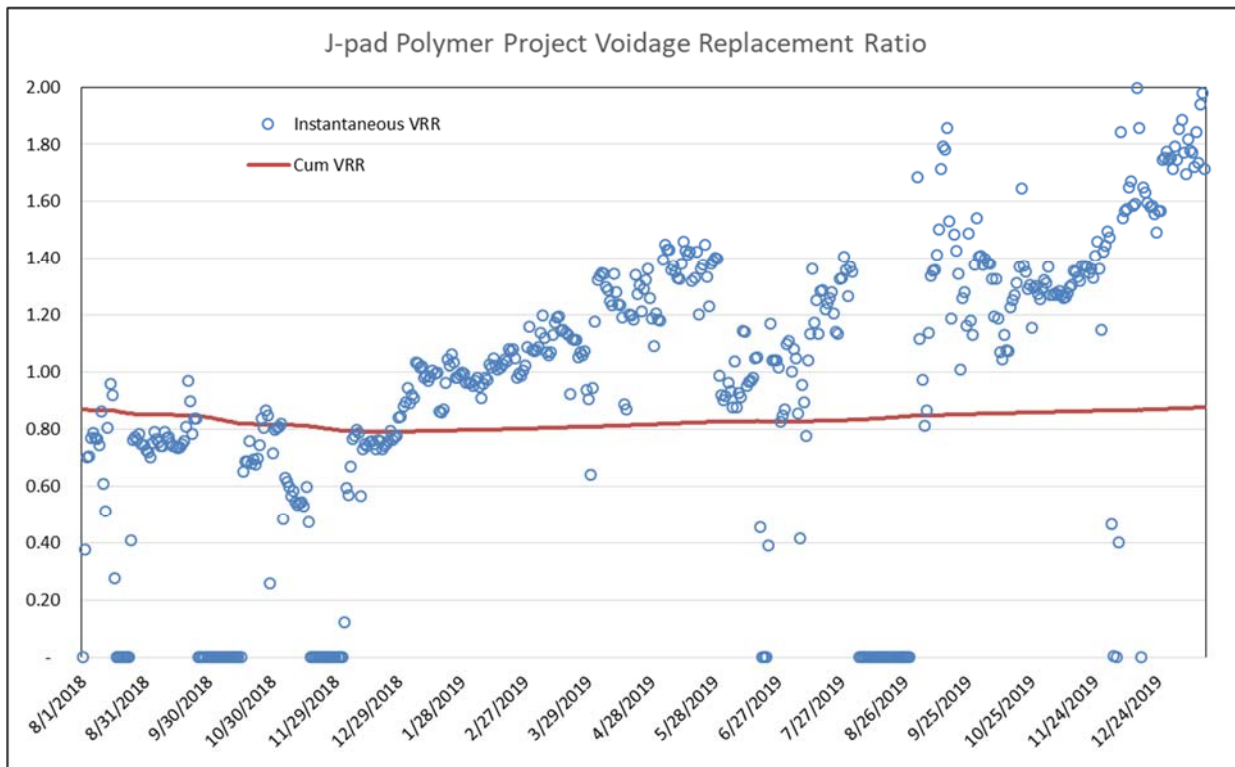
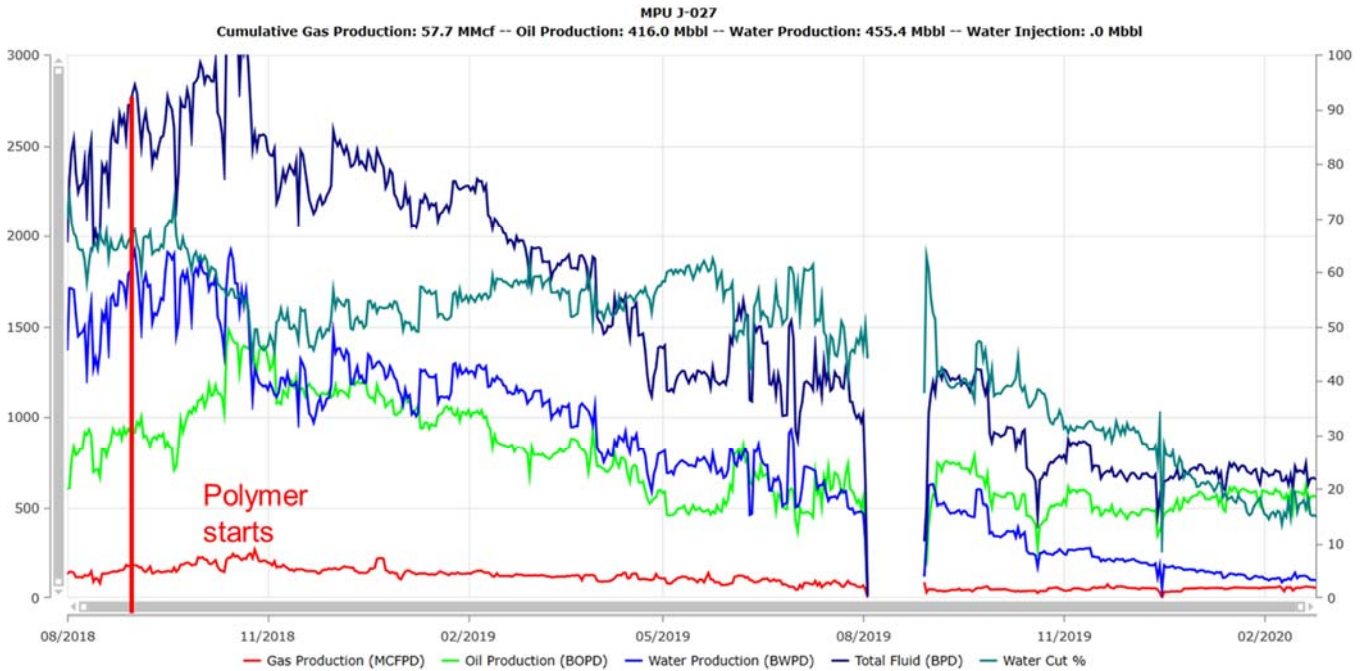


Figure 5.5: Voidage replacement ratio.

**Production Performance**

**Figure 5.6** depicts the production performance of producer J-27 which is supported by both injectors, J-23A from the south side and J-24A from the North. Since the start of polymer injection, water-cut has decreased from 67% to 15% indicating that the injected polymer is helping improve sweep efficiency. The total fluid rate has stabilized and the oil rate is increasing as the water cut decreases.



**Figure 5.6: J-27 production performance.**

**Figure 5.7** depicts the production performance of producer J-28 which is supported only by J-23A from the north since the south side is adjacent to a sealing fault. Water-cut has also decreased from 70% to less than 15% since the start of polymer injection. The fast response in water-cut is most likely caused by polymer blocking off the high permeability channels which were probably responsible for the fast increase in water-cut before polymer injection started. Oil rate increased to ~700 bpd in late 2019 then declined to ~500 bpd which was caused by slowing down the ESP in mid-December. Had polymer injection never started, the oil rate would have been much lower than 500 bpd since the expected water-cut would increase sharply when water-flooding a heavy oil reservoir.

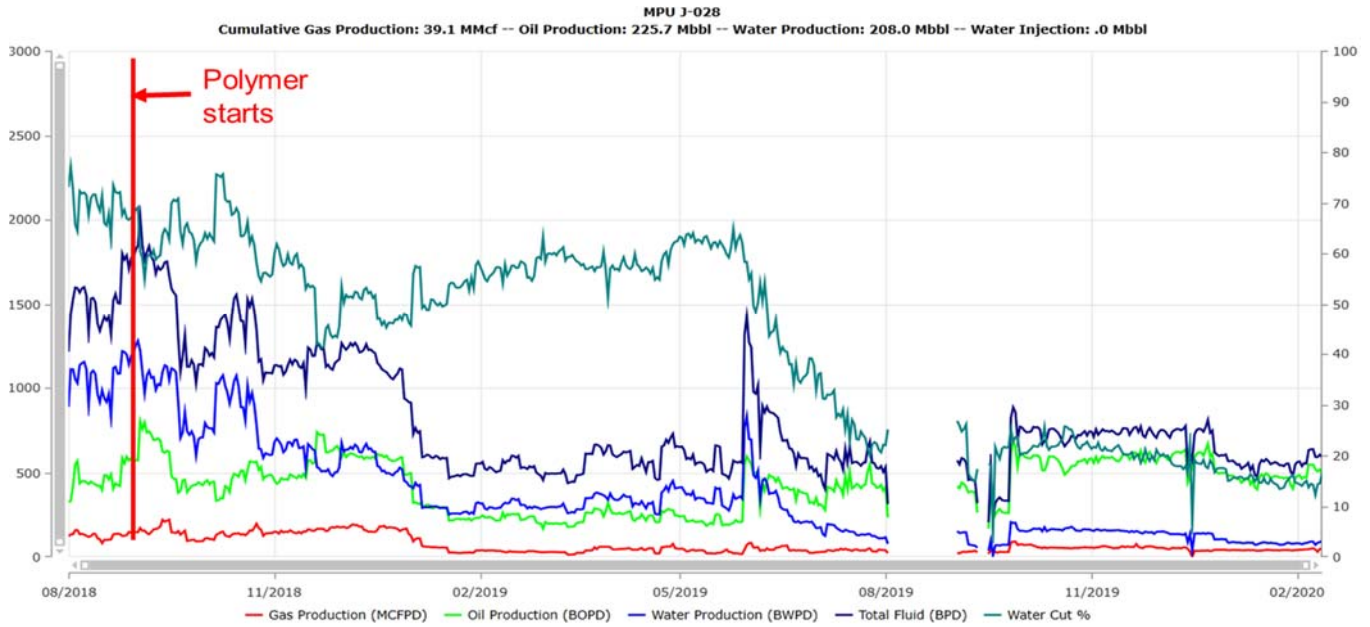


**Figure 5.7: J-28 production performance.**

**Estimated Incremental Oil Rate**

A reservoir simulation model has been developed and history-matched to predict the incremental oil benefit from polymer flood versus waterflood. **Figure 5.8** shows the total predicted oil rate under waterflood (light blue line) and polymer flood (red line) processes from the 2 project wells. The difference between the two represents EOR benefit which is estimated to be approximately 600 bpd at the present time.



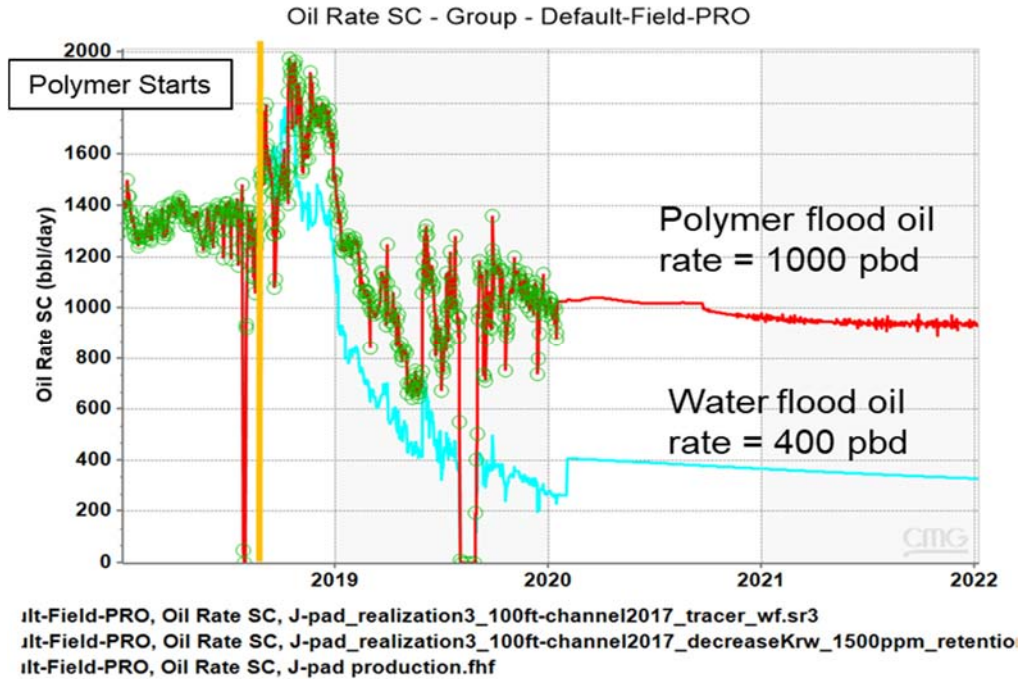


**Figure 5.8: Predicted total oil rate under waterflood and polymer flood processes.**

### Pre-Polymer Tracer Test

Two different tracers named T-140C and T-140A were pumped into injectors J-23A and J-24A respectively on August 3, 2018, 25 days prior to the start of polymer injection. Produced water samples are taken weekly from producers J-27 and J-28 and analyzed to detect tracer concentration. The latest produced tracer concentration is shown in **Figure 5.9**. The time of appearance (breakthrough) and the magnitude of the tracer concentration in the two producers are indicators of injector-producer communication and the volumetric sweep efficiency in the flood pattern.

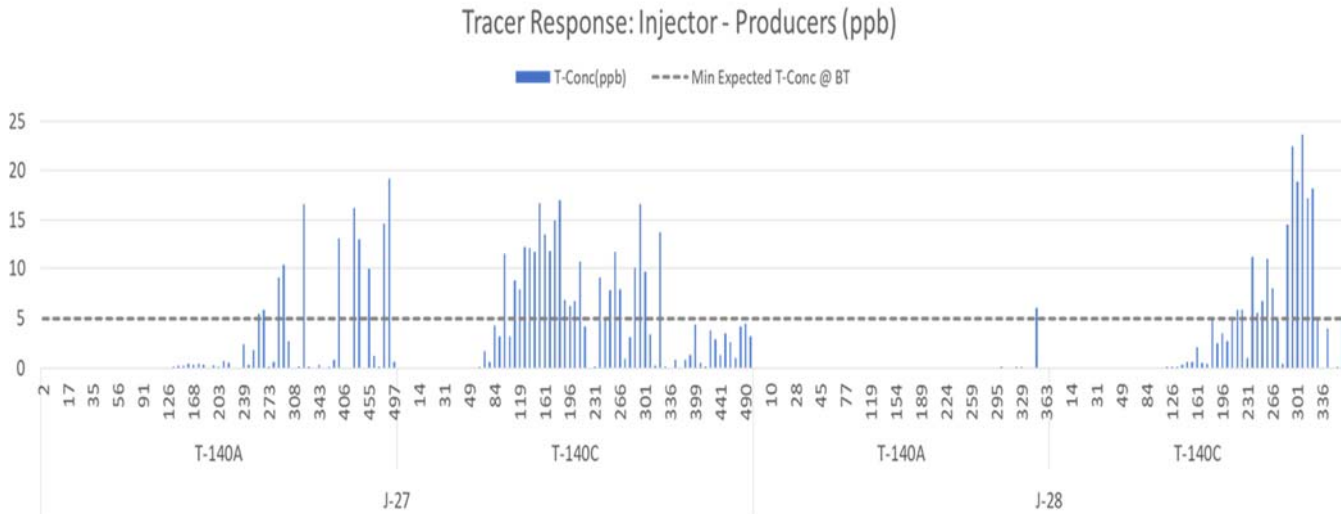


**Figure 5.9: Tracer concentration in produced water.**

Tracer T-140C from J-23A first appeared in producer J-27 after 70 days of injection indicating strong communication between the well pair. However, the fast breakthrough timing also indicates that the sweep efficiency of water displacing oil is low. Assuming no more tracer will be produced from now on, the volumetric sweep efficiency from waterflood was estimated to be less than 3% in the particular reservoir sector between injector J-23A and producer J-27.

Tracer T-140C from J-23A first appeared in producer J-28 after 140 days of injection indicating that communication between the well pair is slower which also means that the injected water was sweeping more oil before being produced out of the reservoir. Estimated volumetric sweep efficiency from waterflood was approximately 9%, assuming no more tracer will be produced from now on.

Tracer T-140A from J-24A also first appeared in producer J-27 after 140 days of injection. The communication in this well pair is slower than from J-23A to J-27. Estimated volumetric sweep efficiency from waterflood was also less than 3%, assuming no more tracer will be produced from now on. It is important to note that the low sweep efficiency by waterflood creates a great opportunity for polymer flood.

**Post-Polymer Tracer Test**

Seven months after polymer injection started, two more tracers, T-803 and T-801, were pumped into injectors J-23A and J-24A respectively to monitor polymer breakthrough timing and estimate sweep efficiency for polymer displacing oil. To date, 12 months after these tracers were injected, no significant tracer concentration has yet been detected from the two producers indicating that all polymer injected so far is still sweeping oil in the reservoir. We plan to continue sampling the produced water and testing for tracer and polymer contents to assess the sweep efficiency of polymer displacing oil. However, in the last couple of months, it has become increasingly difficult to collect produced water samples, whether from the well head or from the test separator, due to the low water cuts and difficulties in separating water from

the produced fluid.

### Monitoring Polymer Breakthrough

Since the start of polymer injection, produced water samples have been collected weekly when possible and analyzed onsite using the clay flocculation test, as well as in the laboratory via nitrogen-fluorescence water composition analyses to detect the presence of produced polymer in the production stream. As of the end of February 2020, 18 months after the start of polymer injection, no polymer has been confirmed in the production stream.

### Main Observations from Field Pilot to Date

1. Adequate polymer injectivity can be achieved with horizontal wells in the Schrader Bluff N-sand reservoir. However, polymer solution quality control is critical to ensure polymer propagation through the reservoir.
2. Water cut has decreased from ~70% to approximately 15% in the project wells since the start of polymer injection. Estimated EOR benefit is approximately 600 bopd at the present time.
3. Eighteen months after the start of polymer injection, no polymer production has been confirmed from the producers yet, compared with waterflood breakthrough timing of 3 months. Furthermore, no post polymer tracer production has been detected 12 months after tracer injection.
4. The drastic decrease in water cut and delayed polymer breakthrough both indicate significant improvement in oil sweep by the injected polymer.
5. More polymer injection is needed to calibrate the reservoir simulation models and accurately quantify the EOR benefit.

### Activity is ongoing.

- Task 6.0 -Analysis of Effective Ways to Treat Produced Water that Contains Polymer

### Experimental details

In the reporting quarter, oil-water separation studies have continued for synthetic emulsions with 75% water cut (WC). The emulsion was prepared by stirring crude oil and synthetic brine at the speed of 15,000 rpm for 3 min. This high shearing intensity is selected to mimic the formation of severe reverse emulsion induced by the jetting pump. The detailed bottle test procedures have been described in previous report, thus they are not repeated here. Various synthetic brines were prepared by increasing the salinity of LSW while keeping the relative ratio of each component constant. The formulation of synthetic brine is listed in **Table 6.1**. The KCl/NaCl mother solution as demulsifier was prepared at the concentration of 200,000 ppm. The volume of KCl/NaCl mother solution is added based on the total volume of the emulsion.

**Table 6.1: Compositions of synthetic brine**

	NaCl (ppm)	KCl (ppm)	CaCl <sub>2</sub> (ppm)	MgCl <sub>2</sub> (ppm)	TDS (ppm)
Sample 1 (LSW)	2,173	8	269	34	2,484
Sample 2	6,998	26	866	110	8,000

Sample 3	10,498	39	1,300	164	12,000
Sample 4	13,997	52	1,733	219	16,000
Sample 5	17,496	64	2,166	274	20,000

*BS&W measurement.* After the water separation reading at 24 hours was recorded, the resolved oil in the graduated cylinder was taken to measure the basic sediments and water (BS&W). A small amount of oil (about 6 mL) was withdrawn with the tip of the syringe and was transferred into the centrifuge tube. Subsequently, an equal volume of an aromatic solvent (i.e. xylene) was added into the centrifuge tube. The tubes were centrifuged at high speed for 10 min after preheated for 30 min. The percent of BS&W was recorded after the centrifugation.

**Results and Discussion**

*The effect of salinity on separation behaviors of synthetic emulsions.* Oil-water separation behavior is characterized by BS&W and oil content in the separated water (Oil in Water, OIW), respectively. **Figure 6.1** shows the effect of salinity on oil-water separation for synthetic emulsion at 75% WC. As seen from **Figure 6.1**, the BS&W remarkably decreased from 12.3% to 7% as the salinity of the synthetic brine increased from 2,484 ppm to 20,000 ppm; meanwhile, the OIW immediately decreased from 730 ppm to less than 50 ppm as the salinity of produced water increased to 8,000 ppm and the OIW was close to 0 when the total salinity was above 8,000 ppm. The decrease of both BS&W and OIW indicates that the higher salinity results in less stable emulsion. However, the degree of decrease in OIW was much more significant than that in BS&W, indicating the great potential of inorganic salt as water clarifier.

*Demulsification of emulsion without polymer.* The emulsion was prepared using crude oil from the wellhead of J28 producer and LSW at the water cut of 75% as blank sample. The NaCl or KCl mother solution was added to the prepared emulsion to investigate their capability to demulsify the prepared emulsion.

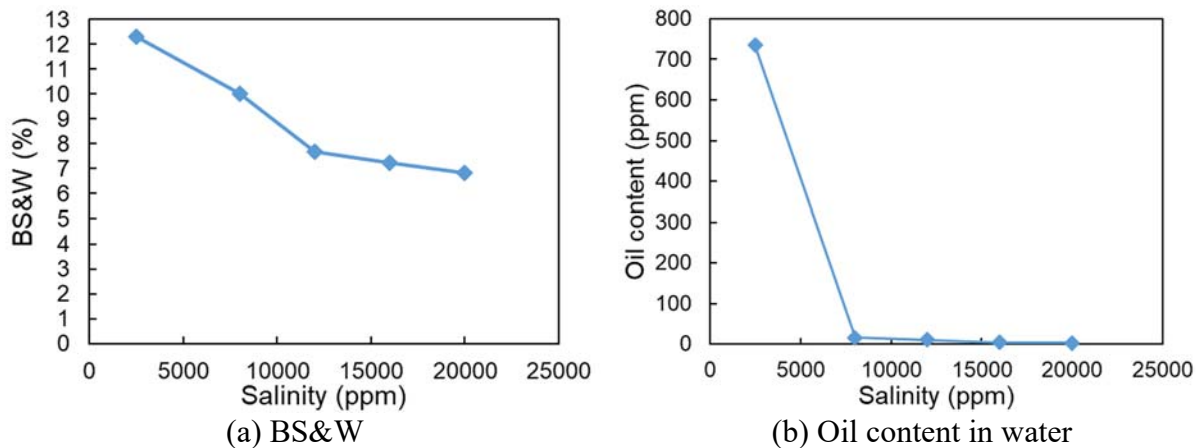


**Figure 6.1: The effect of salinity on oil-water separation**

*The performance of NaCl as demulsifier.* **Figure 6.2** shows the demulsification performance of NaCl for

emulsion at 75% WC. It is obviously seen that the addition of NaCl could effectively reduce the BS&W and the OIW. Comparing to the blank sample (0 ppm NaCl), the addition of 8,000 ppm, 12,000 ppm, 18,000 ppm, and 20,000 ppm NaCl reduced the BS&W by 2%, 6%, 9%, and 9.5%, respectively. The BS&W tended to keep constant with further increasing concentration of NaCl. As seen in **Figure 6.2(b)**, a steep decrease of OIW was observed after the addition of 8,000 ppm NaCl. And the OIW was close to 0 when the added concentration of NaCl was above 8,000 ppm. Thus, the predominant role of NaCl in reducing OIW makes NaCl a good candidate as water clarifier. To be noted, the addition of NaCl could also effectively eliminate the intermediate layer occurring in the blank sample (observed but not shown). However, the interface between the separated oil and water phase was not sharp (observed but not shown), which might bring a challenge for the application of NaCl in field.

*The performance of KCl as demulsifier.* The performance of KCl as demulsifier is also evaluated and compared with that of NaCl, and the results are shown in **Figure 6.3**. Similar to the performance of NaCl, the addition of KCl could also reduce the BS&W and OIW at the same time, accelerating the oil-water separation. However, KCl has a somewhat weaker ability to demulsify the emulsion than NaCl as indicated by the higher BS&W and OIW.

*Demulsification of emulsion containing polymer.* The polymer solution with the concentration of 800 ppm was prepared by dissolving polymer powder into the LSW under gentle mixing. The emulsion was prepared at the water cut of 75% by mixing crude oil and the prepared polymer solution. The KCl or compound emulsion breaker E12+E18 was added to the prepared emulsion to investigate their capability to demulsify the emulsion containing polymer.

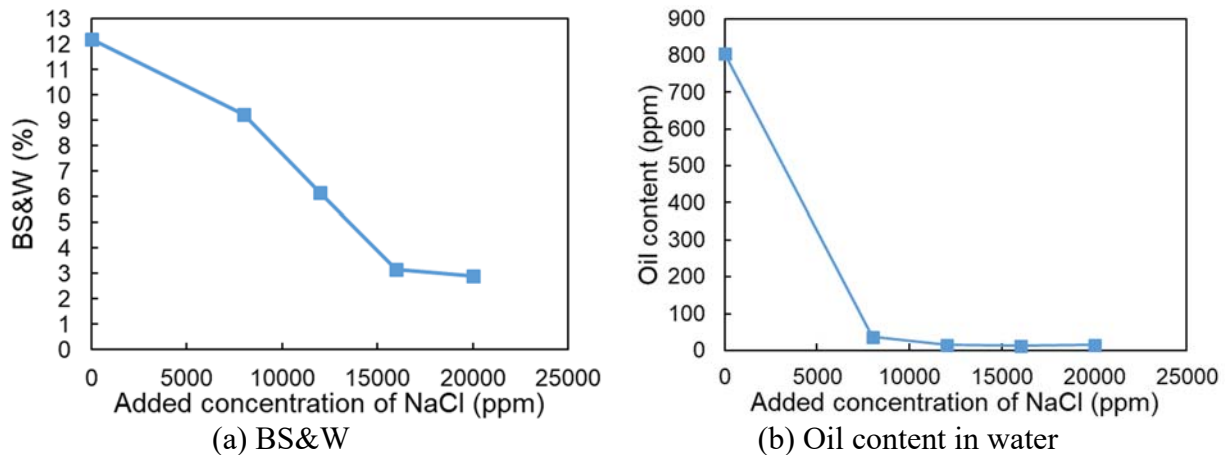


**Figure 6.2: The demulsification performance of NaCl for emulsion at 75% WC**

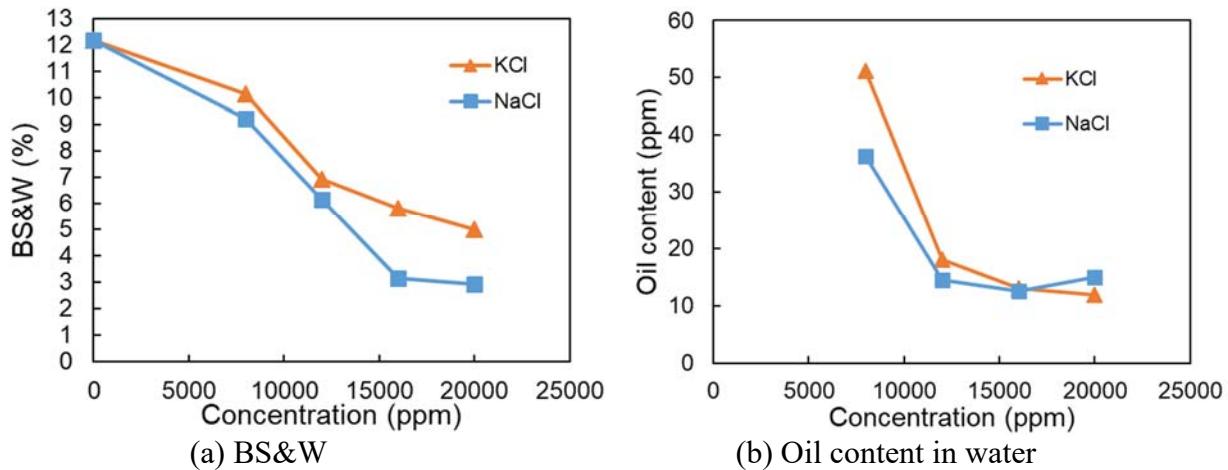
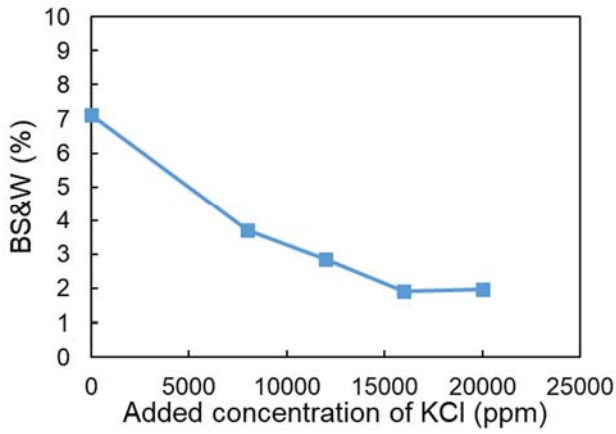
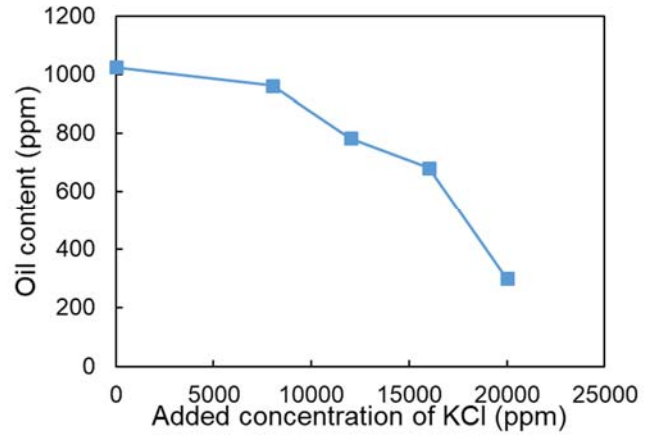


**Figure 6.3: The demulsification performance of KCl for emulsion at 75% WC**

The performance of KCl as demulsifier. **Figure 6.4** shows the demulsification performance of KCl for emulsion with 800 ppm polymer. As seen in **Figure 6.4**, the most significant BS&W reduction occurred when 8,000 ppm KCl was added. The BS&W progressively decreased with increasing concentration of KCl when the concentration of KCl was above 8,000 ppm. Meanwhile, the OIW gradually decreased with the increased concentration of KCl. **Figure 6.5** further illustrated the effect of polymer on the demulsification performance of KCl. Although the polymer tended to lower the BS&W at all tested concentrations of KCl, the presence of polymer hindered the removal of oil droplets from the separated water resulting in higher OIW than that in the case of no polymer. It is evidenced that more than 200 ppm oil remained in the separated polymer solution even when 20,000 ppm of KCl was added. Moreover, regardless of the added concentration of KCl, the interface between the separated oil and water phase is not neat, and the presence of intermediate layer was observed as shown in **Figure 6.6**. Although the intermediate layer became thinner as the concentration of KCl increased, the intermediate layer resulting from the presence of polymer could not be eliminated relying on the addition of KCl. Thus, the negative influence of polymer, i.e. the poor water quality and the presence of the intermediate layer, poses a great challenge to the clarification effect of KCl.

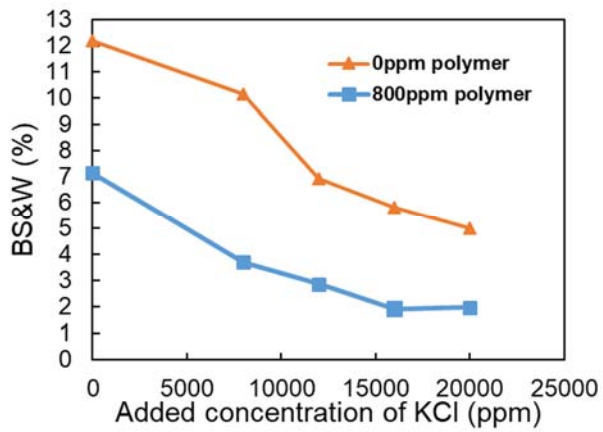


(a) BS&W

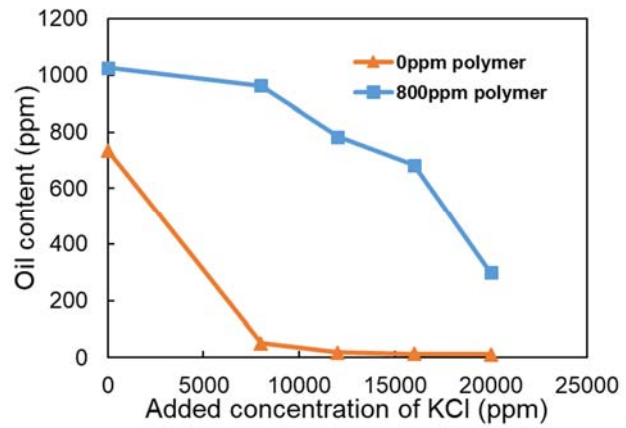


(b) Oil content in water

**Figure 6.4: The demulsification performance of KCl for emulsion with 800 ppm polymer at 75% WC**



(a) BS&W



(b) Oil content in water

**Figure 6.5: The effect of polymer on the demulsification performance of KCl**

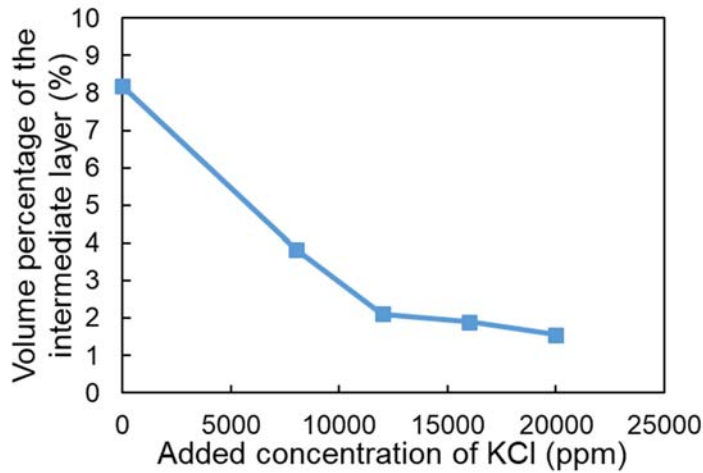


**Figure 6.6: The effect of KCl on the formation of the intermediate layer**

*The performance of the compound emulsion breaker.* As mentioned in the previous quarterly report, compound emulsion breaker E12+E18 (abbreviation for EBs E12085A and E18276A) is considered as the most effective emulsion breaker which has the best potential for deployment in the current ANS polymer flood pilot. The performance of E12+E18 for the emulsion prepared with high shearing intensity (15,000 rpm for 3 min) was also evaluated. **Figure 6.7** shows the demulsification performance of E12+E18 for emulsion containing 800 ppm polymer. The concentration of E12+E18 used in the study is 10 ppm, 50 ppm, and 100 ppm, respectively. As seen in **Figure 6.7**, the BS&W decreased linearly with the concentration of E12+E18, and the OIW declined considerably with increasing concentration of E12+E18. In particular, the intermediate layer was effectively eliminated, the interface between the separated oil and water phase became sharp, and the OIW was no more than 50 ppm when E12+E18 was added at the concentration of 100 ppm. Thus, the emulsion breaker E12+E18 is able to achieve much better performance than KCl even at very low concentration.

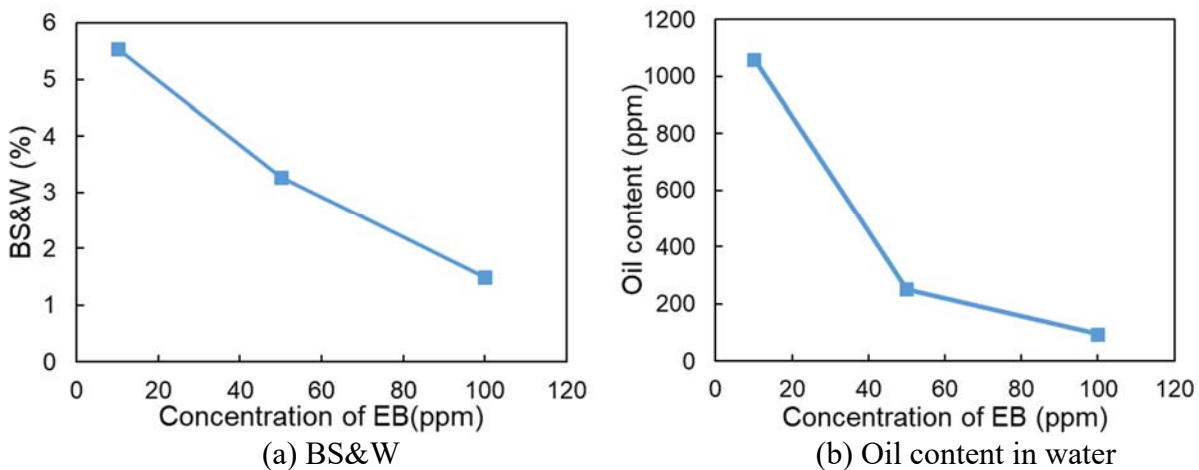


**Figure 6.7: The demulsification performance of E12+E18 for emulsion with 800 ppm polymer at 75% WC**



The performance of KCl combined with demulsifier. Due to the poor performance of KCl and the high cost of emulsion breaker, the performance of KCl combined with demulsifier was evaluated to develop a more cost-effective demulsification formula. The performance of E12+E18 combined with KCl was evaluated in comparison with the performance of KCl, as shown in **Figure 6.8**. As can be seen, the addition of KCl tended to lower the BS&W and the OIW at the same rate, and the most significant reduction occurred at 8,000 ppm KCl. Similarly, the performance of KCl was significantly improved with the addition of 50 ppm E12+E18 as indicated by the lower BS&W and OIW. Moreover, the intermediate layer was not noticed when KCl and E12+E18 coexisted in the emulsion system. Quantitatively, it can be concluded that the performance of 8,000 ppm KCl combined with 50 ppm E12+E18 was almost equivalent to the performance of 100 ppm E12+E18.

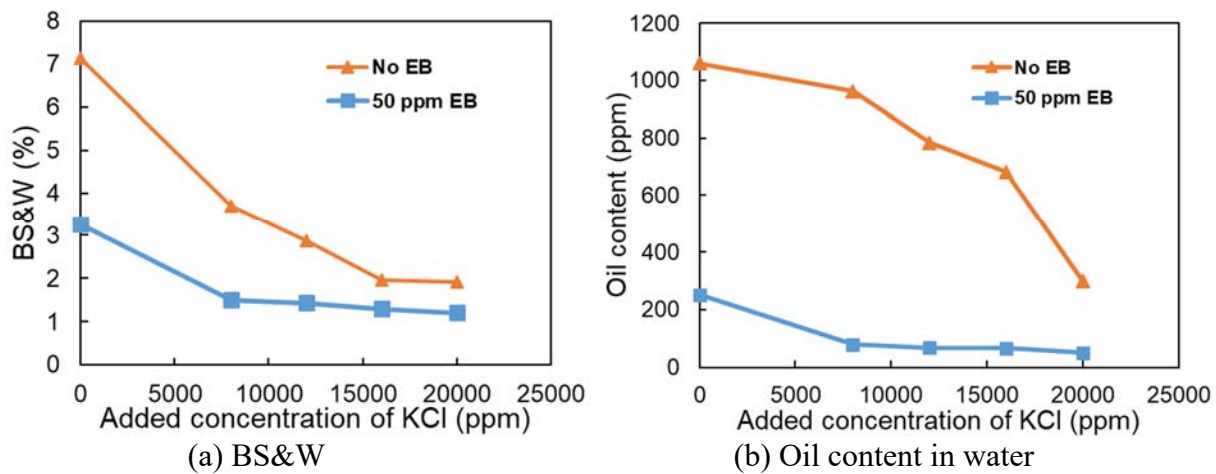


**Figure 6.8: The performance of KCl combined with demulsifier for emulsion with 800 ppm polymer at 75% WC**

### Future Work

This will focus on studying the effect of clay particles on the separation behavior of emulsions and the performance of emulsion breakers.

- Task 6.0a –Polymer Fouling of Heater Tubes

### Experimental Details

In the reporting quarter, fouling experiments were continued on copper tubes. Experiments were completed at 200°F tube skin temperature. For carbon steel tests were done at 165 °F skin temperatures. The polymer concentrations tested were – 80ppm and 600ppm. A repetition of two data points at 200°F were done for 400ppm and 160ppm polymer concentrations as the original results did not represent the expected trend. The procedure for experiments was same as reported in previous quarter. A new type of experiment – cloud point testing was done which basically helps predict the stability of polymer solutions at different temperatures; the detailed procedure is given below.

1. Two solutions were prepared in Milne Point formation brine composition – one with a polymer concentration of 800ppm and the other without polymer that is only brine (0ppm polymer).
2. The solutions were placed in multiple glass containers, sealed using Teflon tape and then these containers were placed in a preheated oven at 160°F and heated for 12 hours.
3. After 12 hours these containers were taken out and pictures were taken to see if any precipitation of polymer has occurred. The precipitation of polymer implies that the solution has reached its cloud point.
4. Then the temperature of oven was increased to 190°F and the containers were placed back inside the oven and heated again for 12 hours. This process was done in the temperature incremental steps shown in the **Table 6.2** below.

**Table 6.2: Experimental approach for cloud point testing**

Temperature (°F)	Heating Hours	Duration of Heating (hours)
160	(0-12)	12
190	(12-24)	12
220	(24-36)	12
240	(36-46)	10
250	(46-60)	14

5. Picture of containers were taken at each data point.

The Dynamic Scale Loop was completely setup and experiments were carried out. The current experimental plan for the Dynamic Scale Loop is given in **Table 6.3** below. The bold font indicates tests conducted in this quarter.

**Table 6.3: Experimental plan for Dynamic Scale Loop (DSL)**

Test #	Temp (°F)	Temp (°C)	Polymer conc. (ppm)	Flow Rate (mL/min)	Velocity (m/s)	Residence Time (min)	% Residence Time of field	% Velocity of Field
1	165	73.88	800	2	0.022	2.354	197.19	0.80
2				60	0.652	0.078	6.57	23.85
3				252	2.740	0.019	1.57	100.19
4	165	73.88	400	2	0.022	2.354	197.19	0.80
5				60	0.652	0.078	6.57	23.85
6				252	2.740	0.019	1.57	100.19
7	165	73.88	0	<b>2</b>	<b>0.022</b>	<b>2.354</b>	<b>197.19</b>	<b>0.80</b>
8				<b>60</b>	<b>0.652</b>	<b>0.078</b>	<b>6.57</b>	<b>23.85</b>
9				252	2.740	0.019	1.57	100.19
10	350	176.66	800	2	0.022	2.354	197.19	0.80

11				60	0.652	0.078	6.57	23.85
12				252	2.740	0.019	1.57	100.19
13	350	176.66	400	2	0.022	2.354	197.19	0.80
14				60	0.652	0.078	6.57	23.85
15				252	2.740	0.019	1.57	100.19
16	350	176.66	0	<b>2</b>	<b>0.022</b>	<b>2.354</b>	<b>197.19</b>	<b>0.80</b>
17				<b>60</b>	<b>0.652</b>	<b>0.078</b>	<b>6.57</b>	<b>23.85</b>
18				252	2.740	0.019	1.57	100.19

The experimental procedure is described below, and a simple schematic is shown in **Figure 6.9**.

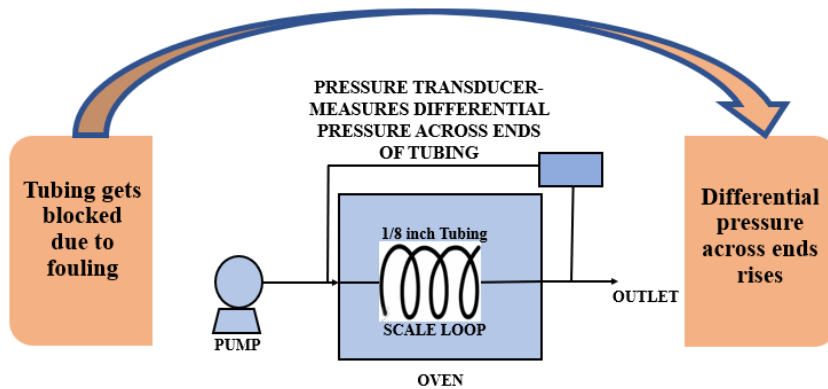


**Figure 6.9: Schematic of Dynamic Scale Loop (DSL)**

1. The coiled tube is placed inside an oven and tubing connections are made to a pump using 1/8” stainless steel tubing.
2. The oven is heated to required temperature to heat the tubing.
3. The pump supplies the testing solution (brine + polymer) at the desired constant flow rate and the solution is made to flow through the tubing.
4. Pressure difference across the inlet and outlet is measured constantly using a pressure transducer and a data logging system.
5. When the differential pressure rises across the ends continuously it implies fouling has led to the tubing being blocked.

### Results and Discussion

*Deposit Rate Test on copper tubes -The effect of polymer concentration and temperature.* Deposit rates for 80ppm and 160ppm concentrations at 200°F were also similar in magnitude to previously tested concentrations indicating that at 200°F there is not a significant amount of fouling on copper tubes. The repeat data points for 200°F at 400ppm and 160ppm were slightly higher than previously obtained values but still significantly less than deposit rates at 250°F and 350°F and consistent with other results. The deposit rates for copper at all tested polymer concentrations and temperatures are shown in the **Figure**

6.10. The yellow bars show the repeated data points. The tubes after the experiment are also shown in Figure 6.11 and compared with the tubes from the 1<sup>st</sup> attempt

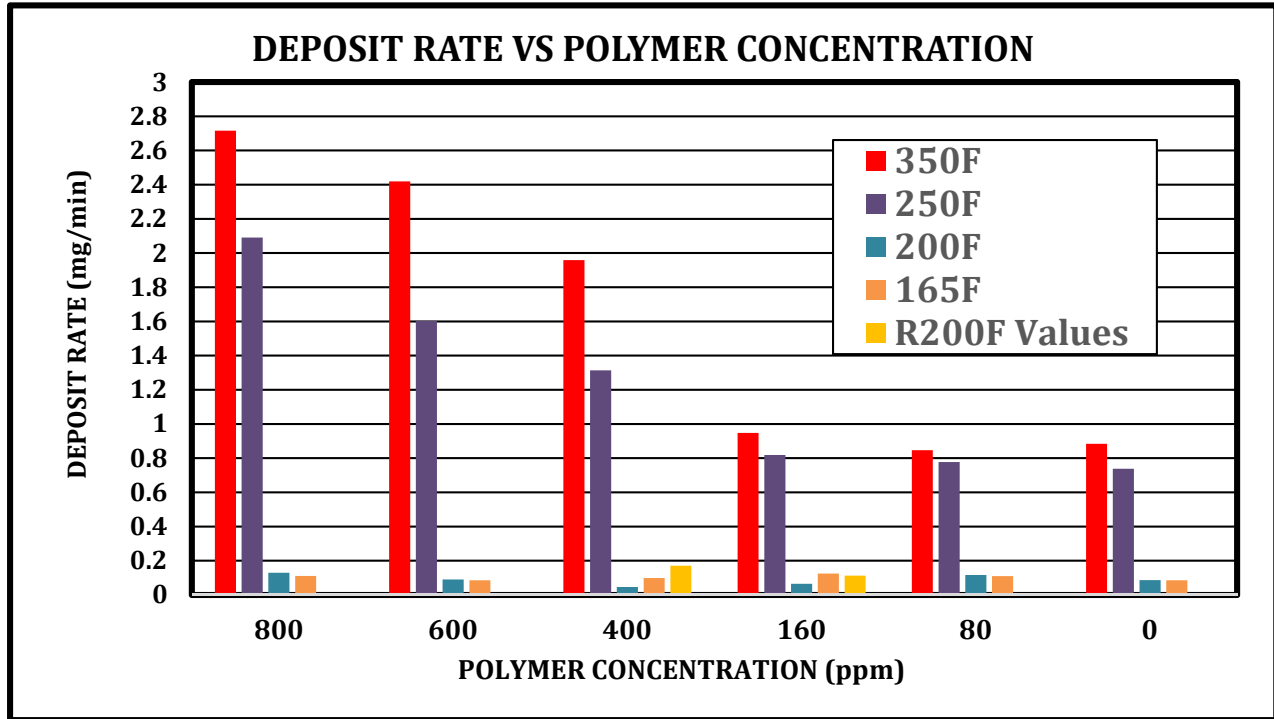


Figure 6.10: Deposit rate comparison at different temperatures and polymer concentrations

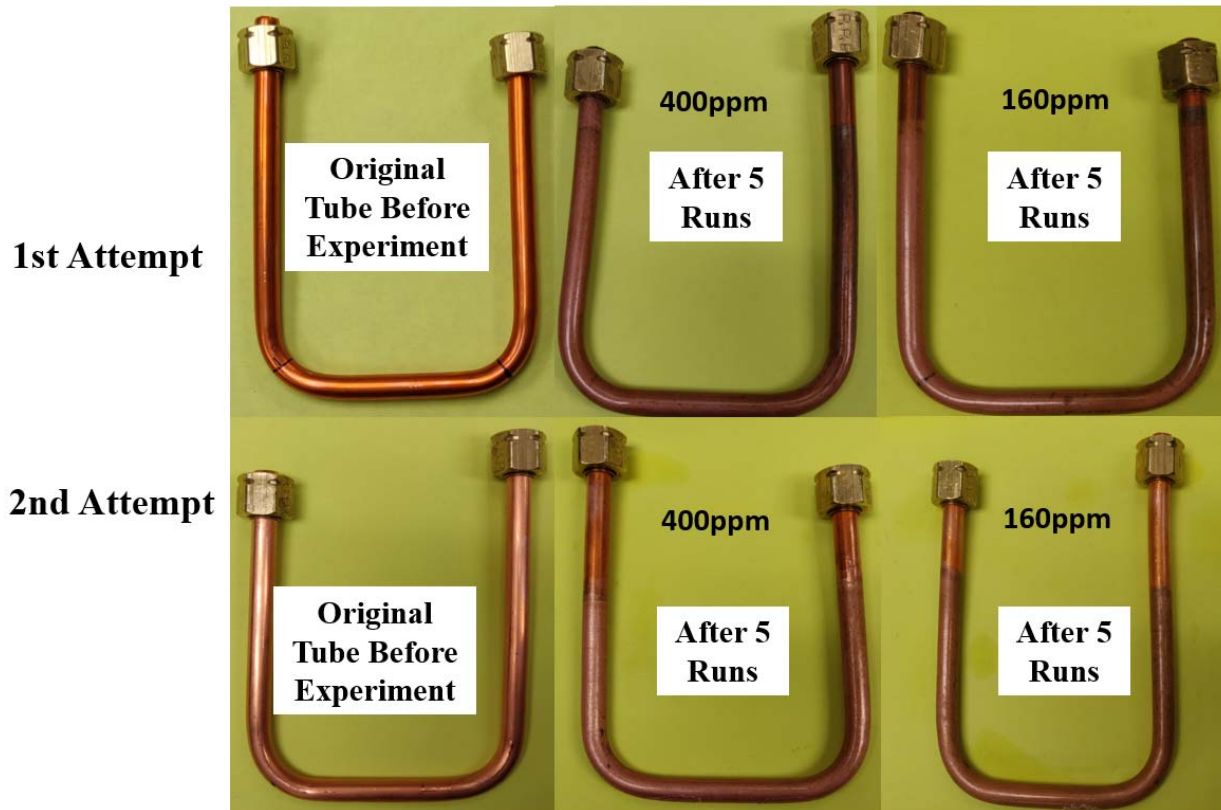


Figure 6.11: Tubes (original and after 5 runs) in both 400ppm and 160ppm test conditions compared with tubes from the 1<sup>st</sup> attempt

*Cloud Point Results* – The results of the cloud point experiment are shown in **Figures 6.12** through **Figure 6.18**.

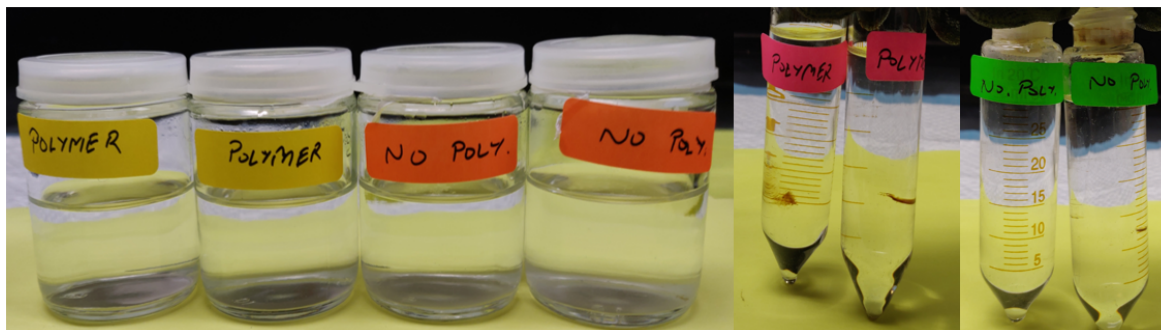


Figure 6.12: Cloud point test solutions after 12 hours at 160°F

No change in solutions was observed after 12 hours at 160°F.

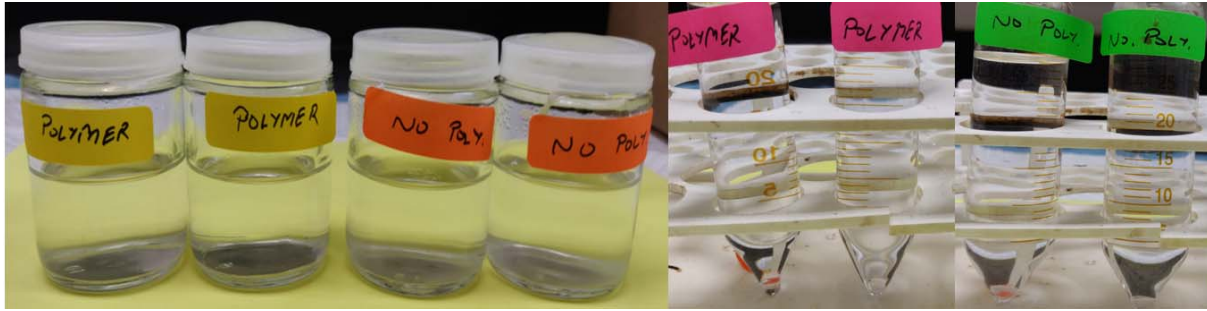


Figure 6.13: Cloud point test solutions after 12 hours at 190°F

No change in solutions was observed after 12 hours at 190°F

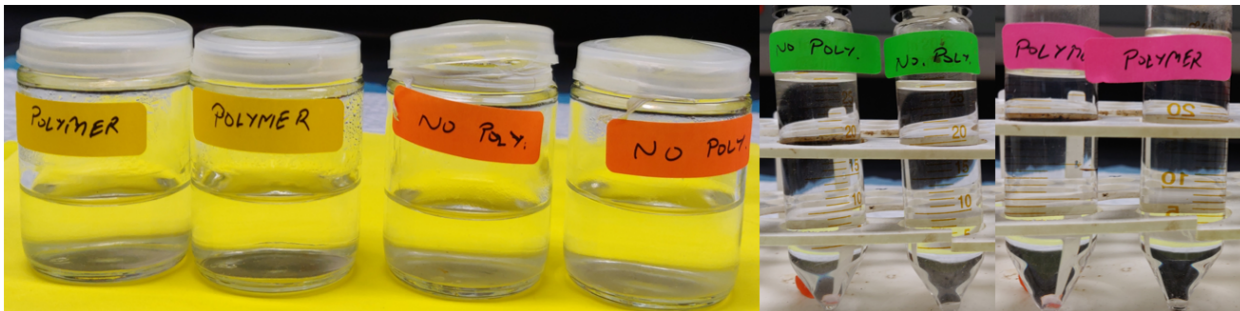


Figure 6.14: Cloud point test solutions after 12 hours at 220°F

No change in solutions was observed after 12 hours at 220°F



Figure 6.15: Cloud point test solutions after 4 hours at 240°F

No change in solutions observed after 4 hours at 240°F. After this point onwards the containers on the left had to be discarded for safety reasons as the plastic caps started melting.

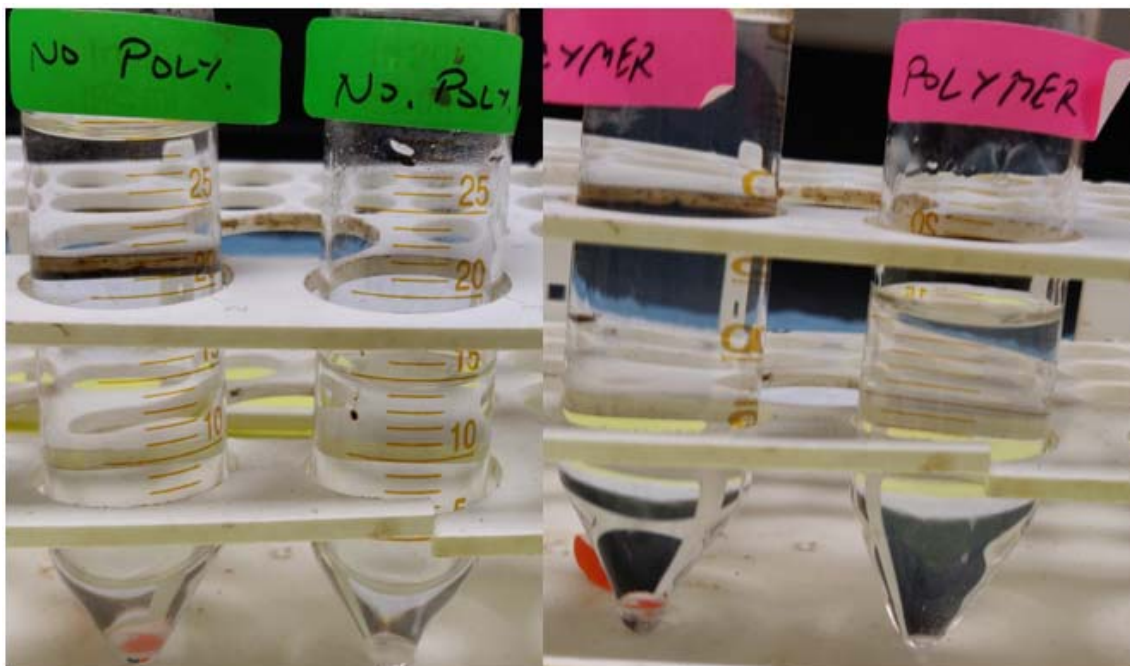


Figure 6.16: Cloud point test solutions after 10 hours at 240°F

No change in solutions observed after 10 hours at 240°F.

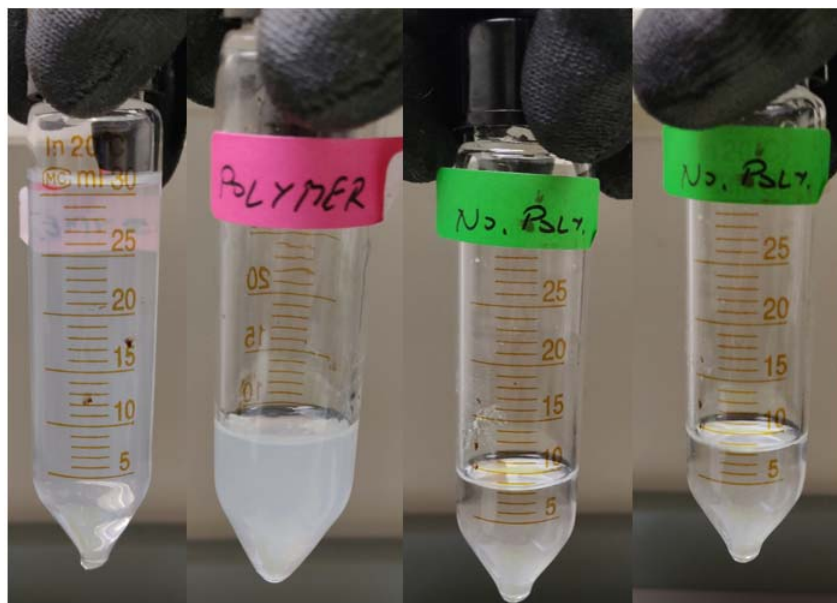


Figure 6.17: Cloud point test solutions after 4 hours at 250°F

Slight milky appearance was seen in the bottle containing the polymer solution after 4 hours at 250°F.



**Figure 6.18: Cloud point test solutions after 12 hours at 250°F.**

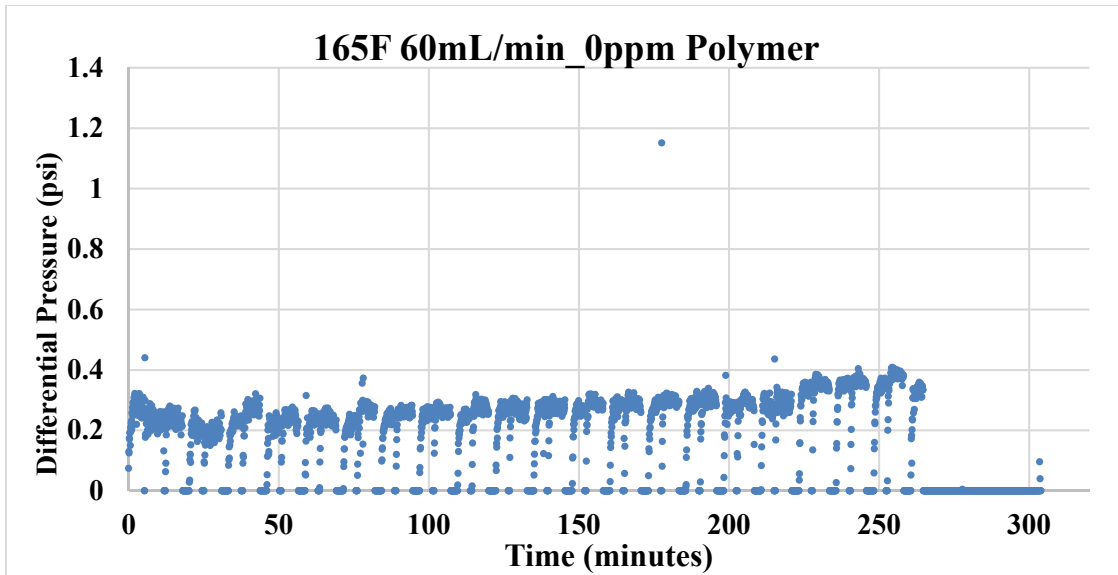
The bottle containing polymer solution showed milky appearance significantly more than the bottle containing only brine. The other containers were not pictured as solution in them evaporated.

*Dynamic Scale Loop Results* – The results of the first experiments of the Dynamic Scale Loop are shown in **Figure 6.19** to **Figure 6.22**. The test conditions of the experiment and their comparison with field parameters at Milne Point are also given below each figure.

The **figure 6.19** shows that when polymer is absent and flow velocity is not too low the differential pressure across the ends of the tubing does not vary much at 165°F skin temperature. In **Figure 6.20** which is for skin temperature of 350°F (all other conditions same) there are minor differential pressure variations although there is not consistent pressure rise which implies the tubing did not get blocked.

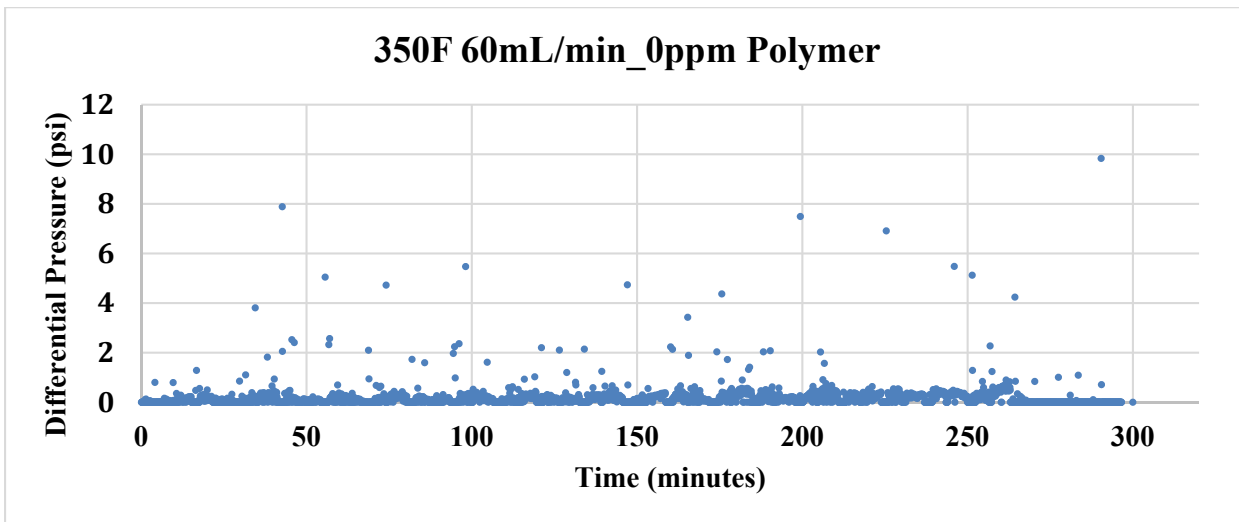
**Figure 6.21** and **Figure 6.22** are for a lower flow rate and hence higher residence time of the test fluids in the tubing. At 165°F a trend similar to the higher flow rate and constant differential pressure was observed throughout the test. **Figure 6.22** is for higher skin temperature of 350°F (all other conditions same) in which a sudden pressure rise was seen after about 35 minutes. At the same time fluids stopped coming out the outlet and both these things imply the tubing got blocked. These preliminary results indicate that higher residence times and higher skin temperatures are critical and can cause severe fouling issues, however these are preliminary results and more tests are needed for confirmed conclusions.





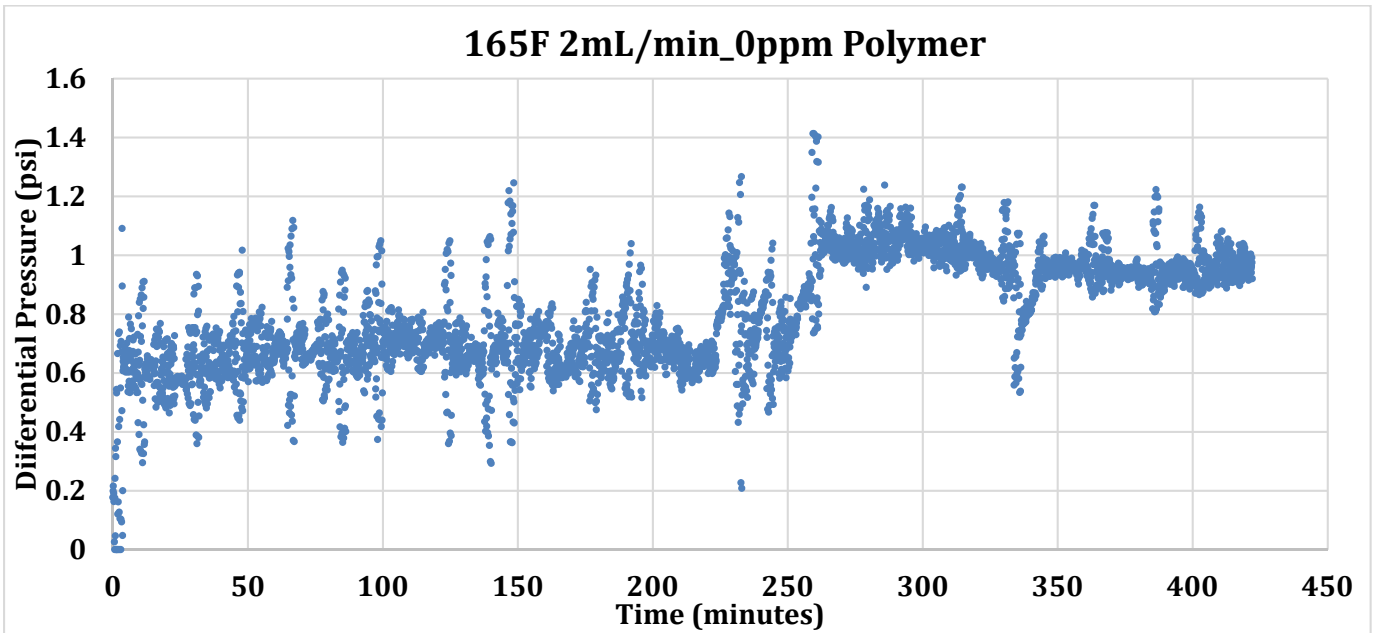
PARAMETER	LAB VALUE	FIELD VALUE
Velocity (m/s)	0.652	2.735
Residence time in Tubing (minutes)	0.078	1.194

Figure 6.19: DSL test result at 165F at 60mL/min with 0ppm polymer



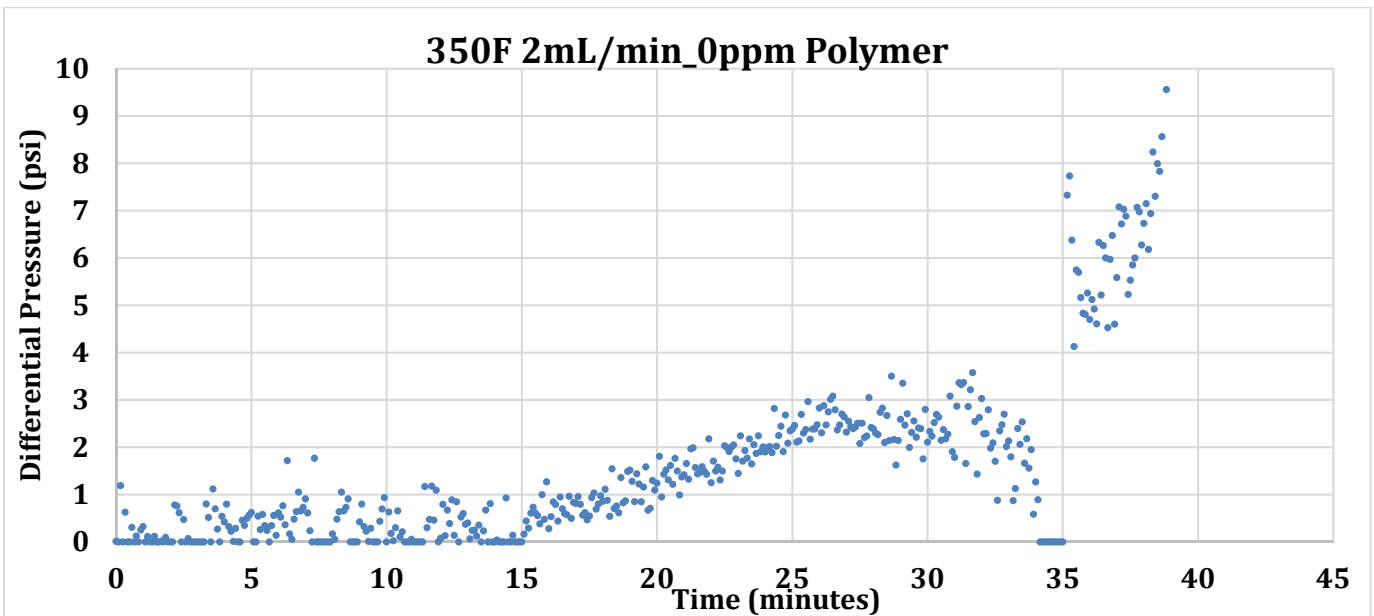
PARAMETER	LAB VALUE	FIELD VALUE
Velocity (m/s)	0.652	2.735
Residence time in Tubing (minutes)	0.078	1.194

Figure 6.20: DSL test result at 350F at 60mL/min with 0ppm polymer



PARAMETER	LAB VALUE	FIELD VALUE
Velocity (m/s)	0.022	2.735
Residence time in Tubing (minutes)	2.35	1.194

Figure 6.21: DSL test result at 165F at 2mL/min with 0ppm polymer



PARAMETER	LAB VALUE	FIELD VALUE
Velocity (m/s)	0.022	2.735
Residence time in Tubing (minutes)	2.35	1.194

**Figure 6.22: DSL test result at 350F at 2mL/min with 0ppm polymer**

**Future Work**

The cloud point experiment will be repeated in new special High Temperature bottles which are expected to prevent the evaporation of the test solution. Additional Dynamic Scale Loop (DSL) experiments will also be conducted in the next quarter with polymer solution with a new pump which can be used to attain high liquid velocities which are representative of the Milne Point field parameters.

**Both activities are ongoing.**

- Task 7.0 - Feasibility of Commercial Application of the Proposed Advanced Polymer Flooding in ANS Heavy Oil Reservoirs

**Activity has not yet started, since it is scheduled for BP4.**

**c. Opportunities for Training and Professional Development**

All the graduate students working on the project are obvious recipients of training and professional development in petroleum engineering. First authors of two of the accepted papers for the 2020 SPE-IOR meeting are UAF MS (Anshul Dhaliwal) and PhD (Hongli Chang) students that are supported by the project, who will present the respective papers at the conference, which will obviously provide them excellent professional development opportunities.

**d. Dissemination of Results to Communities of Interest**

Engineers from ConocoPhillips and Hilcorp continue to communicate about the project on a regular basis. Additionally, most of the project related information is publically available or disseminated through the NETL website, which is accessible to any communities that have interest in the project. Similarly, publications resulting from the project work also serve the same purpose.

**e. Plan for Next Quarter**

Building on the current progress achieved by the research team, work planned for the next quarter will include steadily progressing toward the planned completion dates outlined in **Table A** below.

**Table A: Summary of milestone status.**

Milestones	Task No.	Planned Completion Date	Actual Completion Date	Verification Method	Comments

University of Alaska Fairbanks

Project Management Plan	1a	o 9/30/2022	o Ongoing (latest revision 4/30/2019)	Report/Bi-weekly meetings	None
Data Management Plan	1b	o 8/31/2018	o 7/20/2018 (latest revision 4/30/2019)	Report/Bi-weekly meetings	None
<ul style="list-style-type: none"> <li>Quantify polymer retention</li> </ul>	2	o 3/31/2019	o Several tests completed but continues to be a topic of investigation	Report/Bi-weekly meetings	None
<ul style="list-style-type: none"> <li>Effect of water salinity on <math>S_{or}</math></li> <li>Screening of gel products for conformance control</li> </ul>	3	o 4/30/2019  o 6/30/2019	o Several tests completed per the planned date; however, August 16 <sup>th</sup> marks the true completion.  o Some tests completed, and continues to be a topic of investigation	Report/Bi-weekly meetings	None
<ul style="list-style-type: none"> <li>Pilot area model waterflooding history match</li> <li>Coreflooding model history match</li> <li>Updated area model for polymer flood prediction</li> </ul>	4	o 12/31/2018  o 4/30/2019  o 5/31/2019	o Several iterations, however, an improved history match in the waterflooding period achieved in January 2020.  o Some completed per plan, but the effort continues  o Polymer flooding period WC history match is a challenge,	Report/Bi-weekly meetings	None

<ul style="list-style-type: none"> <li>● Reservoir modeling report</li> </ul>		<ul style="list-style-type: none"> <li>○ 5/31/2019</li> </ul>	<p>but several prediction runs have been completed and are ongoing.</p> <ul style="list-style-type: none"> <li>○ Extensively reported in Quarterlies, but a formal report was submitted on July 11, 2019 as special status report</li> </ul>		
<ul style="list-style-type: none"> <li>● Injection profile with polymer inj.</li> <li>● PFO (post-polymer)</li> <li>● Tracer tests (post-polymer)</li> </ul>	5	<ul style="list-style-type: none"> <li>○ 12/31/2018</li> <li>○ 12/31/2018</li> <li>○ 12/31/2018</li> </ul>	<ul style="list-style-type: none"> <li>○ Ongoing</li> <li>○ Ongoing</li> <li>○ Ongoing</li> </ul> <p><i>Note – all have been completed from the reporting standpoint, but given the dynamic nature of the pilot these are also ongoing</i></p>	Report/Bi-weekly meetings	None

University of Alaska Fairbanks

<ul style="list-style-type: none"> <li>● Initial treatment plan recommendation based upon literature survey</li>   <li>● Static polymer deposition quantification and analyses</li>   <li>● Finalization of the fouling flow loop design</li> </ul>	6	<ul style="list-style-type: none"> <li>○ 12/31/2018</li>   <li>○ 09/30/2019</li>   <li>○ 06/30/2019</li> </ul>	<ul style="list-style-type: none"> <li>○ Ongoing refinement and additional tests. However, recent tests have been used to identify/screen an effective emulsion breaker.</li>   <li>○ Tests on copper, carbon steel and stainless steel already completed and the deposit imaged; mostly complete in this quarter</li>   <li>○ Completed in previous quarter, some tests have been carried out, and ongoing</li> </ul>	Report/Bi-weekly meetings	None
---	---	--	--	---------------------------	------

**2. PRODUCTS**

Samson Ning, John Barnes, Reid Edwards, Walbert Schulpen, Abhijit Dandekar, Yin Zhang, Dave Cercone, Jared Ciferno: First Ever Polymer Flood Field Pilot to Enhance the Recovery of Heavy Oils on Alaska North Slope – Producer Responses and Operational Lessons Learned. Abstract submitted for 2020 SPE ATCE, Denver, CO.

**3. PARTICIPANTS & OTHER COLLABORATING ORGANIZATIONS**

Hilcorp hired two operators dedicated to the project operations. Two reservoir engineers are in charge of the test design and analysis; one facilities engineer is in charge of polymer skid design and installation; and one operations engineer is in charge of downhole well work.

All the listed project personnel identified on the second page, and graduate students working on different tasks formally contribute 2 hours every other Friday in a project working meeting. Additionally, subgroup working meetings, typically lasting for 2-4 hours in a month are also held to discuss specific tasks such as reservoir simulation. For graduate students, the typical formal working hours per week are 20. Besides these, additional hours are typical in preparing reports, presentations for meetings, and potential publications.

**4. IMPACT**

The project continues to be an outreach tool since it is actually showcased (relevant parts of it) in the petroleum engineering curriculum, and is a topic of frequent technical discussions, at many places.

**5. CHANGES/PROBLEMS**

- Current plan is to switch from super bags to bulk transport to simplify operations and reduce polymer transportation cost.
- The team also has discussed reduction in polymer concentration in stages from 1700 ppm to 1400 ppm that will result in a viscosity of ~30 cP and hopefully improve injectivity.

**6. SPECIAL REPORTING REQUIREMENTS**

Nothing to Report.

**7. BUDGETARY INFORMATION**

A summary of the budgetary information for the first budget period of the project is provided in **Table B**. This table shows the planned costs, reported costs, and the variance between the two. Reported costs is the sum of UAF's incurred expenses and the sum of the invoices received from our project partners.

**Table B: Budgetary information for Budget Period 2, Q3.**

Baseline Reporting Quarter	Budget Period 2	
	December 1, 2019-February 29, 2020	
	Q3	Cumulative Total
<b>Baseline Cost Plan</b>		
Federal Share	167,502	4,260,628
Non-Federal Share	114,800	1,193,689
<b>Total Planned</b>	<b>282,302</b>	<b>5,454,317</b>
<b>Actual Incurred Cost</b>		
Federal Share	769,248	2,924,044
Non-Federal Share	161,647	1,599,765
<b>Total Incurred Cost</b>	<b>930,895</b>	<b>4,523,809</b>
<b>Variance</b>		
Federal Share	-601,746	1,336,584
Non-Federal Share	-46,847	-406,076
<b>Total Variance</b>	<b>648,593</b>	<b>930,508</b>

Please note that the PMP also has a spending plan that is based on calendar quarters.

**8. PROJECT OUTCOMES**

Nothing to Report.



## 9. REFERENCES

- Andersen, P. Ø., Lohne, A., Stavland, A., Hiorth, A., & Brattekkås, B. (2018, April 14). Core Scale Simulation of Spontaneous Solvent Imbibition from HPAM Gel. Society of Petroleum Engineers. doi:10.2118/190189-MS
- Bai, B., & Zhang, H. (2011, June 1). Preformed-Particle-Gel Transport Through Open Fractures and Its Effect on Water Flow. Society of Petroleum Engineers. doi:10.2118/129908-PA
- Bai, B., Li, L., Liu, Y., Coste, J., Li, L., 2004, "Preformed Particle Gel for Conformance Control: Transport Mechanism Through Porous Media," Paper SPE 89468, presented at the SPE/DOE 14th Symposium on Improved Oil Recovery, Tulsa, Oklahoma, April, 17-21.
- Chaveteau, G. and Lecourtier, J. 1988. Propagation of Polymer Slugs Through Adsorbent Porous Media. In *Water-Soluble Polymers for Petroleum Recovery*, eds. G.A. Stahl and D.N. Schulz, 53-68. Boston Massachusetts, Springer. [http://dx.doi.org/10.1007/978-1-4757-1985-7\\_3](http://dx.doi.org/10.1007/978-1-4757-1985-7_3).
- Howard, G.C. and Fast, C. R.: Hydraulic Fracturing, Monograph Series, SPE, Richardson, Texas (1970) 2, 32.
- Imqam, A., Bai, B., Al Ramadan, M., Wei, M., Delshad, M., & Sepehrnoori, K. (2014, April 12). Preformed Particle Gel Extrusion through Open Conduits during Conformance Control Treatments. Society of Petroleum Engineers. doi:10.2118/169107-MS
- Manichand, R.N., and Seright, R.S. 2014. Field vs Laboratory Polymer Retention Values for a Polymer Flood in the Tambaredjo Field. *SPE Res Eval & Eng.* **17**(3): 314-325. <http://dx.doi.org/10.2118/169027-PA>.
- Ouyang, L., Zhu, D., & Hill, A. D. (2013, March 26). Theoretical and Numerical Simulation of Herschel-Bulkley Fluid Flow in Propped Fractures. International Petroleum Technology Conference. doi:10.2523/IPTC-17011-MS
- Seright, R.S., **Wang, D.**, Lerner, N., Nguyen, A., Sabid, J., and Tochor, R., 2018. Can 25-cp Polymer Solution Efficiently Displace 1,600-cp Oil during Polymer Flooding. *SPE Journal*, December, Volume 23 (6), 2260-2278. ISSN: 1930-0220. DOI:10.2118/190321-PA.
- Seright, R. S. (2003, February 1). An Alternative View of Filter-Cake Formation in Fractures Inspired by Cr(III)-Acetate-HPAM Gel Extrusion. Society of Petroleum Engineers. doi:10.2118/81829-PA
- Seright, R. S. (2002, January 1). An Alternative View of Filter Cake Formation in Fractures. Society of Petroleum Engineers. doi:10.2118/75158-MS

*University of Alaska Fairbanks*

Wang, Y., & Seright, R. S. (2006, January 1). Correlating Gel Rheology with Behavior during Extrusion through Fractures. Society of Petroleum Engineers. doi:10.2118/99462-MS

Zhang, Guoyin, and Seright, R.S. 2014. Effect of Concentration on HPAM Retention in Porous Media. *SPE Journal* **19**(3): 373-380. Paper 166256. <http://dx.doi.org/10.2118/166256-PA>.